

Saddle Hierarchy in Dense Associative Memory

Robin Thériault^{1*} and Daniele Tantari²

¹Scuola Normale Superiore di Pisa, Piazza dei Cavalieri 7, 56126, Pisa (PI), Italy

²Department of Mathematics, University of Bologna,

Piazza di Porta San Donato 5, 40126, Bologna (BO), Italy

August 2025

Abstract

Dense associative memory (DAM) models have been attracting renewed attention since they were shown to be robust to adversarial examples and closely related to state-of-the-art machine learning paradigms, such as the attention mechanisms in transformers and generative diffusion models. We study a DAM built upon a three-layer Boltzmann machine with Potts hidden units, which represent data clusters and classes. Through a statistical mechanics analysis, we derive saddle-point equations that characterize both the stationary points of DAMs trained on real data and the fixed points of DAMs trained on synthetic data within a teacher-student framework. Based on these results, we propose a novel regularization scheme that makes training significantly more stable. Moreover, we show empirically that our DAM learns interpretable solutions to both supervised and unsupervised classification problems. Pushing our theoretical analysis further, we find that the weights learned by relatively small DAMs correspond to unstable saddle points in larger DAMs. We implement a network-growing algorithm that leverages this saddle-point hierarchy to drastically reduce the computational cost of training dense associative memory.

1 Introduction

Studying the stationary points of machine learning algorithms is crucial to understand how they work. For example, [1, 2] demonstrated that local minima in the loss landscape of large artificial neural networks (NNs) are relatively close to the global minimum, explaining why they generalize well in practice. Moreover, [3, 4] showed that saddle points are much more numerous than local minima in large NNs. These breakthroughs were made by establishing deep connections between the loss landscape of NNs and the energy landscape of disordered systems studied in statistical mechanics. Beyond the broad insights provided by these studies, and despite the progress made by [5, 6, 7, 8], the classification of stationary points in machine learning algorithms remains an open problem. An interesting way forward is through dense associative memory (DAM) models [9, 10]. In fact, the interpretability of DAMs and the relative simplicity of their learning dynamics [11] suggest that their critical points could potentially be characterized using analytical calculations.

*Corresponding author. E-mail address: robin.theriault@sns.it

The Hopfield network was originally introduced as a paradigmatic model of biological associative memory [9]. Generalized Hopfield networks [12, 13, 14, 15, 16, 17] were then developed to improve upon the limited storage capacity of the original [9, 18]. A few years ago, these generalized networks, commonly referred to as dense associative memory (DAM) or modern Hopfield networks [10, 19], were made into trainable machine learning models capable of accurate pattern classification by Krotov and Hopfield (K & H) [10]. In a nutshell, K & H’s DAM learns prototypes of patterns in a trainable weight matrix. Each prototype casts a vote for a class, and the patterns awaiting classification are assigned based on the votes of the prototypes that most closely resemble them. The resulting classification scheme is considerably more adversarially robust and interpretable than that of feedforward NNs with ReLU activation functions [10, 20, 21]. Since their debut as trainable machine learning architectures, deep connections have been made between modern Hopfield networks and transformers [19], as well as generative diffusion models [22, 23]. In particular, modern Hopfield networks were used to implement the attention mechanism of transformers [19, 24], which has been attracting a lot of interest in fundamental [25, 26, 27, 28, 29] and applied research [24, 28, 30, 31]. Recently, it was observed that the trainable weights of K & H’s DAM are channeled toward minima by a low-dimensional network of valleys in the loss landscape [11]. Moreover, the points where valleys branch out from one another were identified as saddles in the simple case where the DAM has two patterns to learn. In general, it is not straightforward to classify the stationary points of machine learning algorithms [8]. However, the results of [11] and the interpretability of DAMs suggest that their stationary points are both fundamental to their learning dynamics and easier to characterize than that of generic NNs. With this goal in mind, we revisit dense associative memory for pattern classification [10] using the framework of Boltzmann machines (BMs) [32, 33, 34, 35] and Statistical Mechanics.

In Section 2, we present the DAM model that we study and the tools that we use to do so. This Section is divided into two subsections. In Section 2.1, we derive a DAM from a BM template. In Section 2.2, we describe the setting in which we study DAM stationary points. In Section 3, we present our theoretical results. This Section is also divided into two subsections. In Section 3.1, we introduce saddle-point equations that characterize DAM stationary points. In Section 3.2, we use these equations to demonstrate the existence of a saddle-point hierarchy according to which the weights learned by DAMs of a given width are embedded in larger DAMs, where they become saddle points. In Section 4, we use our theoretical results to significantly improve DAM training, and we investigate the results. This Section is divided into three subsections. In Section 4.1, we design a theoretically motivated regularization method that facilitates supervised training. In Section 4.2, we show that our DAM, despite being designed for supervised learning, can learn interpretable solutions to both supervised and unsupervised classification problems. Finally, in Section 4.3, we relate our findings to the learning dynamics guided by valleys and saddles studied in [11], and we implement a network-growing algorithm [36, 37] that uses the saddle-point hierarchy to significantly reduce the cost of DAM training. The code and hyperparameter values used in our numerical experiments are available at this public repository [38].

2 Model

The Boltzmann machine (BM) is a canonical graphical model of correlations in discrete data [32]. It is customary to partition BMs into a visible layer $\mathbf{v} = \{v_i\}_{i=1}^N$ and a hidden layer $\mathbf{h} = \{h_\mu\}_{\mu=1}^P$ such that

connections between the two layers are allowed, but connections within them are prohibited [33]. In this case, the visible layer represents concrete features of the data, whose mutual correlations are encoded in connections with the hidden layer. The restricted Boltzmann machine (RBM) obtained using this partition is much easier to train than a generic BM [34, 35] and still has considerable generating power [34, 39], making it more practical in machine learning applications [40, 41, 42]. The visible and hidden units of an RBM follow the Gibbs distribution

$$P_\beta(\mathbf{v}, \mathbf{h}|\mathbf{J}) = Z_\beta(\mathbf{J})^{-1} P_0(\mathbf{v}) P_0(\mathbf{h}) \exp(-\beta H[\mathbf{v}, \mathbf{h}; \mathbf{J}]),$$

where $\beta \geq 0$ is known as the inverse temperature, $P_0(\mathbf{v})$ and $P_0(\mathbf{h})$ are priors on \mathbf{v} and \mathbf{h} , $H[\mathbf{v}, \mathbf{h}; \mathbf{J}] = -\sum_{i=1}^N \sum_{\mu=1}^P J_i^\mu v_i h_\mu$ is called the energy function or Hamiltonian, $\mathbf{J} = \{J_i^\mu\}_{1 \leq i \leq N}^{1 \leq \mu \leq P}$ are trainable weights, and $Z_\beta(\mathbf{J})$ is a normalization constant called the partition function. The inverse temperature β represents the absolute strength of the RBM connections, or equivalently controls the amount of noise $T = 1/\beta$ in the RBM. In this regard, $P_0(\mathbf{v})$ and $P_0(\mathbf{h})$, which restrict the form of the Gibbs distribution to help the RBM represent the data, are the marginal laws of \mathbf{v} and \mathbf{h} when there are no connections, i.e. $\beta = 0$. Their contribution to the Gibbs distribution can be tuned with β , which can therefore be interpreted as a regularization parameter.

2.1 A dense associative memory (DAM) model

As mentioned in the Introduction, we will now derive a dense associative memory (DAM) model for classification from a BM template. We will explain why our model is a DAM at the end of this Section, once we have clearly defined it. We make three basic assumptions on the distribution of data to be classified:

1. the data is scale invariant, i.e. any data point \mathbf{x} is equivalent to $c\mathbf{x}$;
2. the data can be partitioned in disjoint clusters;
3. the clusters can be grouped into mutually exclusive classes.

In order to exploit these three assumptions, we study a BM partitioned into three layers with different roles: the data layer \mathbf{x} , the hidden layer \mathbf{h} and the class layer \mathbf{q} , which represent data, cluster membership and class membership, respectively. The corresponding energy is

$$-H[\mathbf{x}, \mathbf{q}, \mathbf{h}; \mathbf{J}] = \sum_{i=1}^N \sum_{\mu=1}^P w_i^\mu x_i h_\mu + \sum_{y=1}^C \sum_{\mu=1}^P u_y^\mu q_y h_\mu + \sum_{\mu=1}^P h_\mu b^\mu, \quad (1)$$

where $\mathbf{J} = \{\mathbf{w}, \mathbf{u}, \mathbf{b}\}$ is the set of the trainable weights $\mathbf{w} = \{w_i^\mu\}_{1 \leq i \leq N}^{1 \leq \mu \leq P}$, $\mathbf{u} = \{u_y^\mu\}_{1 \leq y \leq C}^{1 \leq \mu \leq P}$ and $\mathbf{b} = \{b^\mu\}_{\mu=1}^P$. There are no direct interactions between the visible layer and the class layer. In other words, conditional on the cluster layer, the visible layer and the class layer are independent. Therefore, this BM is a deep Boltzmann machine (DBM) with 3 layers [43], which can also be thought of as an RBM whose visible layer \mathbf{v} is further divided into \mathbf{x} and \mathbf{q} .

Since the data is scale invariant (Assumption 1), we normalize it by its (Euclidean) norm in the data layer. In other terms, we take the data units x_i to be continuous variables with unit norm $\sqrt{\sum_{i=1}^N (x_i)^2} = 1$. We assume no further knowledge about \mathbf{x} , so we take the prior $P_0(\mathbf{x})$ to be the uniform distribution on the $N - 1$

dimensional unit sphere S^{N-1} . Data normalization is a very common practice in machine learning. For example, normalization by the Euclidean norm is frequent in text document clustering [44, 45, 46]. Various types of normalization also occur in the brain and retina [47].

Since the hidden layer and the class layer represent disjoint clusters and classes, respectively (Assumptions 2 and 3), we take their respective units to be mutually exclusive binary variables, i.e. $\mathbf{h} \in \{0, 1\}^P$ with $\sum_{\mu=1}^P h_{\mu} \in \{0, 1\}$ and $\mathbf{q} \in \{0, 1\}^C$ with $\sum_{y=1}^C q_y \in \{0, 1\}$. In other words, we take each of these two layers to be the vector representation of a single categorical (or Potts [48, 49]) variable with $P + 1$ and $C + 1$ categories, respectively. As such, $P_0(\mathbf{h})$ and $P_0(\mathbf{q})$ simplify to probability mass functions $P_0(\mathbf{h} = \mathbf{e}_{\gamma})$ and $P_0(\mathbf{q} = \mathbf{e}_y)$, where we introduce $\mathbf{e}_{\gamma} = \{\delta_{\gamma\mu}\}_{\mu=1}^P$ for $\gamma \in \{0, \dots, P\}$ and define $\mathbf{e}_y \in \{0, 1\}^C$ analogously for $y \in \{0, \dots, C\}$. In particular $\mathbf{e}_0 = \mathbf{0}$ represents a state outside the P clusters or the C classes.

These priors on the hidden layer and the class layer can also be obtained by introducing fixed inhibitory connections within the hidden layer and the class layer, respectively [50, 51, 52]. Since at most one hidden unit h_{μ} can be activated at once, the hidden layer is a very sparse representation of the visible layer. In machine learning, sparsity can improve interpretability [53], generalization, computational efficiency [54], and adversarial robustness [55, 56, 57, 58, 59, 60]. The sparsity of the brain suggests that it is also beneficial for biological neural networks [61].

Given these priors $P_0(\mathbf{x})$, $P_0(\mathbf{h})$ and $P_0(\mathbf{q})$, we derive the marginal distribution of the visible layer (\mathbf{x}, \mathbf{q}) (see Appendix A for details). We start our derivation by showing that the conditional distribution of the data layer given the hidden layer has the form

$$\begin{aligned} P_{\beta}(\mathbf{x}|\mu, \mathbf{J}) &:= P_{\beta}(\mathbf{x}|\mathbf{h} = \mathbf{e}_{\mu}, \mathbf{J}) \\ &\propto \exp\left(\beta \sum_{i=1}^N w_i^{\mu} x_i\right) \quad \forall \mathbf{x} \in S^{N-1} \text{ and } \mu \in \{1, \dots, P\}. \end{aligned} \quad (2)$$

In other words, the probability density $P_{\beta}(\mathbf{x}|\mu, \mathbf{J})$ corresponding to each cluster $\mu > 0$ is a von Mises-Fisher (vMF) distribution centered on the direction $\mathbf{w}^{\mu} = \{w_i^{\mu}\}_{i=1}^N$ (see Appendix C). In order to interpret the \mathbf{w}^{μ} as centroids for their respective clusters, we assume that they belong to S^{N-1} like the data layer. Under this assumption, we find the normalization constant of $P_{\beta}(\mathbf{x}|\mu, \mathbf{J})$ to be $\Omega_N(\beta) = \frac{(2\pi)^{N/2} I_{N/2-1}(\beta)}{\beta^{N/2-1}}$, where $I_n(x)$ is the modified Bessel function of the first kind of order n (see Appendix C).

After slightly more work, we find the marginal distribution of the visible layer to be

$$\begin{aligned} P_{\beta}(\mathbf{x}, y|\mathbf{w}, \mathbf{p}) &:= P_{\beta}(\mathbf{x}, \mathbf{q} = \mathbf{e}_y|\mathbf{J}) \\ &= \sum_{\mu=1}^P p_y^{\mu} \frac{\exp\left(\beta \sum_{i=1}^N w_i^{\mu} x_i\right)}{\Omega_N(\beta)} + p_y^0 \frac{1}{\Omega_N(0)} \quad \forall \mathbf{x} \in S^{N-1} \text{ and } y \in \{0, \dots, C\}, \end{aligned} \quad (3)$$

where $\mathbf{p} = \{p_y^{\gamma}\}_{0 \leq y \leq C}^{0 \leq \gamma \leq P} = \{P_{\beta}(\mathbf{q} = \mathbf{e}_y, \mathbf{h} = \mathbf{e}_{\gamma}|\mathbf{J})\}_{0 \leq y \leq C}^{0 \leq \gamma \leq P}$. $\Omega_N(0) = \frac{2\pi^{N/2}}{\Gamma(N/2)}$ is the surface area of S^{N-1} , where $\Gamma(x)$ is the Gamma function, so $\frac{1}{\Omega_N(0)}$ is the uniform distribution on S^{N-1} . The uniform distribution term of Eq. (3) encourages the model to ignore very noisy data during training, which may or not be desirable depending on the application.

The detailed derivation of Eq. (3) (in Appendix A) is inspired by the derivation of Gaussian mixtures

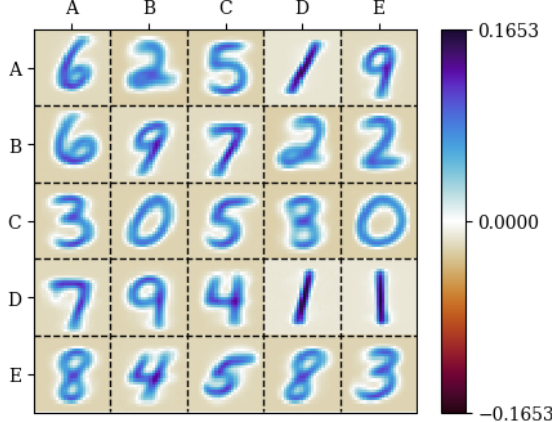


Figure 1: All of the $P = 25$ memories $\{\mathbf{w}^\mu\}_{\mu=1}^{25}$ learned by an instance of our model with $\beta = 16$ when it is trained on the MNIST dataset of handwritten digits [65] using constrained stochastic gradient descent (SGD) of the negative log-likelihood loss (Eq. 4). The hidden units are indexed using pairs of letters from A to E.

from RBMs presented in [62] based on the framework of [50, 51, 52]. In our case, the marginal distribution $P_\beta(\mathbf{x}|\mathbf{w}, \mathbf{p}) = \sum_{y=0}^C P_\beta(\mathbf{x}, y|\mathbf{w}, \mathbf{p})$ and conditional distributions $P_\beta(\mathbf{x}|y; \mathbf{w}, \mathbf{p}) = \frac{P_\beta(\mathbf{x}, y|\mathbf{w}, \mathbf{p})}{\sum_{\gamma=0}^P P_\beta(y, \gamma|\mathbf{w}, \mathbf{p})}$ are convex mixtures between the uniform distribution on S^{N-1} and the vMF distributions $P_\beta(\mathbf{x}|\mu, \mathbf{J})$ (see Eq. 2). Probabilistic models similar to $P_\beta(\mathbf{x}|\mathbf{w}, \mathbf{p})$ are notably used in text document clustering [46]. Mixture distributions that have class-dependent weights like $P_\beta(\mathbf{x}|y; \mathbf{w}, \mathbf{p})$ are also used in Gaussian mixture discriminant analysis [63].

The class weights \mathbf{p} depend on the trainable parameters \mathbf{u} and \mathbf{b} of Eq. (1) (see Appendix A). Without loss of generality, we choose to directly study (and train) \mathbf{p} instead of \mathbf{u} and \mathbf{b} . Recall that p_y^γ is a probability distribution, and in particular $p_y^\gamma \geq 0$ (see Eq. 3). We constrain the marginal $\sum_{y=0}^C p_y^\gamma$, i.e. the fraction of data in each cluster, to a fixed distribution $p_h(\gamma)$ and the marginal $\sum_{\gamma=0}^P p_y^\gamma$, i.e. the proportion of data in each class y , to another fixed distribution $p_q(y)$. In sum, we end up with the constraints $p_y^\gamma \geq 0$, $\sum_{\gamma=0}^P p_y^\gamma = p_q(y)$ and $\sum_{y=0}^C p_y^\gamma = p_h(\gamma)$. Since each cluster belongs to a single class (Assumption 3), we expect the p_y^γ of a trained model to be close to $\sum_{y'=0}^C p_{y'}^\gamma$ for a given y and close to 0 otherwise.

Given a dataset of P^* patterns $\{\mathbf{x}^{*\mu}\}_{\mu=1}^{P^*}$ with soft labels $q_y^{*\mu}$ [64], we can train the weights \mathbf{w} and \mathbf{p} by minimizing the negative log-likelihood loss

$$L(\mathbf{w}, \mathbf{p}) = -\frac{1}{P^*} \sum_{\mu=1}^{P^*} \sum_{y=0}^C q_y^{*\mu} \log P_\beta(\mathbf{x}^{*\mu}, y|\mathbf{w}, \mathbf{p}), \quad (4)$$

which is a form of maximum likelihood estimation. We do so using constrained stochastic gradient descent with momentum (simply called SGD in this paper). We explain how the constraints on \mathbf{w} and \mathbf{p} are enforced in Appendix F, and we briefly discuss the initial conditions and the learning rate in Appendix I.

The weights \mathbf{w}^μ learned by SGD of the loss (Eq. 4) [65] are interpretable prototypes, or memories, of the data (see Fig. 1 in the case of the MNIST dataset of handwritten digits [65]), which is consistent with their role as cluster centroids. Once the model is trained, we can use its conditionals $P_\beta(y|\mathbf{x}; \mathbf{w}, \mathbf{p})$ and $P_\beta(\mathbf{x}|y; \mathbf{w}, \mathbf{p})$

to efficiently reconstruct y from \mathbf{x} or \mathbf{x} from y , respectively. In particular, we can classify unseen patterns using the Bayes classification rule $y = \operatorname{argmax}_{y'} \{\log P_\beta(y'|x; \mathbf{w}, \mathbf{p})\}$ and reconstruct patterns of a given class by finding the local minima of the effective energy $-\log P_\beta(x|y; \mathbf{w}, \mathbf{p})$ as a function of $\mathbf{x} \in S^{N-1}$.

High-dimensional probabilistic models that store or learn prototypes, such as our model, can typically reconstruct a limited number of patterns with non-trivial accuracy. In other words, they have limited storage capacity. For instance, Hopfield's model of associative memory, the Hopfield network [9], has a capacity of up to $\mathcal{O}(N)$ patterns [9, 18]. Dense associative memory (DAM) models are a class of Hopfield network-inspired models with an asymptotically much higher capacity [10, 15]. The effective energy $-\log P_\beta(x|y; \mathbf{w}, \mathbf{p})$ that we can minimize to reconstruct patterns with our model (see Eq. 3) is very similar to that of the DAM studied in [19, 27, 29], which also reconstructs patterns by energy minimization. In fact, according to [29], our model belongs to the class of DAMs with exponential capacity.

2.2 Teacher-student setting

Among the extensive research on the properties of artificial neural networks (NNs) from the perspective of statistical mechanics [2, 3, 4, 14, 15, 16, 17, 18, 29, 62, 66, 67, 68, 69], there have been many studies of simple RBMs trained by maximum likelihood estimation (see Eq. 4) [70, 71, 72, 73, 74, 75] or by averaging samples from the posterior distribution of the weights \mathbf{J} given some observed data \mathcal{D} . The latter approach has notably been used to characterize the fundamental limits of RBM learning [76, 77, 78, 79, 80, 81, 82, 83, 84] in the *teacher-student setting* where the data used to train \mathbf{J} is sampled from another RBM with planted weights \mathbf{J}^* [85, 78, 79, 86]. This teacher-student setting can also be used to study our DAM. In this scenario, a *teacher* DAM with weights \mathbf{w}^* and \mathbf{p}^* generates a large amount $M = \alpha N$ of noisy data $\mathcal{D} = \{\mathbf{x}^c, y^c\}_{c=1}^M$ and feeds them to a *student* DAM, which then trains its weights \mathbf{w} and \mathbf{p} by averaging samples from the posterior distribution

$$P_\beta(\mathbf{w}, \mathbf{p}|\mathcal{D}) = \mathcal{Z}_\beta(\mathcal{D})^{-1} P_0(\mathbf{w}, \mathbf{p}) \prod_{c=1}^M P_\beta(\mathbf{x}^c, y^c|\mathbf{w}, \mathbf{p}), \quad (5)$$

where $\mathcal{Z}_\beta(\mathcal{D}) = \mathbb{E}_{\mathbf{w}, \mathbf{p}} \left[\prod_{c=1}^M P_\beta(\mathbf{x}^c, y^c|\mathbf{w}, \mathbf{p}) \right]$ is the posterior partition function and $P_0(\mathbf{w}, \mathbf{p})$ is the prior on \mathbf{w} and \mathbf{p} , which for simplicity we choose as uniform over the sets in which \mathbf{w} and \mathbf{p} are constrained.

We use a statistical mechanics approach to derive a single set of *saddle-point* equations that simultaneously characterize the weights that are stationary points of maximum likelihood estimation (Eq. 4) for generic data and the typical weight configurations obtained by averaging samples from Eq. (5) in the teacher-student setting. We assume that the student does not know the number of hidden units P^* and the inverse temperature β^* of the teacher, so it cannot match them with its own. In particular, we consider the case where the noise injected by the teacher in the data is relatively small, i.e. $\beta^*/N > 0$ as $N \rightarrow \infty$, while the student chooses a conservative inverse temperature $\beta \ll N$ to avoid overfitting. Moreover, we fix $\sum_{y=0}^C p_y^{*0} = p_{\mathbf{h}}^*(0) = 0$ and $\sum_{y=0}^C p_y^{*\mu} = p_{\mathbf{h}}^*(\mu) = 1/P^*$ for all $\mu > 0$ so that each $\mathbf{g}^{*\mu} := P_\beta(y|\mu; \mathbf{w}, \mathbf{p}) = \mathbf{p}^{*\mu}/p_{\mathbf{h}}^*(\mu) = P^* \mathbf{p}^{*\mu}$ is a soft label for the corresponding $\mathbf{w}^{*\mu}$. On the contrary, we do not give $\sum_{\gamma=0}^{P^*} p_y^{*\gamma} = p_{\mathbf{q}}^*(y)$ a restrictive form. In other words, $p_{\mathbf{q}}^*(y)$ is free to be any given probability mass function.

3 Theoretical results

3.1 Saddle-point equations

In this Section, we introduce a set of equations for the stationary points of the loss (Eq. 4), which we then relate to the saddle-point equations emerging from the statistical mechanics analysis of posterior sampling (see Eq. 5) in the teacher-student setting.

Let us first establish a few definitions that we will use frequently throughout the Section. Given two matrices $\mathbf{w}^* \in \mathbb{R}^{P^* \times N}$ and $\mathbf{w} \in \mathbb{R}^{P \times N}$, we define the overlap matrix $\mathbf{m}(\mathbf{w}^*, \mathbf{w}) = \mathbf{w}^* \mathbf{w}^T \in \mathbb{R}^{P^* \times P}$. We write its entries as $m^{\mu_* \mu}(\mathbf{w}^*, \mathbf{w}) = \sum_{i=1}^N w_i^{*\mu_*} w_i^\mu$ and its row vectors as $m^{\mu_*}(\mathbf{w}^*, \mathbf{w})$, where $1 \leq \mu_* \leq P^*$ and $1 \leq \mu \leq P$. Moreover, for any matrix $\mathbf{m} \in \mathbb{R}^{P^* \times (P+1)}$ with entries $m^{\mu_* \gamma}$ and row vectors m^{μ_*} , we use

$$\sigma_\gamma(m^{\mu_*}) = \frac{\exp(m^{\mu_* \gamma})}{\sum_{\nu=0}^P \exp(m^{\mu_* \nu})}$$

to represent the entry number $\gamma \in \{0, 1, \dots, P\}$ of the softmax function applied to the row vector m^{μ_*} . In this context, m^{μ_*} has a zeroth component $m^{\mu_* 0}$, and so does its softmax.

In Appendix B, we show that the stationary points of the negative log-likelihood loss (Eq. 4) satisfy

$$\begin{aligned} w_i^\mu &= \frac{\bar{w}_i^\mu}{\sqrt{\sum_{j=1}^N [\bar{w}_j^\mu]^2}} \\ p_y^\gamma &= \frac{\bar{p}_y^\gamma}{\zeta_y^\gamma(\bar{\mathbf{p}}; p_{\mathbf{h}})} \\ \text{with } \bar{w}_i^\mu &= \sum_{\mu_*=1}^{P^*} x_i^{*\mu_*} \sum_{y=0}^C q_y^{*\mu_*} \sigma_\mu(\beta m^{\mu_*}(\mathbf{x}^*, \mathbf{w}) + \log[\mathbf{p}_y]) \\ \bar{p}_y^\gamma &= \sum_{\mu_*=1}^{P^*} q_y^{*\mu_*} \sigma_\gamma(\beta m^{\mu_*}(\mathbf{x}^*, \mathbf{w}) + \log[\mathbf{p}_y]) \end{aligned} \quad (6)$$

for all $1 \leq \mu \leq P$ and $0 \leq \gamma \leq P$, where $m^{\mu_* 0}(\mathbf{x}^*, \mathbf{w}) = \frac{1}{\beta} \log[\Omega_N(\beta) / \Omega_N(0)]$ and the normalization constant $\zeta_y^\gamma(\bar{\mathbf{p}}; p_{\mathbf{h}})$ is defined in Appendix F.

Similar equations arise naturally in our statistical mechanics analysis, which amounts to using the replica method [87, 88] to compute the limiting free entropy

$$f(\varrho, v, \beta, P^*, P) = \lim_{\beta^*, M, N \rightarrow \infty} \frac{1}{N} \mathbb{E}_{\mathbf{w}^*, \mathbf{p}^*, \mathcal{D}} \log[\mathcal{Z}_\beta(\mathcal{D})], \quad (7)$$

where $v = \beta^*/N$, $\varrho = \frac{M}{P^* N}$ and $\mathbb{E}_{\mathbf{w}^*, \mathbf{p}^*, \mathcal{D}}$ is the joint expectation over the distribution of examples $\mathcal{D} = \{\mathbf{x}^c, y^c\}_{c=1}^M$ generated by the teacher and the priors on the teacher weights. To be more precise, we show that the free entropy can be computed with a variational principle of the form

$$f(\varrho, v, \beta, P^*, P) = \text{Extr}_{\mathbf{m}, \hat{\mathbf{m}}, \mathbf{p}} f(\mathbf{m}, \hat{\mathbf{m}}, \mathbf{p}), \quad (8)$$

whose extremizer $\mathbf{m} = \{m^{\mu_* \mu}\}_{1 \leq \mu \leq P}^{1 \leq \mu_* \leq P^*}$ can be interpreted as the $N \rightarrow \infty$ limit of the expected value of

the teacher-student overlaps $\mathbf{m}(\mathbf{w}^*, \mathbf{w})$. We show the derivation of the variational principle in Appendix D together with an explicit expression for the trial function $f(\mathbf{m}, \hat{\mathbf{m}}, \mathbf{p})$. If we assume that there are $P^* \ll N$ teacher memories and that the priors on $\mathbf{w}^{*\mu*}$ and \mathbf{g}^* are uniform like those of the student, we find that the expected teacher-student overlaps must satisfy the saddle-point equations

$$\begin{aligned} m^{\mu*\mu} &= \varsigma \left(2\beta_{\text{eff}}\varrho \sqrt{\sum_{\nu*=1}^{P^*} [\hat{m}^{\nu*\mu}]^2} \right) \frac{\hat{m}^{\mu*\mu}}{\sqrt{\sum_{\nu*=1}^{P^*} [\hat{m}^{\nu*\mu}]^2}} \\ p_y^\gamma &= \frac{\bar{p}_y^\gamma}{\zeta_y^\gamma(\bar{\mathbf{p}}; p_{\mathbf{h}})} \\ \text{with } \hat{m}^{\mu*\mu} &= \sum_{y=0}^C p_{\mathbf{q}}^*(y) \sigma_\mu (\beta_{\text{eff}} m^{\mu*} + \log [\mathbf{p}_y]) \\ \bar{p}_y^\gamma &= p_{\mathbf{q}}^*(y) \sum_{\mu*=1}^{P^*} \sigma_\gamma (\beta_{\text{eff}} m^{\mu*} + \log [\mathbf{p}_y]) \end{aligned} \quad (9)$$

for all $1 \leq \mu \leq P$ and $0 \leq \gamma \leq P$, where $\varsigma(x) = \frac{x}{\sqrt{x^2+1+1}}$, $\beta_{\text{eff}} = \varsigma(2v)\beta$ and $m^{\mu*0} = \frac{1}{\beta_{\text{eff}}} \log [\Omega_N(\beta) / \Omega_N(0)]$.

If we instead clamp the teacher weights $\mathbf{w}^{*\mu*}$ and $\mathbf{g}^{*\mu*}$ to fixed patterns $\mathbf{x}^{*\mu*}$ and their corresponding soft labels $\mathbf{q}^{*\mu*}$ [64], respectively, to mimic a more general distribution for the data, then Eqs. (9) become (see Appendix E)

$$\begin{aligned} m^{\mu*\mu} &= \varsigma \left(2\beta_{\text{eff}}\varrho \sqrt{\sum_{i=1}^N [\bar{x}_i^\mu]^2} \right) \frac{\sum_{i=1}^N x_i^{*\mu*} \bar{x}_i^\mu}{\sqrt{\sum_{i=1}^N [\bar{x}_i^\mu]^2}} \\ p_y^\gamma &= \frac{\bar{p}_y^\gamma}{\zeta_y^\gamma(\bar{\mathbf{p}}; p_{\mathbf{h}})} \\ \text{with } \bar{x}_i^\mu &= \sum_{\mu*=1}^{P^*} x_i^{*\mu*} \sum_{y=0}^C q_y^{*\mu*} \sigma_\mu (\beta_{\text{eff}} m^{\mu*} + \log [\mathbf{p}_y]) \\ \bar{p}_y^\gamma &= \sum_{\mu*=1}^{P^*} q_y^{*\mu*} \sigma_\gamma (\beta_{\text{eff}} m^{\mu*} + \log [\mathbf{p}_y]). \end{aligned} \quad (10)$$

for all $1 \leq \mu \leq P$ and $0 \leq \gamma \leq P$, where we recall that $m^{\mu*0} = \frac{1}{\beta_{\text{eff}}} \log [\Omega_N(\beta) / \Omega_N(0)]$.

In the limit of $\varrho, v \rightarrow \infty$, which indicates a large number of examples and a low level of teacher noise, Eqs. (10) become equivalent to Eqs. (6) if we make the identification $\bar{x}_i^\mu = \bar{w}_i^\mu$, i.e.

$$w_i^\mu = \frac{\bar{x}_i^\mu}{\sqrt{\sum_{j=1}^N [\bar{x}_j^\mu]^2}}. \quad (11)$$

Let us explain this limit step by step. For any v and ϱ , the M examples $\{\mathbf{x}^c\}_{c=1}^M$ provided to the student are corrupted versions of the teacher patterns \mathbf{x}^* with a noise level of $1/v$. Therefore, in the limit of $v \rightarrow \infty$ with finite ϱ , each example \mathbf{x}^c provided to the student is one of the original patterns \mathbf{x}^* , as in Eqs. (6). However, even in this case, the empirical distribution of the examples deviates from that of \mathbf{x}^* , of which it is merely

a bootstrap sample. At fixed P^* and P , this mismatch disturbs the accurate learning of \mathbf{x}^* when $\varrho = \frac{M}{P^*N}$ is finite, or equivalently the expected number of repetitions M/P^* of each pattern is not sufficiently large compared to N (see Eq. 10). This influence progressively weakens as ϱ grows and the ς function approaches 1, reflecting the convergence of the empirical distribution of the examples to that of the teacher patterns.

In the limit of $\varrho \rightarrow \infty$ with finite v , Eq. (10) is still very similar to Eq. (6). The only difference between them is that Eq. (10) has β_{eff} instead of β in the argument of σ and in the denominator of the definition of $m^{\mu*0}$. Using ς as a shorthand for $\varsigma(2v)$, we find that the fixed points of Eqs. (10) with $\varrho \rightarrow \infty$ are related, through the identification made by Eq. (11), to the stationary points of the effective loss

$$\mathcal{L}(\mathbf{w}, \mathbf{p}) = -\frac{1}{P^*} \sum_{\mu=1}^{P^*} \sum_{y=0}^C q_y^{*\mu} \log \mathcal{P}_{\beta, \varsigma}(\mathbf{x}^{*\mu}, y | \mathbf{w}, \mathbf{p}), \quad (12)$$

where $\mathcal{P}_{\beta, \varsigma}(\mathbf{x}, y | \mathbf{w}, \mathbf{p}) = \sum_{\mu=1}^P p_y^\mu \frac{\exp\left(\varsigma \beta \sum_{i=1}^N w_i^\mu x_i\right)}{\Omega_N(\beta)} + p_y^0 \frac{1}{\Omega_N(0)}$.

What distinguishes this equation from the standard loss (Eq. 4) is that $\mathcal{P}_{\beta, \varsigma}(\mathbf{x}, y | \mathbf{w}, \mathbf{p})$ has $\beta_{\text{eff}} = \varsigma \beta$ in the argument of the exponential function instead of β . As a consequence, $\mathcal{P}_{\beta, \varsigma}(\mathbf{x}, y | \mathbf{w}, \mathbf{p})$ is not a probability distribution unless $\varsigma = 1$, in the limit of $v \rightarrow \infty$ (see Appendix C). A value of ς less than one in the effective loss (Eq. 12) is reminiscent of the presence of noise in the data generation process, so we propose to use it as a regularizer for the weights. We discuss this point in more detail in Section 4.1.

3.2 Saddle-point hierarchy

As shown in [8], the loss landscape of any NN with unconstrained weights contains the stationary points of narrower NNs with the same architecture. In Appendix G, we show that this result also applies to the teacher-student setting with $\varrho \rightarrow \infty$ and any non-zero v . To be more precise, we show that, if the parameters $\bar{x}_i^{\text{fixed}, \mu}, \bar{p}_y^{\text{fixed}, \gamma}, m^{\text{fixed}, \mu_* \gamma}, p_y^{\text{fixed}, \gamma}$ with hidden unit prior $p_h^{\text{given}}(\gamma)$ are a fixed point of Eqs. (10) with P hidden units, then the duplicated parameters

$$\begin{aligned} \bar{x}_i^{\text{duali}, \mu} &= \begin{cases} \bar{x}_i^{\text{fixed}, \mu} & 0 < \mu \leq P \\ \bar{x}_i^{\text{fixed}, \mu-P} & P < \mu \leq P+R \end{cases} \\ \bar{p}_y^{\text{duali}, \gamma} &= \begin{cases} \bar{p}_y^{\text{fixed}, 0} & \gamma = 0 \\ \frac{1}{2} \bar{p}_y^{\text{fixed}, \gamma} & 0 < \gamma \leq R \\ \bar{p}_y^{\text{fixed}, \gamma} & R < \gamma \leq P \\ \frac{1}{2} \bar{p}_y^{\text{fixed}, \gamma-P} & P < \gamma \leq P+R \end{cases} \\ m^{\text{duali}, \mu_* \gamma} &= \begin{cases} m^{\text{fixed}, \mu_* 0} & \gamma = 0 \\ m^{\text{fixed}, \mu_* \gamma} & 0 < \gamma \leq P \\ m^{\text{fixed}, \mu_*, \gamma-P} & P < \gamma \leq P+R \end{cases} \end{aligned} \quad (13)$$

$$p_y^{\text{dupli},\gamma} = \begin{cases} p_y^{\text{fixed},0} & \gamma = 0 \\ \frac{1}{2}p_y^{\text{fixed},\gamma} & 0 < \gamma \leq R \\ p_y^{\text{fixed},\gamma} & R < \gamma \leq P \\ \frac{1}{2}p_y^{\text{fixed},\gamma-P} & P < \gamma \leq P + R \end{cases}$$

$$\text{along with } p_{\mathbf{h}}(\gamma) = \begin{cases} p_{\mathbf{h}}^{\text{given}}(0) & \gamma = 0 \\ \frac{1}{2}p_{\mathbf{h}}^{\text{given}}(\gamma) & 0 < \gamma \leq R \\ p_{\mathbf{h}}^{\text{given}}(\gamma) & R < \gamma \leq P \\ \frac{1}{2}p_{\mathbf{h}}^{\text{given}}(\gamma-P) & P < \gamma \leq P + R, \end{cases}$$

are a fixed point of the same saddle-point equations with $P + R \in \{P, \dots, 2P\}$ hidden units (See Appendix G for a detailed derivation). In other words, we duplicate some of the weights solving Eqs. (10) to construct a fixed point for a wider network. In that sense, wide DAMs contain the fixed points of narrower DAMs. In particular (see Section 3.1), this property also holds for the stationary points of both the standard loss (Eq. 4) and the effective loss (Eq. 12).

The saddle-point equations (Eq. 10) with duplicated order parameters (Eqs. 13) are invariant to the permutation of any hidden unit $\gamma \in \{1, \dots, R\}$ and its duplicate $\gamma + P$. This kind of symmetry can be spontaneously broken if it leads to a higher free entropy (see Eqs. 7 and 22). However, symmetry-breaking transitions can be prohibitively slow when the symmetric state is stable to local perturbations [89]. Interestingly, the DAM introduced in [10] quickly undergoes many successive permutation symmetry-breaking bifurcations during training [11]. This observation and additional empirical evidence suggest that the symmetric states are unstable, or in other words that they are saddles, which was verified analytically for DAMs with only two data points to memorize [11]. In Appendix G, we prove that, if β is large enough, Eqs. (13) is a saddle, which is a major step toward explaining why permutation symmetry-breaking transitions are relatively fast in DAMs trained with a large number of data points. We call this result *the saddle-point hierarchy principle*.

4 Empirical results

In this Section, we use our theoretical results to improve training, and we show empirically that our DAM learns interpretable solutions to both supervised and unsupervised classification problems. We perform all our numerical experiments on the MNIST dataset of handwritten digits [65]. The code and hyperparameter values used in our numerical experiments are available at this public repository [38].

4.1 Learning by minimizing the effective loss

As the number of hidden units P increases, standard maximum likelihood estimation with fixed inverse temperature β becomes progressively less apt to train our DAM to its full potential. At high P and β , many memories stay stuck in noisy states that do not contribute to classification, which is wasteful. Using a lower β helps the memories converge, but also reduces their resolution and diversity, possibly because it also lowers the

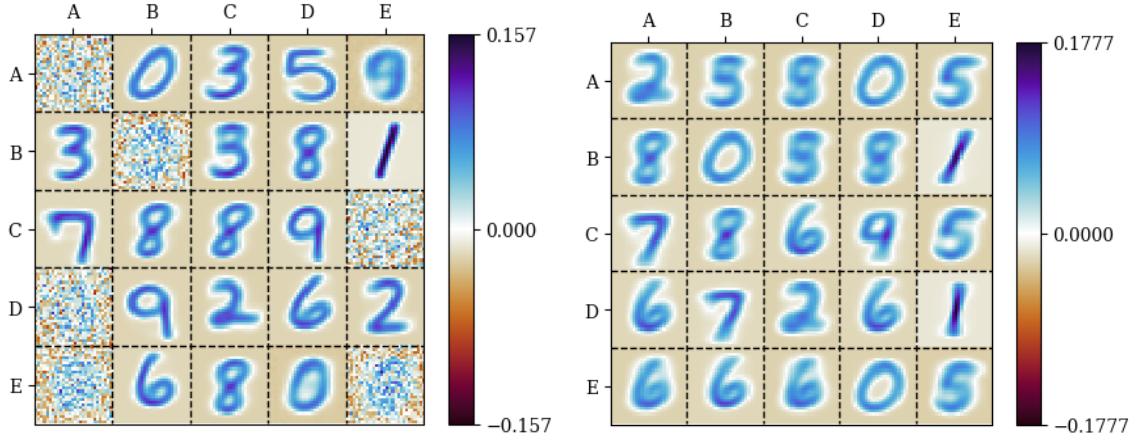


Figure 2: 25 of the $P = 1000$ memories \mathbf{w}^μ learned by two instances of our dense associative memory (DAM) model with different values of β . Both networks are trained on the MNIST dataset of handwritten digits [65] using constrained stochastic gradient descent (SGD) of the negative log-likelihood loss (Eq. 4). The left-panel model has $\beta = 18$, and the right-panel one $\beta = 6$. DAMs with $18 > \beta > 6$ learn memories that interpolate between these two pictures. The hidden units are indexed using pairs of letters from A to E.

DAM’s capacity [29]. This change is far from being only cosmetic. In fact, it comes with a gradual reduction in classification accuracy (see Table 1).

Optimization algorithms with a parameter analogous to β often converge to better solutions when this parameter is increased from a small value during optimization. For example, annealing schedules [90, 91] can be incorporated into minimization algorithms to help them find deeper local minima than they could otherwise. This observation suggests that our DAM would learn better memories if we increased β during training. It is tempting to do so by SGD of Eq. (4) with respect to β , but it makes β increase so quickly that many memories still stay stuck in noisy states.

We find that optimizing the effective loss (Eq. 12) with a suitable ς slows down the evolution of β enough to let the DAM learn much cleaner memories (see Fig. 3, top panel) and achieve much better classification accuracy (see Table 1) than with standard training (Eq. 4). Looking back at Section 3.1, we propose to interpret ς as a regularization parameter that helps the DAM take noise from the data into account during training. There is no obvious theoretically motivated way to find the best value of ς for a generic dataset, so we choose it by hand. Despite this limitation, we believe that the simplicity and interpretability of our method still make it an interesting alternative to annealing schedules.

When we use this training method, we compute the DAM classification accuracy from the effective predictions

$$\mathcal{P}_{\beta, \varsigma} (y|\mathbf{x}; \mathbf{w}, \mathbf{p}) = \frac{\mathcal{P}_{\beta, \varsigma} (\mathbf{x}, y|\mathbf{w}, \mathbf{p})}{\mathcal{P}_{\beta, \varsigma} (\mathbf{x}|\mathbf{w}, \mathbf{p})} \quad (14)$$

where $\mathcal{P}_{\beta, \varsigma} (\mathbf{x}|\mathbf{w}, \mathbf{p}) = \sum_{y=0}^C \mathcal{P}_{\beta, \varsigma} (\mathbf{x}, y|\mathbf{w}, \mathbf{p})$,

instead of the true predictions $P_\beta (y|\mathbf{x}; \mathbf{w}, \mathbf{p}) = P_\beta (\mathbf{x}, y|\mathbf{w}, \mathbf{p}) / P_\beta (\mathbf{x}|\mathbf{w}, \mathbf{p})$. This approach allows us to

Inverse temperature β	Classification accuracy
6	79%
10	85%
14	89%
18	91%
Trained with $\varsigma = 0.25$	96%

Table 1: DAM classification accuracy (rounded down to two significant figures) for $P = 1000$ and various values of β . The last line is for β trained by SGD of the effective loss (Eq. 12) with $\varsigma = 0.25$.

calculate both the accuracy and the loss through a single evaluation of $\mathcal{P}_{\beta, \varsigma}(y|\mathbf{x}; \mathbf{w}, \mathbf{p})$, which is more efficient than computing $\mathcal{P}_{\beta, \varsigma}(\mathbf{x}, y|\mathbf{w}, \mathbf{p})$ and $\mathbf{P}_\beta(\mathbf{x}, y|\mathbf{w}, \mathbf{p})$ separately when monitoring the progress of training.

4.2 Dense associative memory is interpretable, even in unsupervised classification

Now that we understand how to train our DAM reasonably well, we investigate one of the most interesting properties of the solutions that it learns: their interpretability. As advertised in the Introduction, we will explain how to further improve training in the following Section. We already mentioned that the regularization parameter ς of the effective loss is interpretable (see Section 4.1 and Eq. 12). Here, we point out that the learned weights are as well. In fact, each learned \mathbf{p}^μ / p_h (μ) can be interpreted as a soft label for the corresponding \mathbf{w}^μ (see Fig. 3). This property was also observed by [11] in K & H’s DAM for pattern classification [10].

At test time, we observe that our DAM classifies approximately 98% of the test data points into the class $y = \operatorname{argmax}_{y'} \{p_{y'}^\mu\}$ of the memory \mathbf{w}^μ to which they are the most similar. In other words, a 1-nearest neighbor classifier [92] conditioned on the memories \mathbf{w}^μ and their soft labels \mathbf{p}^μ / p_h (μ) approximates the classification of our model with 98% fidelity. This behavior is reminiscent of K & H’s DAM [10], where only a few memories participate in the classification of each data point. The 1-nearest neighbor classifier approximates DAM classification more faithfully for correctly classified data points (approximately 99% fidelity) than incorrectly classified data points (approximately 70% fidelity).

We now show that the notion of interpretability described in this Section extends beyond supervised learning. Given a dataset of P^* unlabeled patterns $\{\mathbf{x}^{*\mu}\}_{\mu=1}^{P^*}$, we find that we can train our DAM for unsupervised classification by replacing the soft labels $q_y^{*\mu}$ in the effective loss (Eq. 12) with the softened DAM predictions $(1 - \varepsilon) \mathcal{P}_{\beta, \varsigma}(y|\mathbf{x}^{*\mu}; \mathbf{w}, \mathbf{p}) + \varepsilon \frac{1}{C+1}$, where $\varepsilon \in [0, 1]$ and $\mathcal{P}_{\beta, \varsigma}(y|\mathbf{x}^{*\mu}; \mathbf{w}, \mathbf{p})$ is defined in Eq. (14). In this scenario, we are minimizing

$$\mathcal{L}_{\text{unsup}}(\mathbf{w}, \mathbf{p}) = -\frac{1}{P^*} \sum_{\mu=1}^{P^*} \sum_{y=0}^C \left[(1 - \varepsilon) \mathcal{P}_{\beta, \varsigma}(y|\mathbf{x}^{*\mu}; \mathbf{w}, \mathbf{p}) + \varepsilon \frac{1}{C+1} \right] \log \mathcal{P}_{\beta, \varsigma}(\mathbf{x}^{*\mu}, y|\mathbf{w}, \mathbf{p}). \quad (15)$$

As before, we do so using constrained SGD (see Appendix F) with the initialization and learning rate described

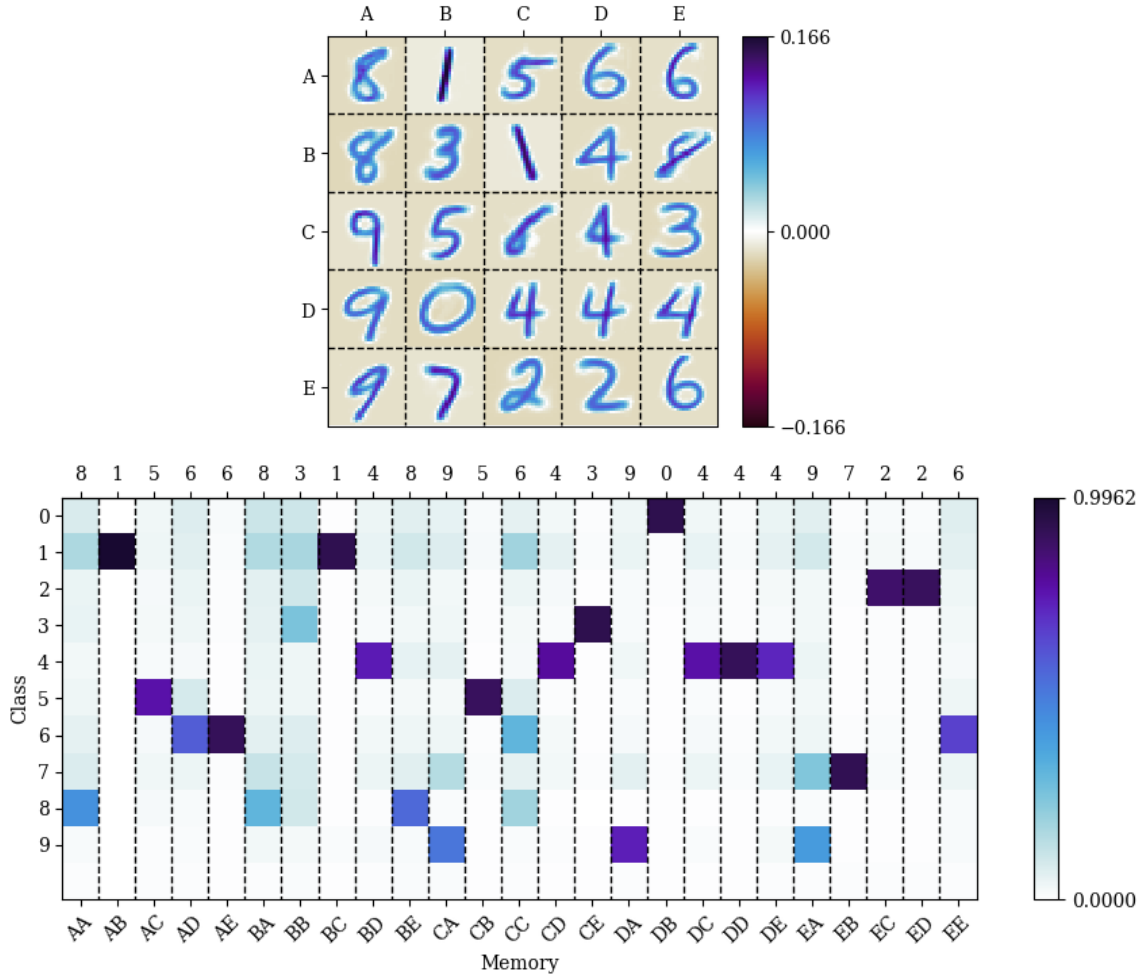


Figure 3: In the top panel, 25 of the $P = 1000$ memories \mathbf{w}^μ learned by an instance of our dense associative memory (DAM) model trained on the MNIST dataset of handwritten digits [65] using constrained stochastic gradient descent (SGD) of the effective loss (Eq. 4) with $\varsigma = 0.25$. In the bottom panel, the corresponding rescaled class weights $\mathbf{p}^\mu / p_h(\mu)$, where $p_h(\gamma) = \frac{1}{P+1}$ for all $0 \leq \gamma \leq P$. The hidden units are indexed using pairs of letters from A to E, and the column-wise maxima of the class weights are the classes of the memories with the corresponding letter indices. Rescaled class weights learned with $p_h(\gamma) \neq \frac{1}{P+1}$ are qualitatively similar to the ones shown in this figure. Approximately 98% of test digits fed to the DAM are given the class of the memory that resembles them the most. For example, a digit that looks like the memory #AA is given the class 8.

in Appendix I. Equivalently, we can also view this algorithm as minimizing the combined loss

$$\mathcal{L}_{\text{total}}(\mathbf{w}, \mathbf{p}) = \mathcal{L}_{\text{margin}}(\mathbf{w}, \mathbf{p}) + \lambda \mathcal{L}_{\text{cond}}(\mathbf{w}, \mathbf{p}), \quad (16)$$

$$\text{where } \mathcal{L}_{\text{margin}}(\mathbf{w}, \mathbf{p}) = -\frac{1}{P^*} \sum_{\mu=1}^{P^*} \log \mathcal{P}_{\beta, \varsigma}(\mathbf{x}^{*\mu} | \mathbf{w}, \mathbf{p})$$

$$\text{and } \mathcal{L}_{\text{cond}}(\mathbf{w}, \mathbf{p}) = -\frac{1}{P^*} \sum_{\mu=1}^{P^*} \sum_{y=0}^C \mathcal{P}_{\beta, \varsigma}(y | \mathbf{x}^{*\mu}; \mathbf{w}, \mathbf{p}) \log \mathcal{P}_{\beta, \varsigma}(y | \mathbf{x}^{*\mu}; \mathbf{w}, \mathbf{p}),$$

where $\mathcal{P}_{\beta, \varsigma}(\mathbf{x}^{*\mu} | \mathbf{w}, \mathbf{p}) = \sum_{y=0}^C \mathcal{P}_{\beta, \varsigma}(\mathbf{x}^{*\mu}, y | \mathbf{w}, \mathbf{p})$ (see Eq. 14). $\mathcal{L}_{\text{cond}}(\mathbf{w}, \mathbf{p})$ is called the minimum entropy regularization term in unsupervised machine learning [93]. Intuitively, it encourages the DAM to learn different class weights p_y^γ for each class y , which is not possible by minimizing only $\mathcal{L}_{\text{margin}}(\mathbf{w}, \mathbf{p})$ because $\mathcal{P}_{\beta, \varsigma}(\mathbf{x}^{*\mu} | \mathbf{w}, \mathbf{p})$ does not depend on y . Exploiting this characteristic, we train our DAM on patches of MNIST digits [65] and find that it learns reasonable latent classes $y = \text{argmax}_{y'} \{p_{y'}^\mu\}$ for the memories \mathbf{w}^μ (see Fig. 4 and Figs. 7, 8, 9 and 10 of Appendix J). This approach could potentially be useful for feature extraction [94].

4.3 Fast training with splitting steepest descent

We now explain how to further improve the training method of Section 4.1. More specifically, we use the saddle-point hierarchy derived in 3.2 to accelerate training.

Machine learning models that experience the permutation symmetry-breaking bifurcations described in Section 3.2 during training—such as the DAM studied in [11], RBMs with binary units [81, 84] and Gaussian mixtures [62, 50, 51, 52, 91, 95, 96]—have characteristic tree-shaped learning dynamics. Intuitively, permutation symmetry-breaking transitions are points where model parameters differentiate from each other, so they correspond to the bifurcations of the tree. In the left panel of Fig. (5), we show that the learning dynamics of our DAM also follows a tree of permutation symmetry-breaking transitions.

The saddle-point hierarchy principle introduced in Section 3.2 suggests the following idea to accelerate learning: train a relatively narrow DAM for cheap, then repeatedly duplicate (or “split”) some of the hidden units μ , escape the corresponding saddle point and continue training. Intuitively, we expect to save a lot of computing resources by using relatively few hidden units at the start of training, when the learning dynamics follows a few branches close to the root of the learning dynamics tree. The splitting steepest descent algorithm introduced in [36] formalizes this idea in an efficient and theoretically motivated way. We implement a variant of this algorithm that takes the constraint $\mathbf{w}^\mu \in S^{N-1}$ into account, but is otherwise very similar to the original version (see Alg. 1), with fast splitting implemented as in [37]. The constraint $\mathbf{w}^\mu \in S^{N-1}$ only matters in steps 5 and 11, which are also arguably the most conceptually difficult parts of Alg. (1), so we explain them in detail in Appendix H. Fig. (5) shows that the learning dynamics tree of splitting steepest descent has a more sparsely populated trunk than that of SGD without splitting (see Fig. 5). In other words, by using a relatively small number P of memories at the beginning of training, we reduce the total number of values $P \times T$ that they take over a period of time T , which is consistent with our intuition that it can save computational resources. The situation could have been different if using fewer memories slowed down training.

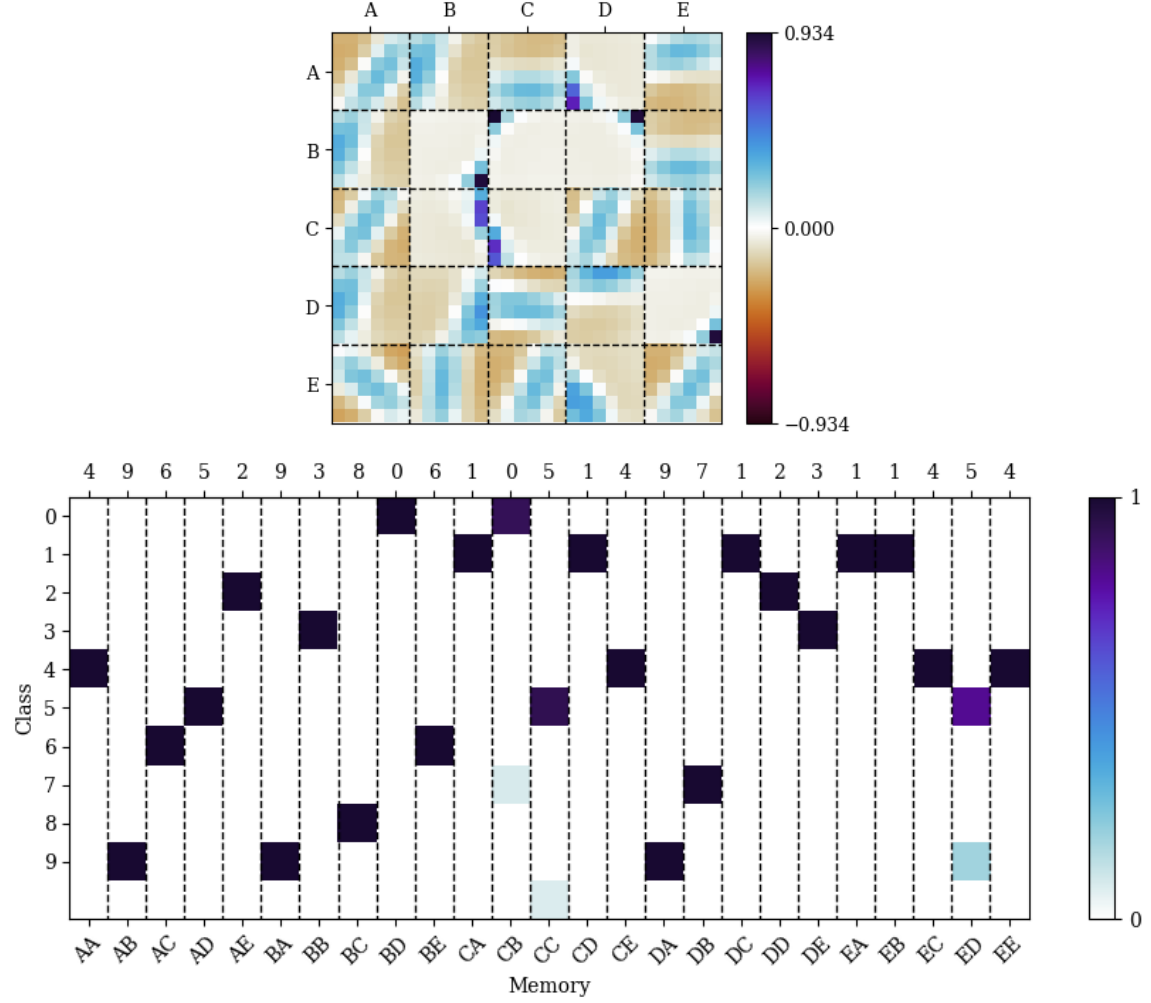


Figure 4: In the top panel, 25 of the $P = 100$ memories w^μ learned by an instance of our dense associative memory (DAM) model trained in an unsupervised way (Eq. 15) on 6×6 patches of the MNIST dataset of handwritten digits [65] while assuming $C = 10$ latent classes and $\varsigma = 0.6$. In the bottom panel, the corresponding rescaled class weights $p^\mu / p_h(\mu)$, where $p_h(\gamma) = \frac{1}{P+1}$ for all $0 \leq \gamma \leq P$. The hidden units are indexed using pairs of letters from A to E, and the column-wise maxima of the class weights are the classes of the memories with the corresponding letter indices.

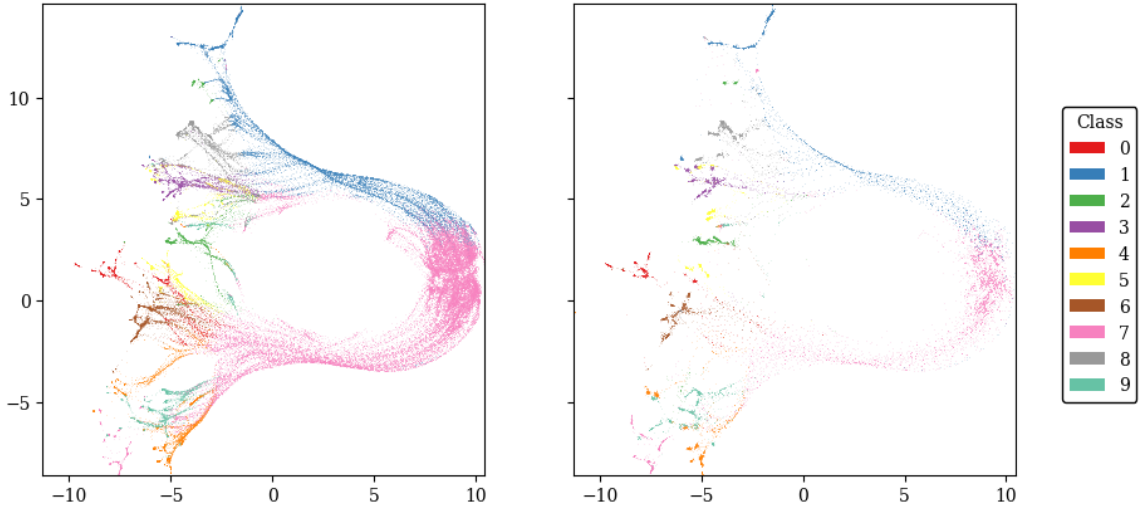


Figure 5: Overlaps $m^{\mu*\mu}(\mathbf{x}^*, \mathbf{w}) = \sum_{i=1}^N x_i^{*\mu*} w_i^\mu$ between the first 1000 digits $\mathbf{x}^{*\mu*} = \{x_i^{*\mu*}\}_{i=1}^N$ of the MNIST training set [65] and the memories $\mathbf{w}^\mu = \{w_i^\mu\}_{i=1}^N$ of our dense associative memory (DAM) model while it is learning them. Each point is one of the high-dimensional magnetization vectors $m_\mu(\mathbf{x}^*, \mathbf{w}) = \{m^{\mu*\mu}(\mathbf{x}^*, \mathbf{w})\}_{\mu*=1}^{P^*}$ projected onto a two-dimensional plane using the UMAP algorithm [97]. On the left, the $m_\mu(\mathbf{x}^*, \mathbf{w})$ found during training without splitting steepest descent. On the right, the $m_\mu(\mathbf{x}^*, \mathbf{w})$ found with splitting steepest descent (Alg. 1). In both cases, UMAP is trained on the $m_\mu(\mathbf{x}^*, \mathbf{w})$ found without splitting steepest descent. The classes $y = \text{argmax}_{y'} \{p_{y'}^\mu\}$ of the memories \mathbf{w}^μ are color-coded in the legend. 7 and 1 are the most numerous classes, so they have the top two largest entries in $\sum_{\gamma=0}^P p_y^\mu = p_{\mathbf{q}}(y)$ (see Appendix I), which is why the memories are classified as either 7 or 1 at the beginning of training.

Algorithm 1 Splitting steepest descent [36, 37]

- 1: Preallocate space for a DAM with P_{\max} hidden units and the corresponding weights \mathbf{w} and \mathbf{p}
- 2: Initialize the weights \mathbf{w}^μ and \mathbf{p}^μ connected to the P_{cur} first hidden units $\mu \in \{1, \dots, P_{\text{cur}}\}$, as well as \mathbf{p}^0
- 3: $\min L(\mathbf{w}, \mathbf{p})$ with SGD
- 4: **while** $P_{\text{cur}} < P_{\max}$ **do**
- 5: Identify a subset $\mu_{\text{copy}} \subseteq \{1, \dots, P_{\text{cur}}\}$ of $R \leq P_{\max} - P_{\text{cur}}$ hidden units to split, **return** if empty
- 6: Let $\mu_{\text{paste}} = \{P_{\text{cur}} + 1, \dots, P_{\text{cur}} + R\}$
- 7: Build weights $\mathbf{w}^{\mu_{\text{paste}}} = \mathbf{w}^{\mu_{\text{copy}}}$ for μ_{paste}
- 8: Rescale $\mathbf{p}^{\mu_{\text{copy}}} \leftarrow \mathbf{p}^{\mu_{\text{copy}}} / 2$ and $p_h(\mu_{\text{split}}) \leftarrow p_h(\mu_{\text{split}}) / 2$
- 9: Build weights $\mathbf{p}^{\mu_{\text{paste}}} = \mathbf{p}^{\mu_{\text{copy}}}$ and $p_h(\mu_{\text{paste}}) = p_h(\mu_{\text{copy}})$ for μ_{paste}
- 10: Update $P_{\text{cur}} \leftarrow P_{\text{cur}} + R$
- 11: Escape the saddle point by 2nd order descent of $L(\mathbf{w}, \mathbf{p})$ w.r.t. \mathbf{w}
- 12: $\min L(\mathbf{w}, \mathbf{p})$ with SGD
- 13: **end while**
- 14: **return**

▷ See Appendix H and [36, 37] for details about steps 5 and 11

We now establish a methodology that we will use to compare the training times of DAMs trained using the effective loss (Eq. 12) on MNIST [65] with and without splitting steepest descent. It is more interesting and meaningful to compare the training times of NNs with similar performance. Therefore, we pick hyperparameters such that DAMs trained with and without splitting have similar classification accuracy. For that purpose, we find the general region of hyperparameter space where DAMs trained without splitting steepest descent have the best classification accuracy. The accuracy does not change much in this region, so we pick generic hyperparameters inside. Next, we manually tune the hyperparameters of splitting steepest descent so that the resulting DAMs have comparable accuracy. Note that we did not find hyperparameters that make the accuracy with splitting steepest descent significantly better than without it.

Once the hyperparameters are set, we collect statistics of the accuracy and training time. We run our experiment on a CPU and manually set the seed of pseudorandom number generation to make training deterministic and reproducible. Two DAMs with the same hyperparameters and the same seed are guaranteed to be trained using the same number of computer operations and to have the same classification accuracy after training. However, background processes and other external factors can change between two runs with the same seed, which adds noise to the bare training time that we want to measure. As such, we approximate the bare training time as the minimum over many runs with the same seed. We then calculate the average and standard deviation of the classification accuracy and bare training time over multiple seeds.

In Fig. (6), we compare DAM training time and accuracy with and without splitting steepest descent, using round markers and error bars to show their respective means and standard deviations as a function of the maximum number of hidden units P_{\max} . Splitting stops at P_{\max} hidden units, and DAMs without splitting have P_{\max} hidden units from the start. All hidden units are split in each while-loop iteration of Alg. (1), except for the last iteration, where exactly $P_{\max} - P_{\text{cur}}$ hidden units are split. As wanted, DAMs have similar accuracy with and without splitting (left panel). Moreover, the relatively small error bars of the training time indicate that the residual noise of the background processes is small and that the seed has a limited impact on the training speed (right panel). Splitting steepest descent has a significant speed advantage that scales very advantageously with P_{\max} (right panel). Without splitting, the training time is proportional to P_{\max} . With splitting, the training time is almost constant. The clearest sign that it increases with P_{\max} is the small jump

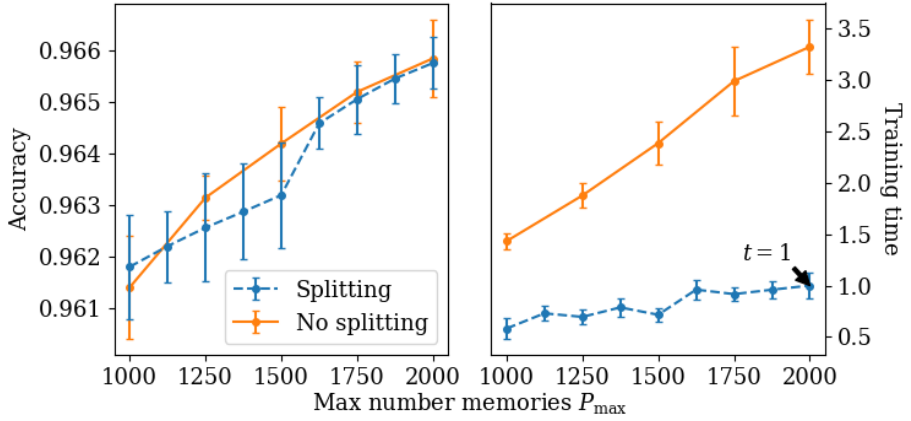


Figure 6: The classification accuracy and training time of dense associative memory (DAM) networks trained with and without splitting as a function of the maximum number of hidden unit P_{\max} . The round markers and their corresponding error bars show the means and standard deviations of the measurements made at each P_{\max} . Statistics are collected from 10 different random seeds. In the left panel, we verify that the DAMs with and without splitting have a similar accuracy. In the right panel, we compare their training times t . To facilitate this comparison, we normalize the t -axis such that the data point indicated by the arrow is at $t = 1$.

between $P_{\max} = 1500$ and $P_{\max} = 1625$, where the number of while-loop iterations in Alg. (1) increases by 1. In other words, the run time of Alg. (1) is better explained as proportional to $\lceil \log P_{\max} \rceil$ than P_{\max} in the range of P_{\max} of our numerical experiment, which is a dramatic improvement over the run time without splitting.

5 Conclusion

In this work, we study a dense associative memory (DAM) model capable of learning interpretable solutions to both supervised and unsupervised problems, which we construct from the framework of Boltzmann machines.

We derive two sets of equations that respectively characterize the stationary points of DAMs trained on real data using maximum likelihood estimation and the fixed points of DAMs trained on synthetic data in the teacher-student setting. Guided by their similarity, we then establish that the maximum likelihood equations are a special case of the teacher-student equations. Building on this equivalence, we introduce an effective loss function that significantly stabilizes training thanks to a regularization parameter that mimics the noise present in the data generation process.

We show that the stationary points of the effective loss of DAMs with a given number of hidden units are saddle points of larger DAMs. We considerably accelerate training using a custom implementation of the splitting steepest descent network-growing algorithm [36, 37] inspired by this *saddle-point hierarchy principle*. In our numerical experiments, the training time of splitting steepest descent is approximately logarithmic in the number of hidden units, which is a huge improvement over the linear training time that we observe without splitting steepest descent. Further research is needed to clearly determine the asymptotic functional form of the training time.

In Section 4.1, we briefly discuss how our DAM is interpretable. The ingredients needed to make an

interpretable neural network are not well understood, and we believe that our DAM offers a promising opportunity to explore that area. Studying the teacher-student setting with teacher inverse temperature β^* less than order N is another interesting research direction that we leave to future work. Beyond the framework of our model, [98, 99] have designed a technique that trains Gaussian mixture models by replicating mixture components. In contrast with our work, it uses a handpicked cooling schedule and breaks permutation symmetries with random noise. By design, splitting steepest descent finds the directions in the loss landscape that allow NNs to escape saddle points with permutation symmetries as quickly as possible, but finding these directions is more expensive than generating random noise (see Appendix H and [36, 37]). It would be interesting to study this tradeoff and identify the regimes where each method is preferable over the other. More generally, one could investigate how permutation symmetry-breaking takes place in energy models related to DAMs, such as attentional BMs [27], and study its relationship with the permutation symmetry-breaking [81, 84] and dynamical transitions [70, 71, 100, 73, 101] found in other types of RBMs. [11, 102] have made connections between DAM learning dynamics and cellular differentiation. Similarly, it could be possible to investigate whether there are similarities between cellular division and splitting steepest descent in our model. Finally, it would be interesting to see if splitting steepest descent and our proposed regularization technique can be used to improve the training of transformers and generative diffusion.

Data availability statement

The code for the numerical experiments presented in this work is available at this public repository [38].

Acknowledgements

This work was partially supported by project SERICS (PE00000014) under the MUR National Recovery and Resilience Plan funded by the European Union - NextGenerationEU. The work was also supported by the project PRIN22TANTARI "Statistical Mechanics of Learning Machines: from algorithmic and information-theoretical limits to new biologically inspired paradigms" 20229T9EAT – CUP J53D23003640001. DT also acknowledges GNFM-Indam.

RT acknowledges the computational resources of the Center for High Performance Computing (CHPC) at the Scuola Normale Superiore of Pisa, as well as Carlo Lucibello and Matteo Negri for insightful discussions.

Conflicts of interest

The authors have no conflicts of interest to declare.

Author contributions

Robin Thériault: Conceptualization, Methodology, Software, Formal analysis, Investigation, Data curation, Writing – original draft, Visualization. **Daniele Tantari:** Conceptualization, Validation, Writing – original draft, Writing – review and editing, Supervision, Project administration, Funding acquisition

A Derivation of the model

Consider the RBM Hamiltonian

$$-\beta H [\mathbf{x}, \mathbf{q}, \mathbf{h}; \mathbf{J}] = \beta \sum_{\mu=1}^P h_\mu \sum_{i=1}^N w_i^\mu x_i + \beta \sum_{\mu=1}^P h_\mu \sum_{y=1}^C u_y^\mu q_y + \beta \sum_{\mu=1}^P h_\mu b^\mu.$$

where $\mathbf{J} = \{\mathbf{w}, \mathbf{u}, \mathbf{b}\}$ is the set of all RBM parameters, i.e. $\mathbf{w} = \{w_i^\mu\}_{1 \leq i \leq N}^{1 \leq \mu \leq P}$, $\mathbf{u} = \{u_y^\mu\}_{1 \leq y \leq C}^{1 \leq \mu \leq P}$ and $\mathbf{b} = \{b^\mu\}_{\mu=1}^P$. The prior densities $P_0(\mathbf{h})$ and $P_0(\mathbf{q})$ are non-zero only when $\mathbf{h} \in \{\mathbf{e}_\gamma\}_{\gamma=0}^P$ and $\mathbf{q} \in \{\mathbf{e}_y\}_{y=0}^C$, in which case we have

$$-\beta H [\mathbf{x}, \mathbf{e}_y, \mathbf{e}_\gamma; \mathbf{J}] = \begin{cases} 0 & \gamma = 0 \\ \beta \sum_{i=1}^N w_i^\gamma x_i + a_y^\gamma & 0 < \gamma \leq P \end{cases}$$

where $a_y^\mu = \begin{cases} \beta b^\mu & y = 0 \\ \beta u_y^\mu + \beta b^\mu & 0 < y \leq C \end{cases}$

For convenience, we write the corresponding Gibbs distribution $P_\beta(\mathbf{x}, \mathbf{q} = \mathbf{e}_y, \mathbf{h} = \mathbf{e}_\gamma | \mathbf{J})$ as $P_\beta(\mathbf{x}, y, \mu | \mathbf{J})$, and the priors $P_0(\mathbf{q} = \mathbf{e}_y)$ and $P_0(\mathbf{h} = \mathbf{e}_\gamma)$ as $\pi_{\mathbf{q}}(y)$ and $\pi_{\mathbf{h}}(\gamma)$, respectively. Given a uniform prior on \mathbf{x} , we find

$$P_\beta(\mathbf{x}, y, \mu | \mathbf{J}) = \frac{1}{Z_\beta(\mathbf{J})} \pi_{\mathbf{q}}(y) \begin{cases} \pi_{\mathbf{h}}(0) & \gamma = 0 \\ \pi_{\mathbf{h}}(\gamma) \exp(a_y^\gamma) \exp\left(\beta \sum_{i=1}^N w_i^\gamma x_i\right) & 0 < \gamma \leq P, \end{cases}$$

where $Z_\beta(\mathbf{J})$ is an unknown normalization constant. The data \mathbf{x} belonging to each cluster $\mu > 0$ follows a von Mises-Fisher (vMF) distribution $P_\beta(\mathbf{x} | \mu, \mathbf{J}) \propto \exp\left(\beta \sum_{i=1}^N w_i^\mu x_i\right)$ centered on $\mathbf{w}^\mu = \{w_i^\mu\}_{i=1}^N$ (see Appendix C). We assume that $\sqrt{\sum_{i=1}^N (w_i^\mu)^2} = 1$ so that the corresponding cluster centroids \mathbf{w}^μ lie on the hypersphere S^{N-1} like the data $\mathbf{x} = \{x_i\}_{i=1}^N$. We marginalize $P_\beta(\mathbf{x}, y, \mu | \mathbf{J})$ over the hidden units μ and get

$$P_\beta(\mathbf{x}, y | \mathbf{J}) = \frac{1}{Z_\beta(\mathbf{J})} \pi_{\mathbf{q}}(y) \left[\sum_{\mu=1}^P \pi_{\mathbf{h}}(\mu) \exp(a_y^\mu) \exp\left(\beta \sum_{i=1}^N w_i^\mu x_i\right) + \pi_{\mathbf{h}}(0) \right].$$

We will now find the normalization constant $Z_\beta(\mathbf{J})$. Marginalizing $P_\beta(\mathbf{x}, y|\mathbf{J})$ over \mathbf{x} , we obtain

$$\begin{aligned}
P_\beta(y|\mathbf{J}) &= \int_{S^{N-1}} d\mathbf{x} P_\beta(\mathbf{x}, y|\mathbf{J}) \\
&= \frac{1}{Z_\beta(\mathbf{J})} \pi_{\mathbf{q}}(y) \int_{S^{N-1}} d\mathbf{x} \left[\sum_{\mu=1}^P \pi_{\mathbf{h}}(\mu) \exp(a_y^\mu) \exp\left(\beta \sum_{i=1}^N w_i^\mu x_i\right) + \pi_{\mathbf{h}}(0) \right] \\
&= \frac{1}{Z_\beta(\mathbf{J})} \pi_{\mathbf{q}}(y) \Omega_N(\beta) \sum_{\mu=1}^P \pi_{\mathbf{h}}(\mu) \exp(a_y^\mu) + \Omega_N(0) \pi_{\mathbf{h}}(0) \\
&= \frac{1}{Z_\beta(\mathbf{J})} \pi_{\mathbf{q}}(y) \Omega_N(\beta) \left[\sum_{\mu=1}^P \pi_{\mathbf{h}}(\mu) \exp(a_y^\mu) + \pi_{\mathbf{h}}(0) \exp(a^0) \right],
\end{aligned}$$

where $a^0 = \log[\Omega_N(0)/\Omega_N(\beta)]$. Normalization of $P_\beta(y|\mathbf{J})$ requires that

$$P_\beta(y|\mathbf{J}) = \frac{\pi_{\mathbf{q}}(y) \left[\sum_{\mu=1}^P \pi_{\mathbf{h}}(\mu) \exp(a_y^\mu) + \pi_{\mathbf{h}}(0) \exp(a^0) \right]}{\sum_{y'=0}^C \pi_{\mathbf{q}}(y') \left[\sum_{\nu=1}^P \pi_{\mathbf{h}}(\nu) \exp(a_{y'}^\nu) + \pi_{\mathbf{h}}(0) \exp(a^0) \right]},$$

so we deduce that $Z_\beta(\mathbf{J}) = \Omega_N(\beta) \sum_{y=0}^C \pi_{\mathbf{q}}(y) \left[\sum_{\mu=1}^P \pi_{\mathbf{h}}(\mu) \exp(a_y^\mu) + \pi_{\mathbf{h}}(0) \exp(a^0) \right]$. We define

$$p_y^\gamma = \begin{cases} \frac{\pi_{\mathbf{q}}(y) \pi_{\mathbf{h}}(0) \exp(a^0)}{\sum_{y'=0}^C \pi_{\mathbf{q}}(y') \left[\sum_{\nu=1}^P \pi_{\mathbf{h}}(\nu) \exp(a_{y'}^\nu) + \pi_{\mathbf{h}}(0) \exp(a^0) \right]} & \gamma = 0 \\ \frac{\pi_{\mathbf{q}}(y) \pi_{\mathbf{h}}(\mu) \exp(a_y^\mu)}{\sum_{y'=0}^C \pi_{\mathbf{q}}(y') \left[\sum_{\nu=1}^P \pi_{\mathbf{h}}(\nu) \exp(a_{y'}^\nu) + \pi_{\mathbf{h}}(0) \exp(a^0) \right]} & 0 < \gamma \leq P, \end{cases}$$

from which we obtain

$$P_\beta(\mathbf{x}, y|\mathbf{J}) = \sum_{\mu=1}^P p_y^\mu \frac{\exp\left(\beta \sum_{i=1}^N w_i^\mu x_i\right)}{\Omega_N(\beta)} + p_y^0 \frac{1}{\Omega_N(0)}.$$

The conditional distributions $P_\beta(\mathbf{x}|y, \mathbf{J})$ and their marginal $P_\beta(\mathbf{x}|\mathbf{J}) = \sum_{y=0}^C P_\beta(\mathbf{x}|y, \mathbf{J}) P_\beta(y|\mathbf{J})$ are von Mises-Fisher mixtures [46] with weights $\frac{p_y^\gamma}{\sum_{\nu=0}^P p_y^\nu}$ and $\sum_{y=0}^C p_y^\gamma$, respectively. As explained in Section 2, we constrain the marginals $\sum_{y=0}^C p_y^\gamma = P_\beta(\gamma|\mathbf{J})$ and $\sum_{\gamma=0}^P p_y^\gamma = P_\beta(y|\mathbf{J})$ to be equal to fixed distributions $p_{\mathbf{h}}(\gamma)$ and $p_{\mathbf{q}}(y)$, respectively. Formally, this means that $\mathbf{p} = \{p_y^\gamma\}_{0 \leq y \leq C}^{0 \leq \gamma \leq P}$ belongs to the transportation polytope with sum constraints $\sum_{\gamma=0}^P p_y^\gamma = p_{\mathbf{q}}(y)$ and $\sum_{y=0}^C p_y^\gamma = p_{\mathbf{h}}(\gamma)$ [103].

B Stationarity conditions of the loss

Since we constrain the memories \mathbf{w}^μ to have unit norm (see Section 2), the method of Lagrange multipliers tells us any set of memories \mathbf{w} that minimizes Eq. (4) must solve the extremization problem

$$\text{Extr}_{\mathbf{w}, \varphi} \left\{ L(\mathbf{w}, \mathbf{p}) + \frac{1}{2} \sum_{\mu=1}^P \varphi^\mu \left(\sum_{i=1}^N [w_i^\mu]^2 - 1 \right) \right\}.$$

The extrema are the points where the gradient vanishes, so they take the form

$$\begin{aligned}\partial_{w_i^\mu} L(\mathbf{w}, \mathbf{p}) + \varphi^\mu w_i^\mu &= 0 \\ \sum_{i=1}^N [w_i^\mu]^2 &= 1\end{aligned}$$

for all $1 \leq \mu \leq P$. We calculate $\partial_{w_i^\mu} L(\mathbf{w}, \mathbf{p})$ and write the solution in the more explicit form

$$\begin{aligned}\bar{w}_i^\mu &= \sum_{\mu_*=1}^{P^*} x_i^{*\mu_*} \sum_{y=0}^C q_y^{*\mu_*} \sigma_\mu(\beta m^{\mu_*}(\mathbf{x}^*, \mathbf{w}) + \log[\mathbf{p}_y]) \\ w_i^\mu &= \frac{\bar{w}_i^\mu}{\sqrt{\sum_{j=1}^N [\bar{w}_j^\mu]^2}},\end{aligned}$$

for all $1 \leq \mu \leq P$, where $\sigma_\gamma(x^{\gamma*}) = \frac{\exp(x^{\gamma*})}{\sum_{\nu=0}^P \exp(x^{\gamma*\nu})}$, $m^{\mu_*\mu}(\mathbf{x}^*, \mathbf{w}) = \sum_{i=1}^N x_i^{*\mu_*} w_i^\mu$ for $1 \leq \mu \leq P$ and $m^{\mu_*0}(\mathbf{x}, \mathbf{w}) = \frac{1}{\beta} \log[\Omega_N(\beta) / \Omega_N(0)]$.

Similarly, any set of class weights \mathbf{p} that minimizes Eq. (4) must solve the extremization problem

$$\text{Extr}_{\mathbf{p}, \omega, \lambda} \left\{ L(\mathbf{w}, \mathbf{p}) + \sum_{y=0}^C \lambda_y \left(\sum_{\gamma=0}^P p_y^\gamma - p_{\mathbf{q}}(y) \right) + \sum_{\gamma=0}^P \omega^\gamma \left(\sum_{y=0}^C p_y^\gamma - p_{\mathbf{h}}(\gamma) \right) \right\}.$$

In Appendix F, we show that its solution is

$$\begin{aligned}\bar{p}_y^\gamma &= \sum_{\mu_*=1}^{P^*} q_y^{*\mu_*} \sigma_\gamma(\beta m^{\mu_*}(\mathbf{x}, \mathbf{w}) + \log[\mathbf{p}_y]) \\ p_y^\gamma &= \frac{\bar{p}_y^\gamma}{\zeta_y^\gamma(\bar{\mathbf{p}}; p_{\mathbf{h}})}\end{aligned}$$

for all $0 \leq \gamma \leq P$, where the normalization constant $\zeta_y^\gamma(\bar{\mathbf{p}}; p_{\mathbf{h}})$ is defined using Eqs. (26) of Appendix F. Combining these equations with the ones for \mathbf{w} , we find the stationarity conditions

$$\begin{aligned}\bar{w}_i^\mu &= \sum_{\mu_*=1}^{P^*} x_i^{*\mu_*} \sum_{y=0}^C q_y^{*\mu_*} \sigma_\mu(\beta m^{\mu_*}(\mathbf{x}^*, \mathbf{w}) + \log[\mathbf{p}_y]) \\ \bar{p}_y^\gamma &= \sum_{\mu_*=1}^{P^*} q_y^{*\mu_*} \sigma_\gamma(\beta m^{\mu_*}(\mathbf{x}^*, \mathbf{w}) + \log[\mathbf{p}_y]) \\ w_i^\mu &= \frac{\bar{w}_i^\mu}{\sqrt{\sum_{j=1}^N [\bar{w}_j^\mu]^2}} \\ p_y^\gamma &= \frac{\bar{p}_y^\gamma}{\zeta_y^\gamma(\bar{\mathbf{p}}; p_{\mathbf{h}})}\end{aligned}$$

for all $1 \leq \mu \leq P$ and $0 \leq \gamma \leq P$.

C Integration of the von Mises-Fisher density

The von Mises-Fisher (vMF) distribution [104] is an isotropic Gaussian distribution restricted to the $N - 1$ dimensional unit sphere S^{N-1} . It takes the form

$$p(\mathbf{x}) = \Omega(r)^{-1} \exp\left(\sum_{i=1}^N r_i x_i\right),$$

where $r = \sqrt{\sum_i [r_i]^2}$ is called the concentration parameter. When $r = 0$, it reduces to the uniform distribution on the unit sphere, whose surface surface area $\frac{2\pi^{N/2}}{\Gamma(N/2)}$ is thus also the normalization constant $\Omega_N(0)$. When $r > 0$, we define the mean direction $\hat{\mathbf{r}} = \{r_i/r\}_{i=1}^N$ and find the normalization constant to be

$$\begin{aligned} \Omega_N(r) &= \int_{S^{N-1}} d\mathbf{x} \exp\left(\sum_{i=1}^N r_i x_i\right) \\ &= \int_{S^{N-1}} d\mathbf{x} \exp\left(r \sum_{i=1}^N \hat{r}_i x_i\right) \\ &= \Omega_{N-1}(0) \int_{-1}^1 du (1-u^2)^{(N-3)/2} \exp(ru) \\ &= \Omega_N(0) \left(\frac{r}{2}\right)^{1-N/2} \Gamma\left(\frac{N}{2}\right) I_{N/2-1}(r), \end{aligned} \tag{17}$$

where $I_n(x)$ is the modified Bessel function of the first kind of order n . The third line of (17) comes from the change of variables $u = \sum_{i=1}^N \hat{r}_i x_i$, and the fourth line is a consequence of Poisson's Bessel function integral [105]. In the limit of large N with $\rho = \frac{r}{N-2} \approx \frac{r}{N}$, we find

$$\begin{aligned} \int_{S^{N-1}} d\mathbf{x} \exp\left(\sum_{i=1}^N r_i x_i\right) &\approx \frac{\Omega_N(0)}{\sqrt{2\pi(N/2-1)}} \left(\frac{N}{2}-1\right)^{1-N/2} (1+(2\rho)^2)^{-1/4} \\ &\quad \Gamma\left(\frac{N}{2}\right) \exp\left[\left(\frac{N}{2}-1\right)(\eta(2\rho)+1)\right] \\ \text{where } \eta(x) &= (1+x^2)^{1/2} - 1 - \log\left[1+(1+x^2)^{1/2}\right] + \log 2, \end{aligned}$$

by exploiting the large N asymptotic expansion of $I_{N/2-1}([N/2-1] \cdot 2\rho)$ found in [106, 107]. We use Stirling's approximation

$$\Gamma\left(\frac{N}{2}\right) \approx \sqrt{2\pi(N/2-1)} \left(\frac{N}{2}-1\right)^{N/2-1} \exp\left(-\frac{N}{2}+1\right)$$

to simplify it to

$$\int_{S^{N-1}} d\mathbf{x} \exp \left(\sum_{i=1}^N r_i x_i \right) \approx \Omega_N(0) \left(1 + (2\rho)^2 \right)^{-1/4} \exp \left[\left(\frac{N}{2} - 1 \right) \eta(2\rho) \right] \quad (18)$$

where $\eta(x) = (1+x^2)^{1/2} - 1 - \log \left[1 + (1+x^2)^{1/2} \right] + \log 2$.

D Replicated partition function and free entropy

Suppose a student dense associative memory (DAM) model is trained using a dataset $\mathcal{D} = \{\mathbf{x}^c, y^c\}_{c=1}^M$ of M i.i.d. examples \mathbf{x}^c with labels y^c . By Bayes' theorem, the student weights \mathbf{w} and \mathbf{p} follow the distribution

$$P_\beta(\mathbf{w}, \mathbf{p} | \mathcal{D}) = \mathcal{Z}(\mathcal{D})^{-1} P(\mathbf{w}, \mathbf{p}) \prod_{c=1}^M P_\beta(\mathbf{x}^c, y^c | \mathbf{w}, \mathbf{p}),$$

where $\mathcal{Z}(\mathcal{D}) = \mathbb{E}_{\mathbf{w}, \mathbf{p}} \left[\prod_{c=1}^M P_\beta(\mathbf{x}^c, y^c | \mathbf{w}, \mathbf{p}) \right]$. Assuming the examples are sampled from a teacher DAM with weights \mathbf{w}^* and \mathbf{p}^* , the average replicated partition takes the form

$$\begin{aligned} \langle \mathcal{Z}^L \rangle &= \sum_{\{y^c\}_{c=1}^M} \int \left[\prod_{c=1}^M d\mathbf{x}^c \right] \mathbb{E}_{\mathbf{w}^*, \mathbf{p}^*} \left[\prod_{c=1}^M P_\beta(\mathbf{x}^c, y^c | \mathbf{w}^*, \mathbf{p}^*) \right] \mathcal{Z}(\mathcal{D})^L \\ &= \sum_{\{y^c\}_{c=1}^M} \int \left[\prod_{c=1}^M d\mathbf{x}^c \right] \mathbb{E}_{\mathbf{w}^*, \mathbf{p}^*} \left[\prod_{c=1}^M P_\beta(\mathbf{x}^c, y^c | \mathbf{w}^*, \mathbf{p}^*) \right] \prod_{a=1}^L \mathbb{E}_{\mathbf{w}^a, \mathbf{p}^a} \left[\prod_{c=1}^M P_\beta(\mathbf{x}^c, y^c | \mathbf{w}^a, \mathbf{p}^a) \right] \\ &= \mathbb{E}_{\mathbf{w}^*, \mathbf{w}} \mathbb{E}_{\mathbf{p}^*, \mathbf{p}} \left[\prod_{c=1}^M \sum_{y^c=0}^C \int_{S^{N-1}} d\mathbf{x}^c P_\beta(\mathbf{x}^c, y^c | \mathbf{w}^*, \mathbf{p}^*) \prod_{a=1}^L P_\beta(\mathbf{x}^c, y^c | \mathbf{w}^a, \mathbf{p}^a) \right] \\ &= \mathbb{E}_{\mathbf{w}^*, \mathbf{w}} \mathbb{E}_{\mathbf{p}^*, \mathbf{p}} \left[\left(\sum_{y=0}^C \int_{S^{N-1}} d\mathbf{x} P_\beta(\mathbf{x}, y | \mathbf{w}^*, \mathbf{p}^*) \prod_{a=1}^L P_\beta(\mathbf{x}, y | \mathbf{w}^a, \mathbf{p}^a) \right)^M \right], \end{aligned}$$

where we redefined $\mathbf{w} = \{\mathbf{w}^a\}_{a=1}^L$ and $\mathbf{p} = \{\mathbf{p}^a\}_{a=1}^L$. In order to simplify the argument of $(\cdot)^M$, it is convenient to write Eq. (3) in the form

$$P_\beta(\mathbf{x}, y | \mathbf{w}^a, \mathbf{p}^a) = \sum_{\gamma=0}^P \Omega_N(\beta [1 - \delta_{\gamma 0}])^{-1} p_y^{a\gamma} \exp \left(\beta [1 - \delta_{\gamma 0}] \sum_{i=1}^N w_i^{a\gamma} x_i \right), \quad (19)$$

where the value of \mathbf{w}^{a0} is arbitrary. Until the end of this Section, all sums over the hidden units will include the index 0 unless explicitly indicated otherwise. Define $I_y(\mathbf{x}) = P_\beta(\mathbf{x}, y | \mathbf{w}^*, \mathbf{p}^*) \prod_{a=1}^L P_\beta(\mathbf{x}, y | \mathbf{w}^a, \mathbf{p}^a)$,

then

$$\begin{aligned}
I_y(\mathbf{x}) &= \left[\sum_{\gamma_*=0}^{P^*} \Omega_N(\beta^*[1-\delta_{\gamma_*0}])^{-1} p_y^{*\gamma_*} \exp\left(\beta^*[1-\delta_{\gamma_*0}] \sum_{i=1}^N w_i^{*\gamma_*} x_i\right) \right] \\
&\quad \prod_{a=1}^L \left[\sum_{\gamma=0}^P \Omega_N(\beta[1-\delta_{\gamma0}])^{-1} p_y^{a\gamma} \exp\left(\beta[1-\delta_{\gamma0}] \sum_{i=1}^N w_i^{a\gamma} x_i\right) \right] \\
&= \sum_{\gamma_*\gamma_1\dots\gamma_L} \Omega_N(\beta^*[1-\delta_{\gamma_*0}])^{-1} \left[\prod_a \Omega_N(\beta[1-\delta_{\gamma_a0}]) \right]^{-1} \\
&\quad p_y^{*\gamma_*} \left[\prod_a p_y^{a\gamma_a} \right] \exp\left(\beta^*[1-\delta_{\gamma_*0}] \sum_i w_i^{*\gamma_*} x_i + \beta \sum_a [1-\delta_{\gamma_a0}] \sum_i w_i^{a\gamma_a} x_i\right).
\end{aligned}$$

We will now evaluate the integral $\int_{S^{N-1}} d\mathbf{x} I_y(\mathbf{x})$. Using Eq. (18) of Appendix C with $\rho = \rho_{\gamma_*\gamma} := \frac{1}{N} \sqrt{\sum_i [\beta^*[1-\delta_{\gamma_*0}] w_i^{*\gamma_*} + \beta \sum_a [1-\delta_{\gamma_a0}] w_i^{a\gamma_a}]^2}$, we get

$$\begin{aligned}
&\int_{S^{N-1}} d\mathbf{x} \exp\left(\beta^*[1-\delta_{\gamma_*0}] \sum_i w_i^{*\gamma_*} x_i + \beta \sum_a [1-\delta_{\gamma_a0}] \sum_i w_i^{a\gamma_a} x_i\right) \\
&\approx \Omega_N(0) \left(1 + (2\rho_{\gamma_*\gamma})^2\right)^{-1/4} \exp\left[\left(\frac{N}{2} - 1\right) \eta(2\rho_{\gamma_*\gamma})\right],
\end{aligned}$$

in the limit of large N . Since $\sqrt{\sum_i (w_i^{*\gamma_*})^2} = 1$, the square of $\rho_{\gamma_*\gamma}$ simplifies to

$$\begin{aligned}
(\rho_{\gamma_*\gamma})^2 &= \left(\frac{1}{N} \sqrt{\sum_i \left[\beta^*[1-\delta_{\gamma_*0}] w_i^{*\gamma_*} + \beta \sum_a [1-\delta_{\gamma_a0}] w_i^{a\gamma_a} \right]^2} \right)^2 \\
&= v^2 [1-\delta_{\gamma_*0}] + 2\frac{\beta}{N} v [1-\delta_{\gamma_*0}] \sum_a [1-\delta_{\gamma_a0}] \sum_i w_i^{*\gamma_*} w_i^{a\gamma_a} \\
&\quad + \frac{\beta^2}{N^2} \sum_{a,b} [1-\delta_{\gamma_a0}] [1-\delta_{\gamma_b0}] \sum_i w_i^{a\gamma_a} w_i^{b\gamma_b},
\end{aligned}$$

where $v = \frac{\beta^*}{N}$. To leading order in $\frac{\beta}{N}$ we find

$$\begin{aligned}
&\left(1 + (2\rho_{\gamma_*\gamma})^2\right)^{-1/4} \approx \left(1 + (2v[1-\delta_{\gamma_*0}])^2\right)^{-1/4} \\
\text{and } &\left(\frac{N}{2} - 1\right) \eta(2\rho_{\gamma_*\gamma}) \approx \left(\frac{N}{2} - 1\right) \eta(2v[1-\delta_{\gamma_*0}]) + \beta_{\text{eff}} [1-\delta_{\gamma_*0}] \sum_a [1-\delta_{\gamma_a0}] \sum_i w_i^{*\gamma_*} w_i^{a\gamma_a} \\
&\quad + \frac{[\beta\xi_{\gamma_*}]^2}{2N} \sum_{a,b} [1-\delta_{\gamma_a0}] [1-\delta_{\gamma_b0}] \sum_i w_i^{a\gamma_a} w_i^{b\gamma_b},
\end{aligned}$$

where $\beta_{\text{eff}} = \frac{2v}{\sqrt{[2v]^2+1+1}}\beta$ and $\xi_{\gamma_*} = \delta_{\gamma_*0} + \sqrt{\frac{2}{\sqrt{[2v]^2+1+1}}} [1 - \delta_{\gamma_*0}]$. Assuming that $v \gg 1/N$ and $\beta \ll N$, we drop the last term. Finally, we use Eq. (18) backwards with $\rho = v [1 - \delta_{\gamma_*0}]$ and obtain

$$\begin{aligned} \Omega_N(\beta^* [1 - \delta_{\gamma_*0}])^{-1} \int_{S^{N-1}} d\mathbf{x} \exp \left(\beta^* [1 - \delta_{\gamma_*0}] \sum_i w_i^{*\gamma_*} x_i + \beta \sum_a [1 - \delta_{\gamma_a0}] \sum_i w_i^{a\gamma_a} x_i \right) \\ \approx \exp \left(\beta_{\text{eff}} [1 - \delta_{\gamma_*0}] \sum_a [1 - \delta_{\gamma_a0}] \sum_i w_i^{*\gamma_*} w_i^{a\gamma_a} \right), \end{aligned}$$

from which we conclude that

$$\begin{aligned} \sum_{y=0}^C \int_{S^{N-1}} d\mathbf{x} I_y(\mathbf{x}) \approx \sum_{\gamma_* \gamma_1 \dots \gamma_L} \sum_y p_y^{*\gamma_*} \left[\prod_a p_y^{a\gamma_a} \right] \left[\prod_a \Omega_N(\beta [1 - \delta_{\gamma_a0}]) \right]^{-1} \\ \exp \left(\beta_{\text{eff}} [1 - \delta_{\gamma_*0}] \sum_a [1 - \delta_{\gamma_a0}] \sum_i w_i^{*\gamma_*} w_i^{a\gamma_a} \right). \end{aligned}$$

We define $\alpha = M/N$, introduce the order parameter

$$m^{a\gamma_*\nu} \text{ for } \sum_i w_i^{*\gamma_*} w_i^{a\nu}, \quad (20)$$

and insert into $\langle \mathcal{Z}^L \rangle$ the identity operator

$$\begin{aligned} 1 &= \int_{\mathbb{R}} \prod_{\gamma_*, \nu; a} dm^{a\gamma_*\nu} \delta \left(m^{a\gamma_*\nu} - \sum_i w_i^{*\gamma_*} w_i^{a\nu} \right) \\ &= \int_{\mathbb{R}} \prod_{\gamma_*, \nu; a} dm^{a\gamma_*\nu} \int_{i\mathbb{R}} \prod_{\gamma_*, \nu; a} d\hat{m}^{a\gamma_*\nu} \exp \left\{ \frac{\beta_{\text{eff}}\alpha}{P^*} \sum_{\gamma_*, \nu; a} \hat{m}^{a\gamma_*\nu} \left(\sum_i w_i^{*\gamma_*} w_i^{a\nu} - m^{a\gamma_*\nu} \right) \right\} \end{aligned}$$

so that we can rewrite it as

$$\begin{aligned} \langle \mathcal{Z}^L \rangle &= \int \prod_{\gamma_*, \nu; a} d\hat{m}^{a\gamma_*\nu} dm^{a\gamma_*\nu} \mathbb{E}_{\mathbf{w}^*, \mathbf{w}} \exp \{ NH_S(\mathbf{w}, \mathbf{w}^*; \hat{\mathbf{m}}) \} \exp \{ -NH_Q(\mathbf{m}, \hat{\mathbf{m}}) \} \\ &\quad \mathbb{E}_{\mathbf{p}^*, \mathbf{p}} \exp \left\{ \alpha N \log \left[\sum_{\gamma_* \gamma_1 \dots \gamma_L} \sum_y p_y^{*\gamma_*} \left[\prod_a p_y^{a\gamma_a} \right] \exp \{ H_E(\gamma, \gamma_*; \mathbf{m}) \} \right] \right\}, \end{aligned} \quad (21)$$

$$\begin{aligned} \text{where } H_S(\mathbf{w}, \mathbf{w}^*; \hat{\mathbf{m}}) &= \frac{\beta_{\text{eff}}\alpha}{P^*} \sum_{\gamma_*, \nu; a} \hat{m}^{a\gamma_*\nu} \sum_i w_i^{*\gamma_*} w_i^{a\nu} \\ H_Q(\mathbf{m}, \hat{\mathbf{m}}) &= \frac{\beta_{\text{eff}}\alpha}{P^*} \sum_{\gamma_*, \nu; a} \hat{m}^{a\gamma_*\nu} m^{a\gamma_*\nu}, \\ H_E(\gamma, \gamma_*; \mathbf{m}) &= - \sum_a \log [\Omega_N(\beta [1 - \delta_{\gamma_a0}])] + \beta_{\text{eff}} [1 - \delta_{\gamma_*0}] \sum_a [1 - \delta_{\gamma_a0}] m^{a\gamma_*\gamma_a}. \end{aligned}$$

Using Eq. (18) of Appendix C, the exponential of H_S integrates to

$$\begin{aligned}
& \mathbb{E}_{\mathbf{w}} \exp \{N H_S(\mathbf{w}, \mathbf{w}^*; \hat{\mathbf{m}})\} \\
&= \Omega_N(0)^{-PL} \int_{S^{N-1}} d\mathbf{w} \exp \left(\frac{\beta_{\text{eff}} \alpha}{P^*} \sum_{\gamma_*, \nu; a} \hat{m}^{a \gamma_* \nu} \sum_i w_i^{*\gamma_*} w_i^{a \nu} \right) \\
&\approx \prod_{\nu; a} \exp \left[-\frac{1}{4} \log \left(1 + \left[\frac{2\beta_{\text{eff}} \alpha}{P^*} \right]^2 \sum_i \left[\sum_{\gamma_*} \hat{m}^{a \gamma_* \nu} w_i^{*\gamma_*} \right]^2 \right) \right] \\
&\quad \exp \left[\left(\frac{N}{2} - 1 \right) \eta \left(\frac{2\beta_{\text{eff}} \alpha}{P^*} \sqrt{\sum_i \left[\sum_{\gamma_*} \hat{m}^{a \gamma_* \nu} w_i^{*\gamma_*} \right]^2} \right) \right].
\end{aligned}$$

In order to continue the calculations, we make the replica-symmetric ansatz

$$\begin{aligned}
m^{a \gamma_* \nu} &= m^{\gamma_* \nu} \text{ and } \hat{m}^{a \gamma_* \nu} = \hat{m}^{\gamma_* \nu} \text{ for all } a; \gamma_*, \nu \\
p_y^{a \nu} &= p_y^\nu \text{ for all } a; \nu
\end{aligned}$$

so that we can use the replica trick to simplify

$$\begin{aligned}
& \frac{1}{L} \log \left[\sum_{\gamma_*} \sum_{\gamma_1 \dots \gamma_L} \sum_y p_y^{*\gamma_*} \left[\prod_a p_y^{a \gamma_a} \right] \exp \{H_E(\gamma, \gamma_*; \mathbf{m})\} \right] \\
&= \frac{1}{L} \log \left[\sum_{\gamma_*} \sum_y p_y^{*\gamma_*} \sum_{\gamma_1 \dots \gamma_L} \left[\prod_a p_y^{a \gamma_a} \right] \exp \{H_E(\gamma, \gamma_*; \mathbf{m})\} \right] \\
&\approx \sum_{\gamma_*} \sum_y p_y^{*\gamma_*} \log \left[\sum_{\gamma} p_y^\gamma \Omega_N(\beta [1 - \delta_{\gamma 0}])^{-1} \exp(\beta_{\text{eff}} [1 - \delta_{\gamma_* 0}] [1 - \delta_{\gamma 0}] m^{\gamma_* \gamma}) \right],
\end{aligned}$$

as we take L to zero. Similarly, we get

$$\begin{aligned}
\frac{1}{L} \log [\mathbb{E}_{\mathbf{w}} \exp \{N H_S(\mathbf{w}, \mathbf{w}^*; \hat{\mathbf{m}})\}] &= -\frac{1}{4} \log \left(1 + \left[\frac{2\beta_{\text{eff}} \alpha}{P^*} \right]^2 \sum_i \left[\sum_{\gamma_*} \hat{m}^{\gamma_* \nu} w_i^{*\gamma_*} \right]^2 \right) \\
&\quad + \left(\frac{N}{2} - 1 \right) \eta \left(\frac{2\beta_{\text{eff}} \alpha}{P^*} \sqrt{\sum_i \left[\sum_{\gamma_*} \hat{m}^{\gamma_* \nu} w_i^{*\gamma_*} \right]^2} \right).
\end{aligned}$$

From now on, we assume for simplicity that $\sum_y p_y^{*0} = p_{\mathbf{h}}^*(0) = 0$ and $\sum_y p_y^{*\mu_*} = p_{\mathbf{h}}^*(\mu_*) = 1/P^*$ for all $\mu_* > 0$. Defining $g_y^{*\mu_*} = P^* p_y^{*\mu_*} = P_{\beta}(y | \mu_*, \mathbf{J})$ for all $\mu_* > 0$, $\mathbf{g}^* = \{g_y^{*\gamma_*}\}_{0 \leq y \leq C}^{1 \leq \mu_* \leq P^*}$ and $\varrho = \frac{\alpha}{P^*} = \frac{M}{P^* N}$,

the free entropy f then takes the form

$$\begin{aligned}
f &\approx \underset{\mathbf{m}, \hat{\mathbf{m}}, \mathbf{p}}{\text{Extr}} \{f(\mathbf{m}, \hat{\mathbf{m}}, \mathbf{p})\} \quad \text{such that} \quad \sum_{\gamma=0}^P p_y^\gamma = p_{\mathbf{q}}(y) \quad \text{and} \quad \sum_{y=0}^C p_y^\gamma = p_{\mathbf{h}}(\gamma) \quad (22) \\
\text{with} \quad f(\mathbf{m}, \hat{\mathbf{m}}, \mathbf{p}) &= -\beta_{\text{eff}} \varrho \sum_{\gamma_*, \gamma=0}^{P^*, P} \hat{m}^{\gamma_* \gamma} m^{\gamma_* \gamma} + \frac{1}{2} \mathbb{E}_{\mathbf{w}^*} \left[\sum_{\gamma=0}^P \eta \left(2\beta_{\text{eff}} \varrho \sqrt{\sum_{i=1}^N \left[\sum_{\gamma_*=0}^{P^*} \hat{m}^{\gamma_* \gamma} w_i^{*\gamma_*} \right]^2} \right) \right] \\
&+ \varrho \sum_{\mu_*=1}^{P^*} \sum_{y=0}^C \mathbb{E}_{\mathbf{g}^*} [g_y^{*\mu_*}] \log \left[\sum_{\gamma=0}^P p_y^\gamma \Omega_N(\beta[1 - \delta_{\gamma 0}])^{-1} \exp(\beta_{\text{eff}}[1 - \delta_{\gamma 0}] m^{\mu_* \gamma}) \right]
\end{aligned}$$

where we approximated the expectation over \mathbf{p} as a (constrained) extremization problem using Laplace's method. By inspection, the order parameters $m^{0\gamma}$ and $\hat{m}^{0\gamma}$ always vanish, so we ignore them in the incoming derivation of the saddle-point equations.

E Saddle-point equations

In this Appendix, we adopt the convention $1 \leq \mu_* \leq P^*$, $0 \leq \gamma \leq P$ and $1 \leq \mu \leq P$. By the Lagrange multiplier theorem, any set of class weights \mathbf{p} that extremizes Eq. (22) must solve the extremization problem

$$\underset{\mathbf{p}, \omega, \lambda}{\text{Extr}} \left\{ f(\mathbf{m}, \hat{\mathbf{m}}, \mathbf{p}) + \sum_{y=0}^C \lambda_y \left(\sum_{\gamma=0}^P p_y^\gamma - p_{\mathbf{q}}(y) \right) + \sum_{\gamma=0}^P \omega^\gamma \left(\sum_{y=0}^C p_y^\gamma - p_{\mathbf{h}}(\gamma) \right) \right\}.$$

In Appendix F, we show that its solution is

$$\begin{aligned}
\bar{p}_y^\gamma &= \sum_{\mu_*=1}^{P^*} \mathbb{E}_{\mathbf{g}^*} [g_y^{*\mu_*}] \sigma_\gamma(\beta_{\text{eff}}[1 - \delta_{\gamma 0}] m^{\mu_*} - \log[\Omega_N(\beta[1 - \delta_{\gamma 0}])] + \log[\mathbf{p}_y]) \\
p_y^\gamma &= \frac{\bar{p}_y^\gamma}{\zeta_y^\gamma(\bar{\mathbf{p}}; p_{\mathbf{h}})},
\end{aligned}$$

for all $0 \leq \gamma \leq P$, where $\zeta_y^\gamma(\bar{\mathbf{p}}; p_{\mathbf{h}})$ is defined using Eqs. (26) of Appendix F and $\sigma_\gamma(x^{\mu_*}) = \frac{\exp(x^{\mu_* \gamma})}{\sum_{\kappa=0}^P \exp(x^{\mu_* \kappa})}$ is the softmax function. We extremize Eq. (22) with respect to the remaining parameters by solving for the gradient equal to zero. $\partial_{m^{\mu_* \gamma}} f(\mathbf{m}, \hat{\mathbf{m}}, \mathbf{p}) = 0$ immediately yields

$$\hat{m}^{\mu_* \gamma} = [1 - \delta_{\gamma 0}] \sum_{y=0}^C \mathbb{E}_{\mathbf{g}^*} [g_y^{*\mu_*}] \frac{p_y^\gamma \Omega_N(\beta[1 - \delta_{\gamma 0}])^{-1} \exp(\beta_{\text{eff}}[1 - \delta_{\gamma 0}] m^{\mu_* \gamma})}{\sum_{\kappa=0}^P p_y^\kappa \Omega_N(\beta[1 - \delta_{\kappa 0}])^{-1} \exp(\beta_{\text{eff}}[1 - \delta_{\kappa 0}] m^{\mu_* \kappa})}. \quad (23)$$

On the other hand, $\partial_{\hat{m}^{\mu_* \gamma}} f(\mathbf{m}, \hat{\mathbf{m}}, \mathbf{p}) = 0$ gives an equation that depends on the choice of prior for the teacher memories $\mathbf{w}^{*\mu_*}$. We first investigate the case where the teacher memories $\mathbf{w}^{*\mu_*}$ and the class weights \mathbf{g}^* are distributed uniformly at random over the sets to which they are constrained (see Section 2.2). In this scenario, we have $\mathbb{E}_{\mathbf{g}^*} [g_y^{*\mu_*}] = p_{\mathbf{q}}^*(y)$. Moreover, assuming that $P^* \ll N$, random vectors on the unit sphere are

orthonormal with high probability, which means that

$$\begin{aligned}
\sum_{i=1}^N \left[\sum_{\mu_*=1}^{P^*} \hat{m}^{\mu_* \gamma} w_i^{*\mu_*} \right]^2 &= \sum_{i=1}^N \sum_{\mu_*, \nu_*=1}^{P^*} \hat{m}^{\mu_* \gamma} \hat{m}^{\nu_* \gamma} w_i^{*\mu_*} w_i^{*\nu_*} \\
&= \sum_{\mu_*=1}^{P^*} [\hat{m}^{\mu_* \gamma}]^2 + \sum_{\mu_* \neq \nu_*} \hat{m}^{\mu_* \gamma} \hat{m}^{\nu_* \gamma} \sum_{i=1}^N w_i^{*\mu_*} w_i^{*\nu_*} \\
&\approx \sum_{\mu_*=1}^{P^*} [\hat{m}^{\mu_* \gamma}]^2.
\end{aligned}$$

Therefore, $\partial_{\hat{m}^{\mu_* \gamma}} f(\mathbf{m}, \hat{\mathbf{m}}, \mathbf{p}) = 0$ gives

$$\begin{aligned}
0 &= \partial_{\hat{m}^{\mu_* \gamma}} f(\mathbf{m}, \hat{\mathbf{m}}, \mathbf{p}) \\
0 &= -\beta_{\text{eff}} \varrho m^{\mu_* \gamma} + \frac{1}{2} \partial_{\hat{m}^{\mu_* \gamma}} \sum_{\kappa=0}^P \eta \left(2\beta_{\text{eff}} \varrho \sqrt{\sum_{\nu_*=1}^{P^*} [\hat{m}^{\nu_* \kappa}]^2} \right) \\
m^{\mu_* \gamma} &= \varsigma \left(2\beta_{\text{eff}} \varrho \sqrt{\sum_{\nu_*=1}^{P^*} [\hat{m}^{\nu_* \gamma}]^2} \right) \frac{\hat{m}^{\mu_* \gamma}}{\sqrt{\sum_{\nu_*=1}^{P^*} [\hat{m}^{\nu_* \gamma}]^2}},
\end{aligned}$$

where $\varsigma(x) = \frac{x}{\sqrt{x^2+1+1}}$. $\hat{m}^{\mu_* \gamma}$ vanishes (see Eqs. 23) and $m^{\mu_* \gamma}$ is arbitrary (see Eqs. 19 and 20) when $\gamma = 0$. Therefore, we may update only $\hat{m}^{\mu_* \mu}$ and $m^{\mu_* \mu}$ with $1 \leq \mu \leq P$ when solving for $\nabla f = 0$ by fixed-point iteration. Defining $m^{\mu_* 0} = \frac{1}{\beta_{\text{eff}}} \log [\Omega_N(\beta) / \Omega_N(0)]$, we then obtain the saddle-point equations

$$\begin{aligned}
\hat{m}^{\mu_* \mu} &= \sum_{y=0}^C p_{\mathbf{q}}^*(y) \sigma_\mu (\beta_{\text{eff}} m^{\mu_*} + \log [\mathbf{p}_y]) \\
m^{\mu_* \mu} &= \varsigma \left(2\beta_{\text{eff}} \varrho \sqrt{\sum_{\nu_*=1}^{P^*} [\hat{m}^{\nu_* \mu}]^2} \right) \frac{\hat{m}^{\mu_* \mu}}{\sqrt{\sum_{\nu_*=1}^{P^*} [\hat{m}^{\nu_* \mu}]^2}},
\end{aligned}$$

for all $1 \leq \mu \leq P$, where we simplified the argument of the softmax function $\sigma_\mu(x^{\mu*}) = \frac{\exp(x^{\mu* \mu})}{\sum_{\kappa=0}^P \exp(x^{\mu* \kappa})}$ using $m^{\mu*0} = \frac{1}{\beta_{\text{eff}}} \log [\Omega_N(\beta) / \Omega_N(0)]$. Putting the equations for $m^{\mu* \mu}$ and p_y^γ together, we find

$$\begin{aligned}\hat{m}^{\mu* \mu} &= \sum_{y=0}^C p_y^*(y) \sigma_\mu(\beta_{\text{eff}} m^{\mu*} + \log [\mathbf{p}_y]) \\ \bar{p}_y^\gamma &= p_y^*(y) \sum_{\mu=1}^{P^*} \sigma_\gamma(\beta_{\text{eff}} m^{\mu*} + \log [\mathbf{p}_y]) \\ m^{\mu* \mu} &= \varsigma \left(2\beta_{\text{eff}} \varrho \sqrt{\sum_{\nu_*=1}^{P^*} [\hat{m}^{\nu_* \mu}]^2} \right) \frac{\hat{m}^{\mu* \mu}}{\sqrt{\sum_{\nu_*=1}^{P^*} [\hat{m}^{\nu_* \mu}]^2}} \\ p_y^\gamma &= \frac{\bar{p}_y^\gamma}{\zeta_y^\gamma(\bar{\mathbf{p}}; p_{\mathbf{h}})}\end{aligned}$$

for all $1 \leq \mu \leq P$ and $0 \leq \gamma \leq P$. If we instead clamp $\mathbf{w}^{*\mu*}$ and $\mathbf{g}^{*\mu*}$ to some fixed patterns $\mathbf{x}^{*\mu*}$ and their soft labels $\mathbf{q}^{*\mu*}$, respectively, then the solutions of Eq. (22) take the form

$$\begin{aligned}\hat{m}^{\mu* \mu} &= \sum_{y=0}^C q_y^{*\mu*} \sigma_\mu(\beta_{\text{eff}} m^{\mu*} + \log [\mathbf{p}_y]) \\ \bar{p}_y^\gamma &= \sum_{\mu_*=1}^{P^*} q_y^{*\mu*} \sigma_\gamma(\beta_{\text{eff}} m^{\mu*} + \log [\mathbf{p}_y]) \\ m^{\mu* \mu} &= \varsigma \left(2\beta_{\text{eff}} \varrho \sqrt{\sum_{i=1}^N \left[\sum_{\nu_*=1}^{P^*} \hat{m}^{\nu_* \mu} x_i^{*\nu_*} \right]^2} \right) \frac{\sum_{i=1}^N x_i^{*\nu_*} \sum_{\nu_*=1}^{P^*} \hat{m}^{\nu_* \mu} x_i^{*\nu_*}}{\sqrt{\sum_{i=1}^N \left[\sum_{\nu_*=1}^{P^*} \hat{m}^{\nu_* \mu} x_i^{*\nu_*} \right]^2}} \\ p_y^\gamma &= \frac{\bar{p}_y^\gamma}{\zeta_y^\gamma(\bar{\mathbf{p}}; p_{\mathbf{h}})}.\end{aligned}$$

Defining $\bar{x}_i^\mu = \sum_{\mu_*} \hat{m}^{\mu* \mu} x_i^{*\mu*}$, we thus find

$$\begin{aligned}\bar{x}_i^\mu &= \sum_{\mu_*=1}^{P^*} x_i^{*\mu_*} \sum_{y=0}^C q_y^{*\mu*} \sigma_\mu(\beta_{\text{eff}} m^{\mu*} + \log [\mathbf{p}_y]) \\ \bar{p}_y^\gamma &= \sum_{\mu_*=1}^{P^*} q_y^{*\mu*} \sigma_\gamma(\beta_{\text{eff}} m^{\mu*} + \log [\mathbf{p}_y]) \\ m^{\mu* \mu} &= \varsigma \left(2\beta_{\text{eff}} \varrho \sqrt{\sum_{i=1}^N [\bar{x}_i^\mu]^2} \right) \frac{\sum_{i=1}^N x_i^{*\mu_*} \bar{x}_i^\mu}{\sqrt{\sum_{i=1}^N [\bar{x}_i^\mu]^2}} \\ p_y^\gamma &= \frac{\bar{p}_y^\gamma}{\zeta_y^\gamma(\bar{\mathbf{p}}; p_{\mathbf{h}})},\end{aligned}$$

for all $1 \leq \mu \leq P$ and $0 \leq \gamma \leq P$.

F Normalization of the weights

In order to enforce $\sqrt{\sum_{i=1}^N (w_i^\mu)^2} = 1$ at each SGD step, we project \mathbf{w}^μ and the gradient of the loss with respect to \mathbf{w}^μ onto the unit sphere S^{N-1} and the tangent space of \mathbf{w}^μ , respectively. We divide w_i^μ by its norm to project it onto S^{N-1} , and we multiply the gradient by $\delta_{jk} - w_j^\mu w_k^\mu$ to project it onto the tangent space. Projecting the gradient onto the tangent space is a mathematically sound way to obtain the gradient of a function restricted to a manifold embedded in \mathbb{R}^N [108].

The tasks of deriving the saddle-point equations for \bar{p}_y^γ (Eqs. 10), finding the stationarity condition of the loss with respect to the class weights p_y^γ (Eqs. 6) and efficiently training p_y^γ all amount to solving the extremization problem

$$\text{Extr}_{\mathbf{p}, \omega, \lambda} \left\{ f(\mathbf{p}) + \sum_{y=0}^C \lambda_y \left(\sum_{\gamma=0}^P p_y^\gamma - p_{\mathbf{q}}(y) \right) + \sum_{\gamma=0}^P \omega^\gamma \left(\sum_{y=0}^C p_y^\gamma - p_{\mathbf{h}}(\gamma) \right) \right\}, \quad (24)$$

where λ_y and ω^γ are Lagrange multipliers that enforce the constraints $\sum_{\gamma} p_y^\gamma = p_{\mathbf{q}}(y)$ and $\sum_y p_y^\gamma = p_{\mathbf{h}}(\gamma)$. In the former task, $f(\mathbf{p})$ is the free entropy (Eq. 22) at fixed \mathbf{m} and $\hat{\mathbf{m}}$. In the latter two, it is the negative log-likelihood loss (Eq. 4) at a given \mathbf{w} . To find the saddle-point equations and the stationarity conditions of the loss, we derive an implicit solution of Eq. (24) that is useful in analytical calculations. On the other hand, to train p_y^γ , we design an algorithm to quickly compute a numerical solution of Eq. (24). We start by noting that, since the extrema of Eq. (24) are the points where the gradient vanishes, they take the form

$$\begin{aligned} \partial_{p_y^\gamma} f(\mathbf{p}) &= \lambda_y + \omega^\gamma \\ \sum_{\gamma=0}^P p_y^\gamma &= p_{\mathbf{q}}(y) \\ \sum_{y=0}^C p_y^\gamma &= p_{\mathbf{h}}(\gamma). \end{aligned} \quad (25)$$

Define $\bar{p}_y^\gamma = \partial_{p_y^\gamma} \exp(f(\mathbf{p})) = p_y^\gamma \partial_{p_y^\gamma} f(\mathbf{p})$, then

$$\frac{\bar{p}_y^\gamma}{p_y^\gamma} = \lambda_y + \omega^\gamma,$$

along with the previously established row and column sum constraints on \mathbf{p} . Rearranging terms, we get

$$p_y^\gamma = \frac{1}{\lambda_y + \omega^\gamma} \bar{p}_y^\gamma.$$

Using the row and column constraints $\sum_{\gamma=0}^P p_y^\gamma = p_{\mathbf{q}}(y)$ and $\sum_{y=0}^C p_y^\gamma = p_{\mathbf{h}}(\gamma)$, we find that the Lagrange

multipliers λ_y and ω^γ solve the non-linear equations

$$\begin{aligned}\lambda_y &= \frac{1}{p_{\mathbf{q}}(y)} \sum_{\gamma=0}^P \frac{\lambda_y}{\lambda_y + \omega^\gamma} \bar{p}_y^\gamma \\ \omega^\gamma &= \frac{1}{p_{\mathbf{h}}(\gamma)} \sum_{y=0}^C \frac{\omega^\gamma}{\lambda_y + \omega^\gamma} \bar{p}_y^\gamma,\end{aligned}\quad (26)$$

For conciseness, we define $\zeta_y^\gamma(\bar{\mathbf{p}}; p_{\mathbf{h}}) = \lambda_y(\bar{\mathbf{p}}; p_{\mathbf{h}}) + \omega^\gamma(\bar{\mathbf{p}}; p_{\mathbf{h}})$, where $\lambda_y(\bar{\mathbf{p}}; p_{\mathbf{h}})$ and $\omega^\gamma(\bar{\mathbf{p}}; p_{\mathbf{h}})$ are the λ_y and ω^γ solving Eqs. (26) at given P and $p_{\mathbf{h}}$. Using these definitions, we find the implicit solution $p_y^\gamma = \bar{p}_y^\gamma / \zeta_y^\gamma(\bar{\mathbf{p}}; p_{\mathbf{h}})$. As wanted, this equation is useful in analytical calculations involving the saddle-point equations and the stationarity conditions of the loss. However, it is also quite slow to solve numerically for a given $\bar{\mathbf{p}}$, as reported in [109, 110, 111]. Therefore, although we can train p_y^γ by iterating $p_y^\gamma = \bar{p}_y^\gamma / \zeta_y^\gamma(\bar{\mathbf{p}}; p_{\mathbf{h}})$, it is not a very efficient method.

In order to efficiently train p_y^γ , we devise a faster way to solve Eqs. (25) than through Eq. (26). Exponentiating both sides of the first line of Eqs. (25), we find

$$\begin{aligned}\exp\left(\eta \partial_{p_y^\gamma} f(\mathbf{p})\right) \exp(-\eta \lambda_y) \exp(-\eta \omega^\gamma) &= 1 \\ \exp(-\eta \omega^\gamma) p_y^\gamma \exp\left(\eta \partial_{p_y^\gamma} f(\mathbf{p})\right) \exp(-\eta \lambda_y) &= p_y^\gamma,\end{aligned}$$

where η is an arbitrary scalar that will play the role of a learning rate. Fix $k_y^\gamma = p_y^\gamma \exp\left(\eta \partial_{p_y^\gamma} f(\mathbf{p})\right)$. By the Sinkhorn-Knopp theorem [112, 113, 114], there is a rescaled matrix of the form $p_y'^\gamma = D_L^\gamma(\mathbf{k}) k_y^\gamma D_R^\gamma(\mathbf{k})$ that satisfies the same constraints $p_y'^\gamma \geq 0$, $\sum_{\gamma=0}^P p_y'^\gamma = p_{\mathbf{q}}(y)$ and $\sum_{y=0}^C p_y'^\gamma = p_{\mathbf{h}}(\gamma)$ as p_y^γ if some technical conditions are satisfied [114]. Moreover, if $p_y'^\gamma$ exists, then it is unique [115, 116, 114], and we can quickly compute suitable scaling factors $D_L^\gamma(\mathbf{k})$ and $D_R^\gamma(\mathbf{k})$ for $\mathbf{k} = \{k_y^\gamma\}_{0 \leq y \leq C}^{0 \leq \gamma \leq P}$ using the Sinkhorn-Knopp algorithm [112, 113, 114, 117]. $p_y'^\gamma$ is generally not equal to p_y^γ . However, we observe that the iteration

$$\begin{aligned}k_y^\gamma(t) &= p_y^\gamma(t) \exp\left(\eta \partial_{p_y^\gamma(t)} f(\mathbf{p}(t))\right) \\ p_y^\gamma(t+1) &= D_L^\gamma(\mathbf{k}(t)) k_y^\gamma(t) D_R^\gamma(\mathbf{k}(t))\end{aligned}\quad (27)$$

converges at small η (for example $\sim 0.1/P$), which means that it must converge to a solution of Eqs. (25). Since the Sinkhorn-Knopp algorithm is fast, it is significantly more efficient to iterate Eqs. (27) than $p_y^\gamma = \bar{p}_y^\gamma / \zeta_y^\gamma(\bar{\mathbf{p}}; p_{\mathbf{h}})$ to solve Eqs. (25).

In practice, we train p_y^γ using a stochastic variant of Eqs. (27) where the gradient is estimated over small batches of data and smoothed with a momentum hyperparameter. Furthermore, we multiply the gradient by $\delta_{yy'} - p_y^\gamma / p_{\mathbf{h}}(\gamma)$ to reduce the size of the components of $\exp\left(\eta \partial_{p_y^\gamma(t)} f(\mathbf{p}(t))\right)$ that move p_y^γ away from the constraints $\sum_{\gamma=0}^P p_y^\gamma = p_{\mathbf{q}}(y)$ and $\sum_{y=0}^C p_y^\gamma = p_{\mathbf{h}}(\gamma)$. This step is a simple approximation of the gradient projection proposed in [118].

G Saddle-point hierarchy

Suppose that the set of parameters $\bar{x}_i^{\text{fixed},\mu}$, $\bar{p}_y^{\text{fixed},\gamma}$, $m^{\text{fixed},\mu*\gamma}$, $p_y^{\text{fixed},\gamma}$ with hidden unit prior $p_h^{\text{given}}(\gamma)$ is a fixed point of Eqs. (10) with P hidden units. Substitute into the same saddle-point equations with $P + R \in \{P, \dots, 2P\}$ hidden units the duplicated order parameters

$$\begin{aligned}\bar{x}_i^{\text{duali},\mu} &= \begin{cases} \bar{x}_i^{\text{fixed},\mu} & 0 < \mu \leq P \\ \bar{x}_i^{\text{fixed},\mu-P} & P < \mu \leq P + R \end{cases} \\ \bar{p}_y^{\text{duali},\gamma} &= \begin{cases} \bar{p}_y^{\text{fixed},0} & \gamma = 0 \\ \frac{1}{2}\bar{p}_y^{\text{fixed},\gamma} & 0 < \gamma \leq R \\ \bar{p}_y^{\text{fixed},\gamma} & R < \gamma \leq P \\ \frac{1}{2}\bar{p}_y^{\text{fixed},\gamma-P} & P < \gamma \leq P + R \end{cases} \\ m^{\text{duali},\mu*\gamma} &= \begin{cases} m^{\text{fixed},\mu*0} & \gamma = 0 \\ m^{\text{fixed},\mu*\gamma} & 0 < \gamma \leq P \\ m^{\text{fixed},\mu*,\gamma-P} & P < \gamma \leq P + R \end{cases} \\ p_y^{\text{duali},\gamma} &= \begin{cases} p_y^{\text{fixed},0} & \gamma = 0 \\ \frac{1}{2}p_y^{\text{fixed},\gamma} & 0 < \gamma \leq R \\ p_y^{\text{fixed},\gamma} & R < \gamma \leq P \\ \frac{1}{2}p_y^{\text{fixed},\gamma-P} & P < \gamma \leq P + R \end{cases} \\ \text{along with } p_h(\gamma) &= \begin{cases} p_h^{\text{given}}(0) & \gamma = 0 \\ \frac{1}{2}p_h^{\text{given}}(\gamma) & 0 < \gamma \leq R \\ p_h^{\text{given}}(\gamma) & R < \gamma \leq P \\ \frac{1}{2}p_h^{\text{given}}(\gamma - P) & P < \gamma \leq P + R, \end{cases}\end{aligned}$$

where the hidden units $\gamma \in \{P + 1, \dots, P + R\}$ and their corresponding order parameters are duplicates, or copies, of $\gamma \in \{1, \dots, R\}$. $\gamma = 0$ can also be duplicated, but the result is less interesting. By definition (see Eqs. 26), $\zeta_y^\gamma(\bar{\mathbf{p}}^{\text{duali}}; p_h) = \lambda_y(\bar{\mathbf{p}}^{\text{duali}}; p_h) + \omega^\gamma(\bar{\mathbf{p}}^{\text{duali}}; p_h)$, where $\lambda_y(\bar{\mathbf{p}}^{\text{duali}}; p_h)$ and $\omega^\gamma(\bar{\mathbf{p}}^{\text{duali}}; p_h)$ are the

λ_y and ω^γ solving

$$\begin{aligned}
\omega^\gamma &= \frac{1}{p_{\mathbf{h}}(\gamma)} \sum_{y=0}^C \frac{\omega^\gamma}{\lambda_y + \omega^\gamma} \bar{p}_y^{\text{duplici}, \gamma} \\
&= \frac{1}{p_{\mathbf{h}}^{\text{given}}(\gamma)} \sum_{y=0}^C \frac{\omega^\gamma}{\lambda_y + \omega^\gamma} \bar{p}_y^{\text{fixed}, \gamma} \\
\lambda_y &= \frac{1}{p_{\mathbf{q}}(y)} \sum_{\gamma=0}^{P+R} \frac{\lambda_y}{\lambda_y + \omega^\gamma} \bar{p}_y^{\text{duplici}, \gamma} \\
&= \frac{1}{p_{\mathbf{q}}(y)} \sum_{\gamma=0}^P \frac{\lambda_y}{\lambda_y + \omega^\gamma} \bar{p}_y^{\text{fixed}, \gamma}.
\end{aligned}$$

Therefore, $\zeta_y^\gamma(\bar{\mathbf{p}}^{\text{duplici}}, p_{\mathbf{h}}) = \zeta_y^\gamma(\bar{\mathbf{p}}^{\text{fixed}}, p_{\mathbf{h}}^{\text{given}})$, and the saddle-point equations simplify to

$$\begin{aligned}
\bar{x}_i^{\text{fixed}, \mu} &= \frac{1}{2} (1 + \mathbb{I}(\mu > R)) \sum_{\mu_*=1}^{P^*} x_i^{*\mu_*} \sum_{y=0}^C q_y^{*\mu_*} \sigma_\mu (\beta_{\text{eff}} m^{\text{fixed}, \mu_*} + \log [\mathbf{p}_y^{\text{fixed}}]) \\
\bar{p}_y^{\text{fixed}, \gamma} &= \sum_{\mu_*=1}^{P^*} q_y^{*\mu_*} \sigma_\gamma (\beta_{\text{eff}} m^{\text{fixed}, \mu_*} + \log [\mathbf{p}_y^{\text{fixed}}]) \\
m^{\text{fixed}, \mu_* \mu} &= \varsigma \left(2\beta_{\text{eff}} \varrho \sqrt{\sum_{i=1}^N [\bar{x}_i^{*\text{fixed}, \mu}]^2} \right) \frac{\sum_{i=1}^N x_i^{*\mu_*} \bar{x}_i^{*\text{fixed}, \mu}}{\sqrt{\sum_{i=1}^N [\bar{x}_i^{*\text{fixed}, \mu}]^2}} \\
p_y^{\text{fixed}, \gamma} &= \frac{\bar{p}_y^{\text{fixed}, \gamma}}{\zeta_y^\gamma(\bar{\mathbf{p}}^{\text{fixed}}, p_{\mathbf{h}}^{\text{given}})},
\end{aligned} \tag{28}$$

where $\mathbb{I}(\mu > R)$ is the indicator function equal to 1 when $\mu > R$ and 0 otherwise. Assume that $\varrho \rightarrow \infty$ so that $\varsigma \left(2\beta_{\text{eff}} \varrho \sqrt{\sum_{i=1}^N [\bar{x}_i^\mu]^2} \right) \rightarrow \mathbb{I} \left(\sqrt{\sum_{i=1}^N [\bar{x}_i^\mu]^2} > 0 \right)$, then the saddle-point equations are the same no matter how the prefactor of $\frac{1}{2} (1 + \mathbb{I}(\mu > R))$ affects the norm of \bar{x}_i^μ , and Eqs. (13) are a fixed point of the saddle-point equations with $P + R$ hidden units. In particular, Eq. (13) is a stationary point of the loss (Eq. 4) when $\beta_{\text{eff}} = \beta$.

For the rest of this Appendix, all sums are understood as having the same bounds as Eqs. (28) and (10). The stability of any fixed point of the form $\mathbf{x} = \mathbf{F}(\mathbf{x})$, such as those of Eqs. (10), can be evaluated using the Jacobian matrix \mathbf{J} of \mathbf{F} . If all eigenvalues λ of the Jacobian satisfy $|\lambda| < 1$, then the fixed point is stable. Conversely, if the Jacobian has an eigenvalue λ with $|\lambda| > 1$, then the fixed point is unstable. In particular, if the quadratic form $\mathbf{v}^T \mathbf{J} \mathbf{v}$ is larger than 1 for some \mathbf{v} with $\|\mathbf{v}\| = 1$, then the fixed point is unstable. For the rest of this Appendix, we evaluate the stability of Eqs. (10) with duplicated order parameters. Keeping $\bar{\mathbf{p}}$ and

\mathbf{p} fixed, the Jacobian of the saddle-point equation for $\bar{\mathbf{x}}$ is

$$\begin{aligned}
\partial_{\bar{x}_k^\nu} \bar{x}_j^\mu &= \sum_{\mu_*} x_j^{*\mu_*} \partial_{\bar{x}_k^\nu} m^{\mu_* \nu} \sum_y q_y^{*\mu_*} \partial_{m^{\mu_* \nu}} \sigma_\mu (\beta_{\text{eff}} m^{\mu_*} + \log [\mathbf{p}_y]) \\
&= \beta_{\text{eff}} \sum_{\mu_*} x_j^{*\mu_*} \partial_{\bar{x}_k^\nu} m^{\mu_* \nu} \sum_y q_y^{*\mu_*} \sigma_\mu (\beta_{\text{eff}} m^{\mu_*} + \log [\mathbf{p}_y]) (\delta_{\mu\nu} - \sigma_\nu (\beta_{\text{eff}} m^{\mu_*} + \log [\mathbf{p}_y])) \\
&= \beta_{\text{eff}} \sum_{\mu_*} x_j^{*\mu_*} \frac{1}{\sqrt{\sum_i [\bar{x}_i^\nu]^2}} \left(x_k^{*\mu_*} - \left[\sum_i x_i^{*\mu_*} \tilde{x}_i^\nu \right] \tilde{x}_k^\nu \right) \\
&\quad \sum_y q_y^{*\mu_*} \sigma_\mu (\beta_{\text{eff}} m^{\mu_*} + \log [\mathbf{p}_y]) (\delta_{\mu\nu} - \sigma_\nu (\beta_{\text{eff}} m^{\mu_*} + \log [\mathbf{p}_y])),
\end{aligned}$$

where $\tilde{x}_j^\nu = \frac{\bar{x}_j^\nu}{\sqrt{\sum_i [\bar{x}_i^\nu]^2}}$. Suppose that \bar{x}_i^μ , \bar{p}_y^γ , $m^{\mu_* \gamma}$ and p_y^γ are the duplicated parameters of Eq. (13) with $0 < \mu, \nu \leq R$ or $P < \mu, \nu \leq P + R$, then

$$\begin{aligned}
\partial_{\bar{x}_k^\nu} \bar{x}_j^\mu &= \beta_{\text{eff}} \sum_{\mu_*} x_j^{*\mu_*} \frac{1}{\sqrt{\sum_i [\bar{x}_i^\nu]^2}} \left(x_k^{*\mu_*} - \left[\sum_i x_i^{*\mu_*} \tilde{x}_i^\nu \right] \tilde{x}_k^\nu \right) \\
&\quad \sum_y q_y^{*\mu_*} \frac{1}{2} \sigma_{\theta(\mu)} (\beta_{\text{eff}} m^{\text{fixed}, \mu_*} + \log [\mathbf{p}_y^{\text{fixed}}]) \left(\delta_{\mu\nu} - \frac{1}{2} \sigma_{\theta(\nu)} (\beta_{\text{eff}} m^{\text{fixed}, \mu_*} + \log [\mathbf{p}_y^{\text{fixed}}]) \right), \\
\text{where } \theta(\mu) &= \begin{cases} \mu & 0 < \mu \leq R \\ \mu - P & 0 < \mu \leq P + R. \end{cases}
\end{aligned}$$

If β_{eff} is relatively large (for instance of order \sqrt{N}), then the softmax $\sigma_{\theta(\mu)}$ splits the indices μ_* into a cover \mathcal{S} of sets $\mathcal{S}(\mu)$ such that $\sigma_{\theta(\mu)} (\beta_{\text{eff}} m^{\text{fixed}, \mu_*} + \log [\mathbf{p}_y]) \approx \mathbb{I}(\mu_* \in \mathcal{S}(\mu))$. Therefore, we have

$$\begin{aligned}
\partial_{\bar{x}_k^\nu} \bar{x}_j^\mu &\approx \beta_{\text{eff}} \sum_{\mu_*} x_j^{*\mu_*} \frac{1}{\sqrt{\sum_i [\bar{x}_i^\nu]^2}} \left(x_k^{*\mu_*} - \left[\sum_i x_i^{*\mu_*} \tilde{x}_i^\nu \right] \tilde{x}_k^\nu \right) \\
&\quad \frac{1}{2} \mathbb{I}(\mu_* \in \mathcal{S}(\mu)) \left(\delta_{\mu\nu} - \frac{1}{2} \mathbb{I}(\mu_* \in \mathcal{S}(\nu)) \right).
\end{aligned}$$

The subcovers $\mathcal{S}(0 < \mu \leq P)$ and $\mathcal{S}(R < \mu \leq P + R)$ are both partitions of the indices μ_* . As such, $[\partial_{\bar{x}_k^\nu} \bar{x}_j^\mu]_{\mu, \nu=1}^{P+R}$ is block-diagonal with 2×2 blocks coupling the indices $0 < \mu \leq R$ and $\nu = \mu + P$. Without loss of generality, we investigate the stability of the block

$$\begin{aligned}
&\begin{bmatrix} \partial_{\bar{x}_k^1} \bar{x}_j^1 & \partial_{\bar{x}_k^{P+1}} \bar{x}_j^1 \\ \partial_{\bar{x}_k^1} \bar{x}_j^{P+1} & \partial_{\bar{x}_k^{P+1}} \bar{x}_j^{P+1} \end{bmatrix} \\
&= \frac{1}{2} \frac{\beta_{\text{eff}}}{\sqrt{\sum_i [x_i^1]^2}} \sum_{\mu_* \in \mathcal{S}(1)} \begin{bmatrix} x_j^{*\mu_*} (x_k^{*\mu_*} - [\sum_i x_i^{*\mu_*} \tilde{x}_i^1] \tilde{x}_k^1) & -x_j^{*\mu_*} (x_k^{*\mu_*} - [\sum_i x_i^{*\mu_*} \tilde{x}_i^1] \tilde{x}_k^1) \\ -x_j^{*\mu_*} (x_k^{*\mu_*} - [\sum_i x_i^{*\mu_*} \tilde{x}_i^1] \tilde{x}_k^1) & x_j^{*\mu_*} (x_k^{*\mu_*} - [\sum_i x_i^{*\mu_*} \tilde{x}_i^1] \tilde{x}_k^1) \end{bmatrix}.
\end{aligned}$$

where $x_i'^1 = \sum_{\mu_* \in \mathcal{S}(1)} x_i^{*\mu_*}$. Let \mathbf{u}^1 be an arbitrary vector orthogonal to $\tilde{\mathbf{x}}^1$ and define

$$v_j^\mu = \frac{1}{\sqrt{2}} \begin{cases} u_j^1 & \mu = 1 \\ -u_j^1 & \mu = P + 1, \end{cases}$$

then we have the quadratic form

$$\begin{aligned} \sum_{\nu \in \{1, P+1\}} \sum_{k=1}^N v_k^\nu \partial_{\bar{x}_k} \bar{x}_j^\mu &= \frac{\beta_{\text{eff}}}{\sqrt{\sum_i [x_i'^1]^2}} \sum_{\mu_* \in \mathcal{S}(1)} \frac{1}{\sqrt{2}} \begin{bmatrix} x_j^{*\mu_*} \sum_k x_k^{*\mu_*} u_k^1 \\ -x_j^{*\mu_*} \sum_k x_k^{*\mu_*} u_k^1 \end{bmatrix} \\ \sum_{\mu, \nu \in \{1, P+1\}} \sum_{j, k=1}^N v_j^\mu v_k^\nu \partial_{\bar{x}_k} \bar{x}_j^\mu &= \frac{\beta_{\text{eff}}}{\sqrt{\sum_i [x_i'^1]^2}} \sum_{\mu_* \in \mathcal{S}(1)} \left[\sum_j x_j^{*\mu_*} u_j^1 \right]^2. \end{aligned}$$

If \mathbf{u}^1 is orthogonal to all the $\mathbf{x}^{*\mu_*}$ such that $\mu_* \in \mathcal{S}(1)$, and in particular if $\mathcal{S}(1)$ contains a single pattern $\mathbf{x}^{*\mu_*} = \tilde{\mathbf{x}}^1$, then $\sum_{\mu_* \in \mathcal{S}(1)} \left[\sum_j x_j^{*\mu_*} u_j^1 \right]^2 = 0$, so the quadratic form vanishes. In this case, \mathbf{u}^1 is a stable direction of the saddle-point equations. Otherwise, the quadratic form does not vanish, so there is a β_{split} such that the direction \mathbf{u}^1 is unstable when $\beta_{\text{eff}} > \beta_{\text{split}}$.

H Splitting steepest descent

Steps 5 and 11 of splitting steepest descent (Alg. 1) involve the splitting matrices $\mathcal{S}_\mu(\mathbf{w}, \mathbf{p})$ derived in [36]. In this appendix, we explain their role in the algorithm. Consult [36] for a detailed explanation of their interpretation and theoretical underpinnings.

Define the thresholds $\tau_{\text{thres}} \in (0, 1]$ and $\lambda_{\text{thres}} \leq 0$. At step 5 of Alg. (1), we duplicate the hidden units corresponding to the $R \leq \min \{\tau_{\text{thres}} P_{\text{cur}}, P_{\text{max}} - P_{\text{cur}}\}$ most negative minimum eigenvalues λ_{\min}^μ of the splitting matrices $\mathcal{S}_\mu(\mathbf{w}, \mathbf{p})$ such that $\lambda_{\min}^\mu \leq \lambda_{\text{thres}}$ [36]. To make Fig. (6), we pick $\tau_{\text{thres}} = 1$ and $\lambda_{\text{thres}} \approx 0$. Our splitting matrices are

$$\mathcal{S}_\mu(\mathbf{w}, \mathbf{p}) = -\mathbb{E}_{\mathbf{x}^*, y^*} \left[\frac{p_y^\mu \bar{\nabla}_{\mathbf{w}^\mu} \bar{\nabla}_{\mathbf{w}^\mu}^T \exp \left(\beta_{\text{eff}} \sum_{i=1}^N w_i^\mu x_i \right)}{\sum_{\nu=1}^P p_y^\nu \exp \left(\beta_{\text{eff}} \sum_{i=1}^N w_i^\nu x_i \right) + p_y^0 \frac{\Omega_N(\beta)}{\Omega_N(0)}} \right],$$

where $\bar{\nabla}_{\theta}$ is the gradient constrained to the unit hypersphere S^{N-1} (see Appendix F) and β_{eff} can be written explicitly in terms of β as $\beta_{\text{eff}} = \varsigma \beta$ (see Eqs. 12 and 10). At step 11 of Alg. (1), we break permutation symmetries in the memories \mathbf{w}^μ by descending along the eigenvectors $\mathbf{u}^\mu \in S^{N-1}$ corresponding to the eigenvalues λ_{\min}^μ . To be more precise, we update the memories \mathbf{w}^μ and their duplicates $\mathbf{w}^{\text{dupli}, \mu}$ according to $\mathbf{w}^\mu \leftarrow \mathbf{w}^\mu + \delta \mathbf{u}^\mu$ and $\mathbf{w}^{\text{dupli}, \mu} \leftarrow \mathbf{w}^{\text{dupli}, \mu} - \delta \mathbf{u}^\mu$, respectively, where δ is a relatively small learning rate [36]. In physics terminology, the eigenvectors \mathbf{u}^μ are excitation modes that break the permutation symmetries of the memories. N and P are generally large, so it is prohibitively expensive to store $\mathcal{S}_\mu(\mathbf{w}, \mathbf{p})$ explicitly for all hidden units $1 \leq \mu \leq P$. Therefore, as proposed in [37], we find the eigenvectors \mathbf{u}^μ and their eigenvalues λ_{\min}^μ by minimizing the Rayleigh quotients $Q_\mu[\mathbf{w}, \mathbf{p}] : S^{N-1} \ni \mathbf{u}^\mu \mapsto [\mathbf{u}^\mu]^T \mathcal{S}_\mu(\mathbf{w}, \mathbf{p}) \mathbf{u}^\mu$, which can be evaluated without constructing $\mathcal{S}_\mu(\mathbf{w}, \mathbf{p})$ explicitly. To derive $Q_\mu[\mathbf{w}, \mathbf{p}]$, we first compute

$\bar{\nabla}_{\mathbf{w}^\mu} \bar{\nabla}_{\mathbf{w}^\mu}^T \exp(\beta_{\text{eff}} \sum_i w_i^\mu x_i)$. Given $f(\boldsymbol{\theta}) = \sum_i \theta_i x_i$, we find

$$\bar{\nabla}_{\boldsymbol{\theta}} \bar{\nabla}_{\boldsymbol{\theta}}^T \exp(\beta_{\text{eff}} f(\boldsymbol{\theta})) = \exp(\beta_{\text{eff}} f(\boldsymbol{\theta})) (\beta_{\text{eff}} \bar{\nabla}_{\boldsymbol{\theta}} \bar{\nabla}_{\boldsymbol{\theta}}^T f(\boldsymbol{\theta}) + \beta_{\text{eff}}^2 \bar{\nabla}_{\boldsymbol{\theta}} f(\boldsymbol{\theta}) \bar{\nabla}_{\boldsymbol{\theta}}^T f(\boldsymbol{\theta})).$$

As mentioned at the beginning of Appendix F, $\bar{\nabla}_{\boldsymbol{\theta}} f(\boldsymbol{\theta})$ is the unrestricted gradient of $f(\boldsymbol{\theta})$ projected onto the tangent space of $\boldsymbol{\theta}$. It remains to calculate $\bar{\nabla}_{\boldsymbol{\theta}} \bar{\nabla}_{\boldsymbol{\theta}}^T f(\boldsymbol{\theta})$. Following [108], we find it to be the iterated projected gradient

$$\begin{aligned} [\bar{\nabla}_{\boldsymbol{\theta}} \bar{\nabla}_{\boldsymbol{\theta}}^T f(\boldsymbol{\theta})]_{i\ell} &= \sum_k (\delta_{k\ell} - \theta_k \theta_\ell) \partial_{\theta_i} \left(\sum_j (\delta_{jk} - \theta_j \theta_k) \partial_{\theta_j} \left[\sum_h \theta_h x_h \right] \right) \\ &= \sum_k (\delta_{k\ell} - \theta_k \theta_\ell) \partial_{\theta_i} \left(x_k - \left[\sum_j \theta_j x_j \right] \theta_k \right) \\ &= - \sum_k (\delta_{k\ell} - \theta_k \theta_\ell) \left(x_i \theta_k + \left[\sum_j \theta_j x_j \right] \delta_{ik} \right) \\ &= - \left[\sum_j \theta_j x_j \right] (\delta_{i\ell} - \theta_i \theta_\ell), \end{aligned}$$

so we obtain

$$Q_\mu [\mathbf{w}, \mathbf{p}] (\mathbf{u}^\mu) = -\mathbb{E}_{\mathbf{x}^*, y^*} \left[\frac{p_y^\mu \exp(\beta_{\text{eff}} \sum_{i=1}^N w_i^\mu x_i)}{\sum_{\nu=1}^P p_y^\nu \exp(\beta_{\text{eff}} \sum_{i=1}^N w_i^\nu x_i) + p_y^0 \frac{\Omega_N(\beta)}{\Omega_N(0)}} F(\mathbf{u}^\mu; \mathbf{w}^\mu, \mathbf{x}) \right]$$

$$\text{where } F(\boldsymbol{\varphi}; \boldsymbol{\theta}, \mathbf{x}) = \boldsymbol{\varphi}^T [\beta_{\text{eff}} \bar{\nabla}_{\boldsymbol{\theta}} \bar{\nabla}_{\boldsymbol{\theta}}^T f(\boldsymbol{\theta}) + \beta_{\text{eff}}^2 \bar{\nabla}_{\boldsymbol{\theta}} f(\boldsymbol{\theta}) \bar{\nabla}_{\boldsymbol{\theta}}^T f(\boldsymbol{\theta})] \boldsymbol{\varphi}$$

$$\begin{aligned} &= \beta_{\text{eff}}^2 \left(\sum_k \varphi_k x_k - \left[\sum_k \varphi_k \theta_k \right] \left[\sum_j \theta_j x_j \right] \right)^2 \\ &\quad + \beta_{\text{eff}} \left[\sum_j \theta_j x_j \right] \left[\sum_i \varphi_i \theta_i - 1 \right] \left[\sum_\ell \varphi_\ell \theta_\ell + 1 \right]. \end{aligned}$$

We can directly minimize $Q[\mathbf{w}, \mathbf{p}](\mathbf{u}) = \sum_\mu Q_\mu [\mathbf{w}, \mathbf{p}] (\mathbf{u}^\mu)$ to find the set of all eigenvectors \mathbf{u}^μ simultaneously. However, it is more convenient to integrate the eigenvector calculations into the DAM architecture. As such, we define the modified loss

$$\begin{aligned} \mathcal{L}_\epsilon(\mathbf{w}, \mathbf{p}, \mathbf{u}) &= -\log \left[\sum_{\mu=1}^P p_y^\mu \exp \left(\varsigma \beta \sum_{i=1}^N w_i^\mu x_i \right) [1 + \epsilon F(\mathbf{u}^\mu; \mathbf{w}^\mu, \mathbf{x})] + p_y^0 \frac{\Omega_N(\beta)}{\Omega_N(0)} \right] \\ &= -\log \left[\sum_{\mu=1}^P p_y^\mu \exp \left(\varsigma \beta \sum_{i=1}^N w_i^\mu x_i + \log [1 + \epsilon F(\mathbf{u}^\mu; \mathbf{w}^\mu, \mathbf{x})] \right) + p_y^0 \frac{\Omega_N(\beta)}{\Omega_N(0)} \right], \end{aligned}$$

so that the four gradients used to trained the DAM can be calculated using the equations

$$\begin{aligned}\nabla_{\mathbf{u}} \mathcal{Q}[\mathbf{w}, \mathbf{p}](\mathbf{u}) &= \lim_{\epsilon \rightarrow 0} \left\{ \frac{1}{\epsilon} \nabla_{\mathbf{u}} \mathcal{L}_\epsilon(\mathbf{w}, \mathbf{p}, \mathbf{u}) \right\}, \\ \nabla_{\mathbf{w}} \mathcal{L}(\mathbf{w}, \mathbf{p}) &= \nabla_{\mathbf{w}} \mathcal{L}_0(\mathbf{w}, \mathbf{p}, \mathbf{u}) \\ \nabla_{\mathbf{p}} \mathcal{L}(\mathbf{w}, \mathbf{p}) &= \nabla_{\mathbf{p}} \mathcal{L}_0(\mathbf{w}, \mathbf{p}, \mathbf{u}) \\ \text{and } \nabla_{\beta} \mathcal{L}(\mathbf{w}, \mathbf{p}) &= \nabla_{\beta} \mathcal{L}_0(\mathbf{w}, \mathbf{p}, \mathbf{u}).\end{aligned}$$

This technique is based on the automatic differentiation trick proposed in [37]. We numerically implement the limit in the first equation by setting $\epsilon = 0$ during loss evaluation and $\epsilon = 1$ during gradient computation. When we optimize $\mathcal{Q}[\mathbf{w}, \mathbf{p}](\mathbf{u})$, the minima of the different Rayleigh quotients $Q_\mu[\mathbf{w}, \mathbf{p}](\mathbf{u}^\mu)$ can span multiple orders of magnitude, so we normalize the gradients $\nabla_{\mathbf{u}^\mu} Q_\mu[\mathbf{w}, \mathbf{p}](\mathbf{u}^\mu)$ by a running average of their magnitudes to facilitate convergence. This is inspired by the use of RMSProp in [37]. Moreover, we constrain the eigenvectors \mathbf{u}^μ and the gradients $\nabla_{\mathbf{u}^\mu} Q_\mu[\mathbf{w}, \mathbf{p}](\mathbf{u}^\mu)$ to the unit hypersphere as we do for \mathbf{w}^μ (see Appendix F). To make Fig. (6), we train the eigenvectors for 1 epoch, during which we monitor $\min_\mu \left\{ \frac{1}{2} [\mathbf{u}^\mu]^T \nabla_{\mathbf{u}^\mu} \mathcal{Q}[\mathbf{w}, \mathbf{p}](\mathbf{u}^\mu) \right\} = \min_\mu \{ \mathcal{Q}[\mathbf{w}, \mathbf{p}](\mathbf{u}^\mu) \} \sim \min_\mu \{ \lambda_{\min}^\mu \}$ as a metric. The Rayleigh quotients converge very quickly, and using a higher patience does not seem to improve the quality of the learned eigenvectors.

I Initialization and learning rate

To make all our figures, except Fig. (5), we initialize the memories \mathbf{w}^μ uniformly at random on the unit hypersphere S^{N-1} [119]. To make Fig. 5, we instead use the algorithm of [120] to sample the initial memories \mathbf{w}^μ from a vMF distribution (see Appendix C) with mean direction $\tilde{\mathbf{x}}^* = \bar{\mathbf{x}}^* / \|\bar{\mathbf{x}}^*\|$, where $\bar{\mathbf{x}}^* = \frac{1}{N} \sum_{\mu_*=1}^{P^*} \mathbf{x}^{*\mu_*}$ is the mean of the patterns $\mathbf{x}^{*\mu_*}$ and $\|\bar{\mathbf{x}}^*\| = \sqrt{\sum_{i=1}^N [\bar{x}_i^*]^2}$. By construction, the mean direction $\tilde{\mathbf{x}}^*$ is the ordered solution of Eq. (10) with the most permutation symmetries, or in other words the root of the learning dynamics tree shown in Fig. 5, so initializing the memories around it helps reveal the tree structure.

We use a learning rate of $\eta \sim 0.1$ to train the memories \mathbf{w}^μ . Based on our experience, \mathbf{p} trains well when its own learning rate is approximately $\left(1 + \frac{p_h(0)}{1-p_h(0)}\right) P$ times smaller. Without this rescaling, the multiplicative update factor $\exp\left(\eta \partial_{p_y} \mathcal{L}(\mathbf{w}, \mathbf{p})\right)$ described in Appendix F can be relatively large even when η is relatively small, making it ill-behaved. Equivalently, we can also train $g_y^\gamma = \left(1 + \frac{p_h(0)}{1-p_h(0)}\right) P \mathbf{p}$ with the same learning rate η as \mathbf{w} . We adopt this approach in our code available at [38].

Let $P_0 = \frac{p_h(0)}{1-p_h(0)} P$ so that $g_y^\gamma = (P + P_0) p_y^\gamma$. In terms of $g_y^{\text{fixed}, \gamma} = (P + P_0) p_y^{\text{fixed}, \gamma}$, the duplicated parameters (Eq. 13) of the saddle-point hierarchy principle are

$$\bar{x}_i^{\text{duali}, \mu} = \begin{cases} \bar{x}_i^{\text{fixed}, \mu} & 0 < \mu \leq P \\ \bar{x}_i^{\text{fixed}, \mu-P} & P < \mu \leq P + R \end{cases}$$

$$\begin{aligned}
\bar{g}_y^{\text{dupli},\gamma} &= \frac{P+R}{P} \begin{cases} \bar{g}_y^{\text{fixed},0} & \gamma = 0 \\ \frac{1}{2}\bar{g}_y^{\text{fixed},\gamma} & 0 < \gamma \leq R \\ \bar{g}_y^{\text{fixed},\gamma} & R < \gamma \leq P \\ \frac{1}{2}\bar{g}_y^{\text{fixed},\gamma-P} & P < \gamma \leq P+R \end{cases} \\
m^{\text{dupli},\mu_*\gamma} &= \begin{cases} m^{\text{fixed},\mu_*0} & \gamma = 0 \\ m^{\text{fixed},\mu_*\gamma} & 0 < \gamma \leq P \\ m^{\text{fixed},\mu_*,\gamma-P} & P < \gamma \leq P+R \end{cases} \\
g_y^{\text{dupli},\gamma} &= \frac{P+R}{P} \begin{cases} g_y^{\text{fixed},0} & \gamma = 0 \\ \frac{1}{2}g_y^{\text{fixed},\gamma} & 0 < \gamma \leq R \\ g_y^{\text{fixed},\gamma} & R < \gamma \leq P \\ \frac{1}{2}g_y^{\text{fixed},\gamma-P} & P < \gamma \leq P+R \end{cases} \\
\text{along with } g_h(\gamma) &= \frac{P+R}{P} \begin{cases} g_h^{\text{given}}(0) & \gamma = 0 \\ \frac{1}{2}g_h^{\text{given}}(\gamma) & 0 < \gamma \leq R \\ g_h^{\text{given}}(\gamma) & R < \gamma \leq P \\ \frac{1}{2}g_h^{\text{given}}(\gamma-P) & P < \gamma \leq P+R, \end{cases}
\end{aligned}$$

where $g_h^{\text{given}}(\gamma) = (P+P_0)p_h^{\text{given}}(\gamma)$ and $g_h(\gamma) = (P+P_0)p_h(\gamma)$. The newly introduced scaling factor of $\frac{P+R}{P}$ must be taken into account in our implementation of splitting steepest descent (Alg. 1), which gives Alg. (2), shown below.

Algorithm 2 Rescaled splitting steepest descent [36, 37]

- 1: Preallocate space for a DAM with P_{\max} hidden units and the corresponding weights \mathbf{w} and \mathbf{g}
- 2: Initialize the weights \mathbf{w}^μ and \mathbf{g}^μ connected to the P_{cur} first hidden units $\mu \in \{1, \dots, P_{\text{cur}}\}$, as well as \mathbf{g}^0
- 3: $\min L(\mathbf{w}, \mathbf{g})$ with SGD
- 4: **while** $P_{\text{cur}} < P_{\max}$ **do**
- 5: Identify a subset $\mu_{\text{copy}} \subseteq \{1, \dots, P_{\text{cur}}\}$ of $R \leq P_{\max} - P_{\text{cur}}$ hidden units to split, **return** if empty
- 6: Let $\mu_{\text{paste}} = \{P_{\text{cur}} + 1, \dots, P_{\text{cur}} + R\}$ and $\mu_{\text{dupli}} = \{1, \dots, P_{\text{cur}} + R\}$
- 7: Build weights $\mathbf{w}^{\mu_{\text{paste}}} = \mathbf{w}^{\mu_{\text{copy}}}$ for μ_{paste}
- 8: Rescale $\mathbf{g}^{\mu_{\text{copy}}} \leftarrow \mathbf{g}^{\mu_{\text{copy}}} / 2$ and $g_h(\mu_{\text{split}}) \leftarrow g_h(\mu_{\text{split}}) / 2$
- 9: Build weights $\mathbf{g}^{\mu_{\text{paste}}} = \mathbf{g}^{\mu_{\text{copy}}}$ and $g(\mu_{\text{paste}}) = g(\mu_{\text{copy}})$ for μ_{paste}
- 10: Rescale $\mathbf{g}^{\mu_{\text{dupli}}} \leftarrow \frac{P_{\text{cur}}+R}{P_{\text{cur}}} \mathbf{g}^{\mu_{\text{dupli}}}$ and $g_h(\mu_{\text{dupli}}) \leftarrow \frac{P_{\text{cur}}+R}{P_{\text{cur}}} g_h(\mu_{\text{dupli}})$
- 11: Update $P_{\text{cur}} \leftarrow P_{\text{cur}} + R$
- 12: Escape the saddle point by 2nd order descent of $L(\mathbf{w}, \mathbf{g})$ w.r.t. \mathbf{w}
- 13: $\min L(\mathbf{w}, \mathbf{g})$ with SGD
- 14: **end while**
- 15: **return** See Appendix H and [36, 37] for details about steps 5 and 12

We initialize the weights \mathbf{g}^γ and the hidden unit distribution $g_{\mathbf{h}}(\gamma)$ according to

$$g_y^\gamma = \begin{cases} P_0 p_{\mathbf{q}}(y) & \gamma = 0 \\ p_{\mathbf{q}}(y) & \gamma > 0 \end{cases}$$

and $g_{\mathbf{h}}(\gamma) = \begin{cases} \frac{P_0}{P+P_0} & \gamma = 0 \\ \frac{1}{P+P_0} & \gamma > 0. \end{cases}$

When we train our DAM without splitting steepest descent, we set $P_0 = 1$. The resulting weights are, in some sense, the most “typical” [121, 122] for the constraints $g_y^\gamma \geq 0$, $\sum_{y=0}^P g_y^\gamma = (P+1) p_{\mathbf{q}}(y)$ and $\sum_{y=0}^C g_y^\gamma = (P+1) p_{\mathbf{h}}(\gamma) = 1$ (see Section 2). With splitting steepest descent, we set $P_0 = P_{\text{cur}}/P_{\text{final}}$ to ensure that $g_{\mathbf{h}}(0) = \sum_{y=0}^C g_y^0$ is approximately the same size as the other entries of $g_{\mathbf{h}}(\gamma)$ after training. For simplicity, we set $p_{\mathbf{q}}(y)$ to the proportions of classes in the data during supervised training. For unsupervised training (see Section 4.2), we break the permutation symmetry between the different classes by using different values for all the entries of $p_{\mathbf{q}}(y)$. Otherwise, class weights with unbroken permutation symmetries stay stuck at their initial conditions.

J Weights learned with unsupervised training

This Appendix contains plots of DAM weights learned in an unsupervised way (see Section 4.2) and sorted in increasing $y = \text{argmax}_{y'} \{p_{y'}^\mu\}$. They are not in the main text because they take a lot of space.

References

- [1] A. Auffinger, G. B. Arous, and J. Černý, “Random matrices and complexity of spin glasses,” *Communications on Pure and Applied Mathematics*, vol. 66, no. 2, pp. 165–201, 2013. [Online]. Available: <https://onlinelibrary.wiley.com/doi/abs/10.1002/cpa.21422>
- [2] A. Choromanska, M. Henaff, M. Mathieu, G. Ben Arous, and Y. LeCun, “The Loss Surfaces of Multilayer Networks,” in *Proceedings of the Eighteenth International Conference on Artificial Intelligence and Statistics*, ser. Proceedings of Machine Learning Research, G. Lebanon and S. V. N. Vishwanathan, Eds., vol. 38. San Diego, California, USA: PMLR, 09–12 May 2015, pp. 192–204. [Online]. Available: <https://proceedings.mlr.press/v38/choromanska15.html>
- [3] R. Pascanu, Y. N. Dauphin, S. Ganguli, and Y. Bengio, “On the saddle point problem for non-convex optimization,” *arXiv e-prints*, p. arXiv:1405.4604, May 2014.
- [4] Y. N. Dauphin, R. Pascanu, C. Gulcehre, K. Cho, S. Ganguli, and Y. Bengio, “Identifying and attacking the saddle point problem in high-dimensional non-convex optimization,” in *Advances in Neural Information Processing Systems*, Z. Ghahramani, M. Welling, C. Cortes, N. Lawrence, and K. Weinberger, Eds., vol. 27. Curran Associates, Inc., 2014. [Online]. Available: https://proceedings.neurips.cc/paper_files/paper/2014/file/17e23e50bedc63b4095e3d8204ce063b-Paper.pdf

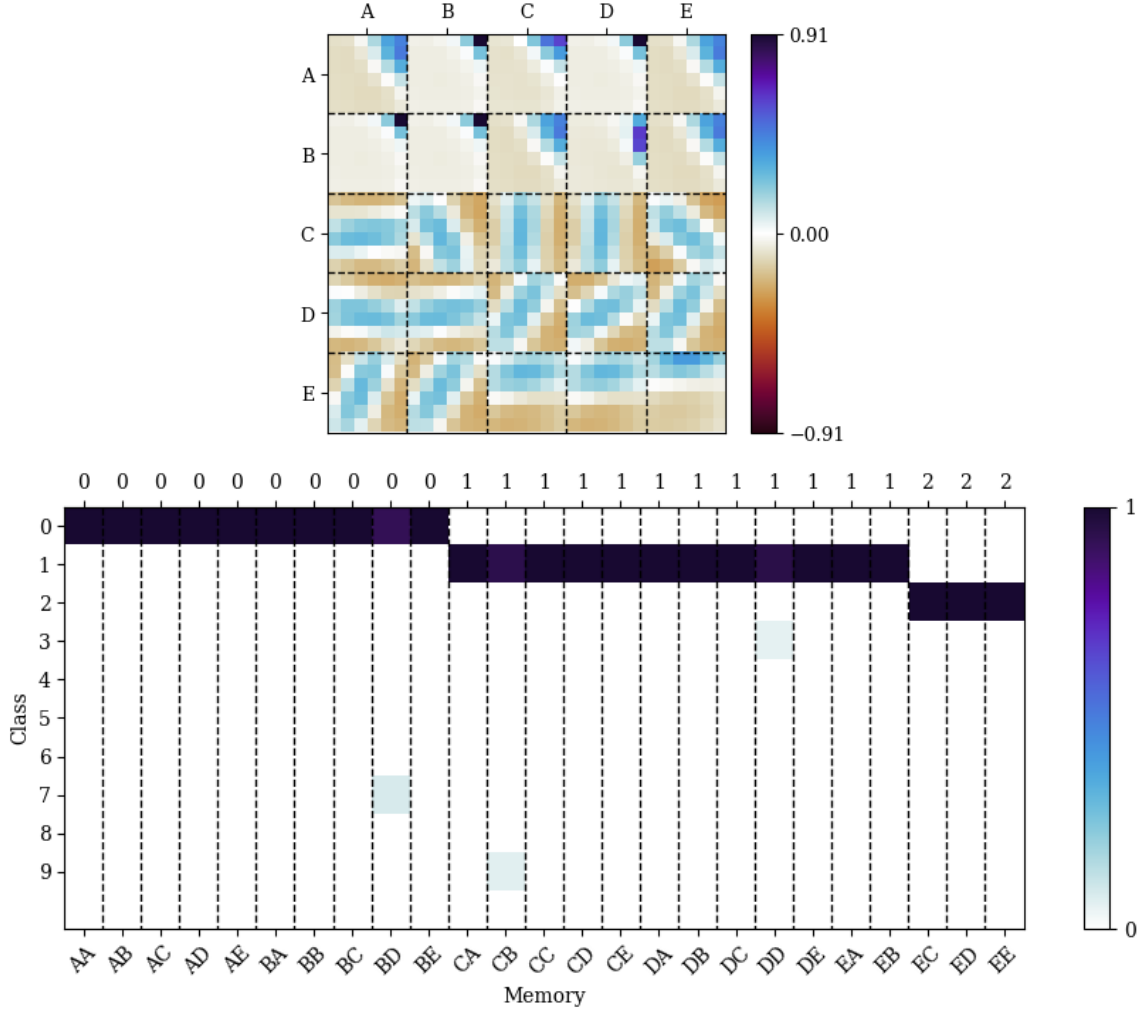


Figure 7: In the top panel, 25 of the $P = 100$ memories \mathbf{w}^μ learned by an instance of our dense associative memory (DAM) model trained in an unsupervised way (Eq. 15) on 6×6 patches of the MNIST dataset of handwritten digits [65] while assuming $C = 10$ latent classes and $\varsigma = 0.6$. In the bottom panel, the corresponding rescaled class weights $\mathbf{p}^\mu / p_h(\mu)$, where $p_h(\gamma) = \frac{1}{P+1}$ for all $0 \leq \gamma \leq P$. The hidden units are indexed using pairs of letters from A to E, and the column-wise maxima of the class weights are the classes of the memories with the corresponding letter indices. \mathbf{w}^μ and \mathbf{p}^μ are sorted in increasing $y = \text{argmax}_{y'} \{p_{y'}^\mu\}$, and this figure shows $1 \leq \mu \leq 25$.

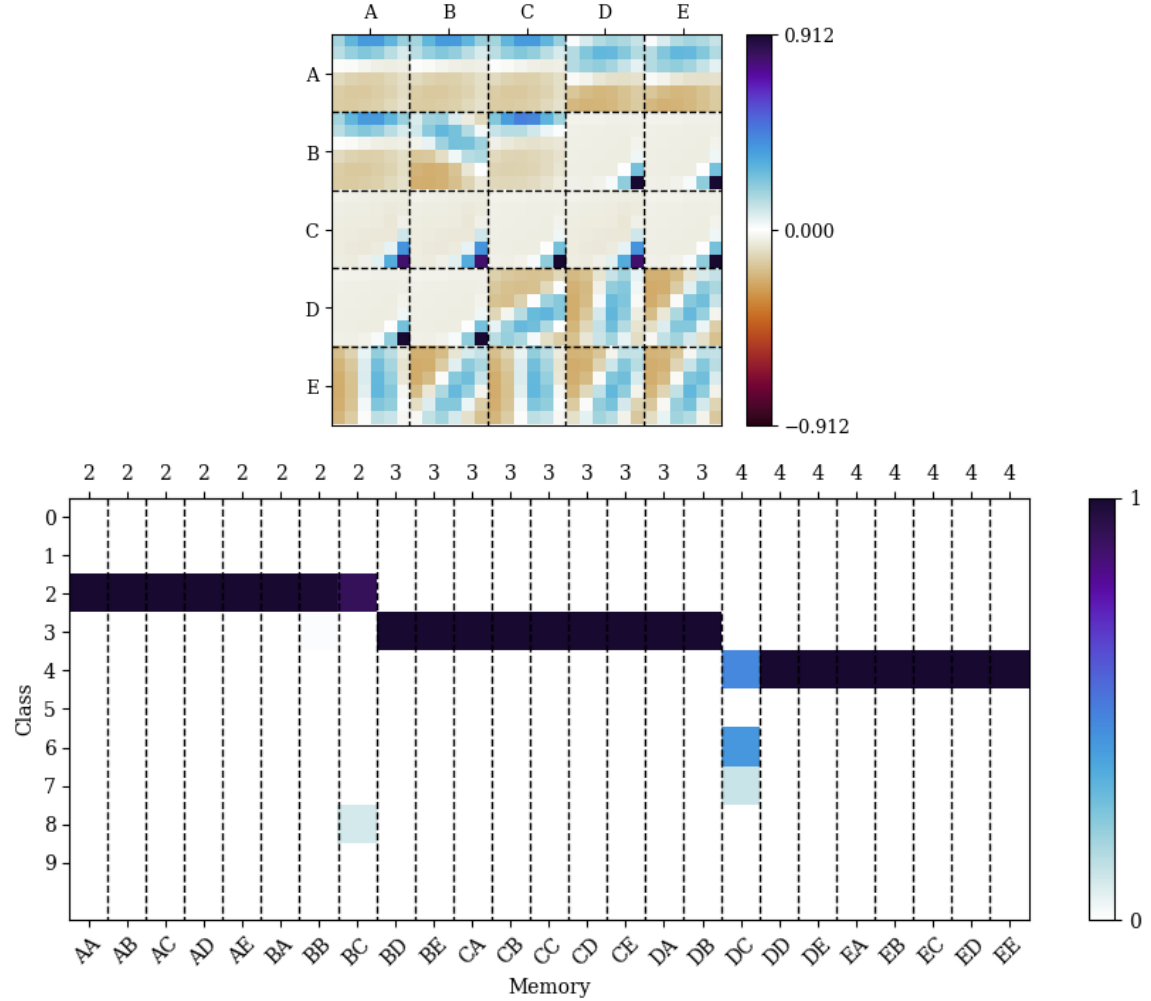


Figure 8: In the top panel, 25 of the $P = 100$ memories w^μ learned by an instance of our dense associative memory (DAM) model trained in an unsupervised way (Eq. 15) on 6×6 patches of the MNIST dataset of handwritten digits [65] while assuming $C = 10$ latent classes and $\varsigma = 0.6$. In the bottom panel, the corresponding rescaled class weights $p^\mu / p_h(\mu)$, where $p_h(\gamma) = \frac{1}{P+1}$ for all $0 \leq \gamma \leq P$. The hidden units are indexed using pairs of letters from A to E, and the column-wise maxima of the class weights are the classes of the memories with the corresponding letter indices. w^μ and p^μ are sorted in increasing $y = \text{argmax}_{y'} \{p_{y'}^\mu\}$, and this figure shows $26 \leq \mu \leq 50$.

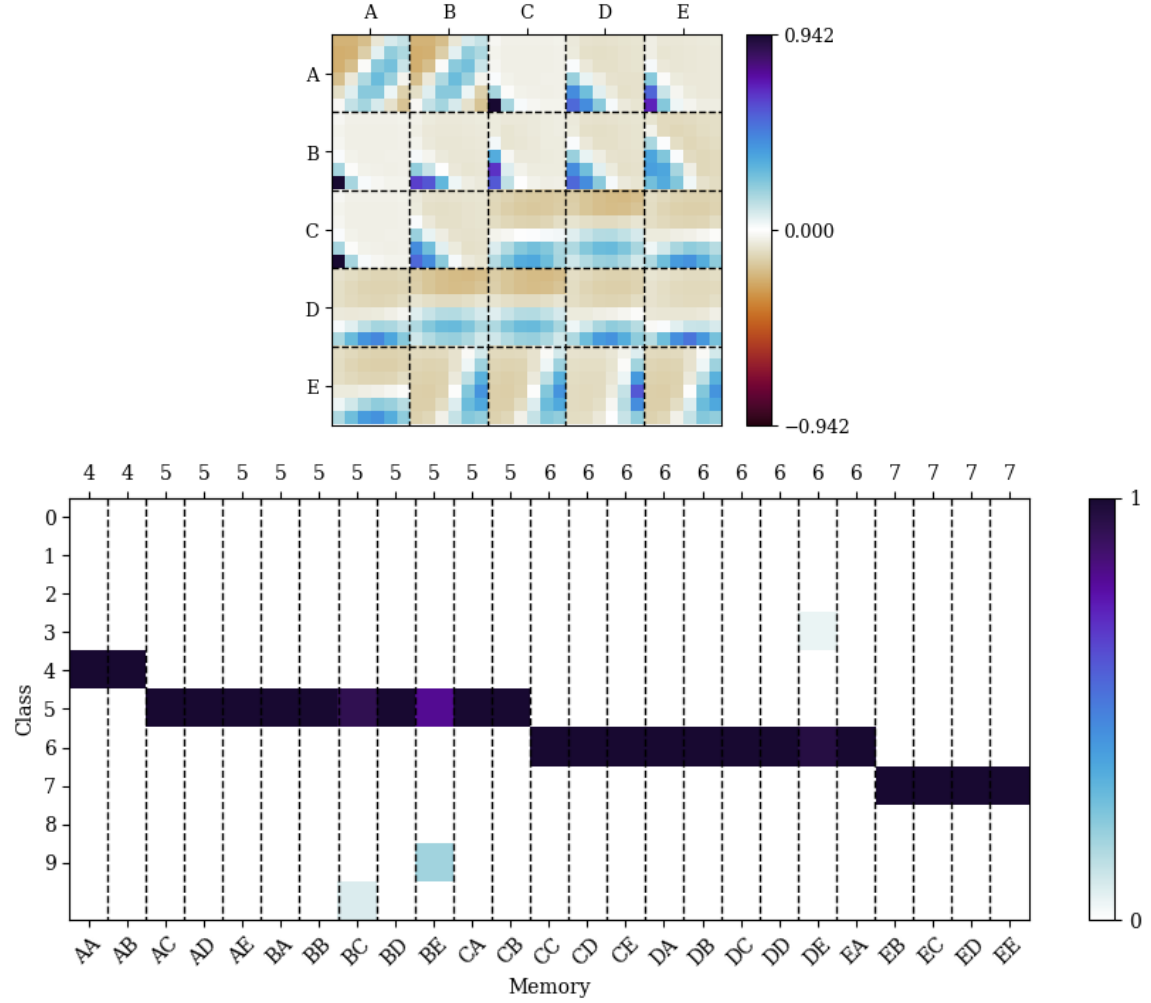


Figure 9: In the top panel, 25 of the $P = 100$ memories \mathbf{w}^μ learned by an instance of our dense associative memory (DAM) model trained in an unsupervised way (Eq. 15) on 6×6 patches of the MNIST dataset of handwritten digits [65] while assuming $C = 10$ latent classes and $\varsigma = 0.6$. In the bottom panel, the corresponding rescaled class weights $\mathbf{p}^\mu / p_h(\mu)$, where $p_h(\gamma) = \frac{1}{P+1}$ for all $0 \leq \gamma \leq P$. The hidden units are indexed using pairs of letters from A to E, and the column-wise maxima of the class weights are the classes of the memories with the corresponding letter indices. \mathbf{w}^μ and \mathbf{p}^μ are sorted in increasing $y = \text{argmax}_{y'} \{p_{y'}^\mu\}$, and this figure shows $51 \leq \mu \leq 75$.

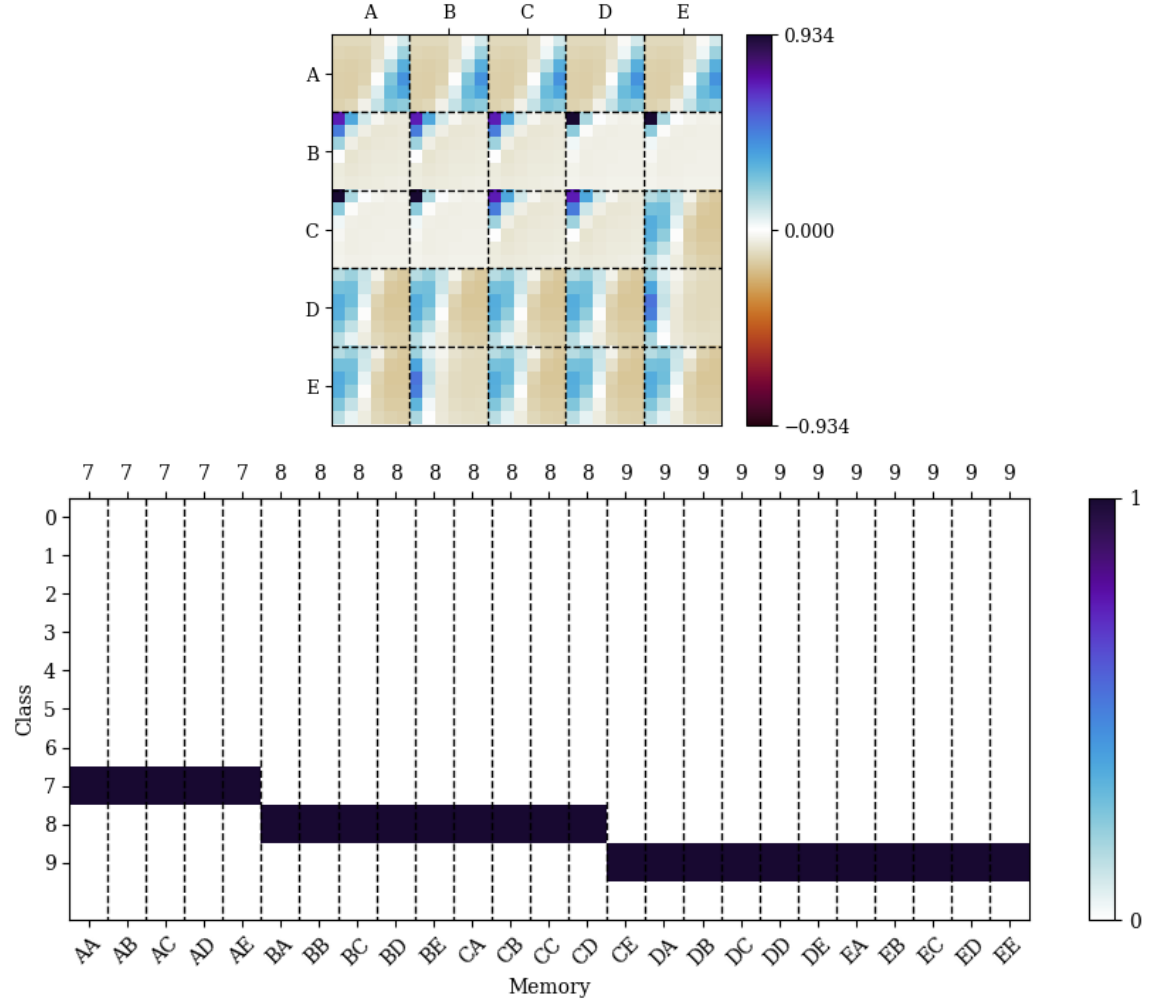


Figure 10: In the top panel, 25 of the $P = 100$ memories \mathbf{w}^μ learned by an instance of our dense associative memory (DAM) model trained in an unsupervised way (Eq. 15) on 6×6 patches of the MNIST dataset of handwritten digits [65] while assuming $C = 10$ latent classes and $\varsigma = 0.6$. In the bottom panel, the corresponding rescaled class weights $\mathbf{p}^\mu / p_h(\mu)$, where $p_h(\gamma) = \frac{1}{P+1}$ for all $0 \leq \gamma \leq P$. The hidden units are indexed using pairs of letters from A to E, and the column-wise maxima of the class weights are the classes of the memories with the corresponding letter indices. \mathbf{w}^μ and \mathbf{p}^μ are sorted in increasing $y = \text{argmax}_{y'} \{p_{y'}^\mu\}$, and this figure shows $76 \leq \mu \leq 100$.

[5] K. Fukumizu and S. Amari, “Local minima and plateaus in hierarchical structures of multilayer perceptrons,” *Neural Networks*, vol. 13, no. 3, pp. 317–327, 2000. [Online]. Available: <https://www.sciencedirect.com/science/article/pii/S0893608000000095>

[6] K. Fukumizu, S. Yamaguchi, Y.-i. Mototake, and M. Tanaka, “Semi-flat minima and saddle points by embedding neural networks to overparameterization,” in *Advances in Neural Information Processing Systems*, H. Wallach, H. Larochelle, A. Beygelzimer, F. d’Alché-Buc, E. Fox, and R. Garnett, Eds., vol. 32. Curran Associates, Inc., 2019. [Online]. Available: https://proceedings.neurips.cc/paper_files/paper/2019/file/a4ee59dd868ba016ed2de90d330acb6a-Paper.pdf

[7] B. Simsek, F. Ged, A. Jacot, F. Spadaro, C. Hongler, W. Gerstner, and J. Brea, “Geometry of the loss landscape in overparameterized neural networks: Symmetries and invariances,” in *Proceedings of the 38th International Conference on Machine Learning*, ser. Proceedings of Machine Learning Research, M. Meila and T. Zhang, Eds., vol. 139. PMLR, 18–24 Jul 2021, pp. 9722–9732. [Online]. Available: <https://proceedings.mlr.press/v139/simsek21a.html>

[8] Y. Zhang, Z. Zhang, T. Luo, and Z. J. Xu, “Embedding principle of loss landscape of deep neural networks,” in *Advances in Neural Information Processing Systems*, M. Ranzato, A. Beygelzimer, Y. Dauphin, P. Liang, and J. W. Vaughan, Eds., vol. 34. Curran Associates, Inc., 2021, pp. 14 848–14 859. [Online]. Available: https://proceedings.neurips.cc/paper_files/paper/2021/file/7cc532d783a7461f227a5da8ea80bfe1-Paper.pdf

[9] J. J. Hopfield, “Neural networks and physical systems with emergent collective computational abilities.” *Proceedings of the National Academy of Sciences*, vol. 79, no. 8, pp. 2554–2558, 1982. [Online]. Available: <https://www.pnas.org/doi/abs/10.1073/pnas.79.8.2554>

[10] D. Krotov and J. J. Hopfield, “Dense associative memory for pattern recognition,” in *Advances in Neural Information Processing Systems*, D. Lee, M. Sugiyama, U. Luxburg, I. Guyon, and R. Garnett, Eds., vol. 29. Curran Associates, Inc., 2016. [Online]. Available: https://proceedings.neurips.cc/paper_files/paper/2016/file/eaae339c4d89fc102edd9dbdb6a28915-Paper.pdf

[11] N. E. Boukacem, A. Leary, R. Thériault, F. Gottlieb, M. Mani, and P. François, “Waddington landscape for prototype learning in generalized hopfield networks,” *Phys. Rev. Res.*, vol. 6, p. 033098, Jul 2024. [Online]. Available: <https://link.aps.org/doi/10.1103/PhysRevResearch.6.033098>

[12] H. H. Chen, Y. C. Lee, G. Z. Sun, H. Y. Lee, T. Maxwell, and C. L. Giles, “High order correlation model for associative memory,” *AIP Conference Proceedings*, vol. 151, no. 1, pp. 86–99, 08 1986. [Online]. Available: <https://doi.org/10.1063/1.36224>

[13] D. Psaltis and C. H. Park, “Nonlinear discriminant functions and associative memories,” *AIP Conference Proceedings*, vol. 151, no. 1, pp. 370–375, 08 1986. [Online]. Available: <https://doi.org/10.1063/1.36241>

[14] P. Baldi and S. S. Venkatesh, “Number of stable points for spin-glasses and neural networks of higher orders,” *Phys. Rev. Lett.*, vol. 58, pp. 913–916, Mar 1987. [Online]. Available: <https://link.aps.org/doi/10.1103/PhysRevLett.58.913>

- [15] E. Gardner, “Multiconnected neural network models,” *Journal of Physics A: Mathematical and General*, vol. 20, no. 11, p. 3453, aug 1987. [Online]. Available: <https://dx.doi.org/10.1088/0305-4470/20/11/046>
- [16] L. F. Abbott and Y. Arian, “Storage capacity of generalized networks,” *Phys. Rev. A*, vol. 36, pp. 5091–5094, Nov 1987. [Online]. Available: <https://link.aps.org/doi/10.1103/PhysRevA.36.5091>
- [17] Horn, D. and Usher, M., “Capacities of multiconnected memory models,” *J. Phys. France*, vol. 49, no. 3, pp. 389–395, 1988. [Online]. Available: <https://doi.org/10.1051/jphys:01988004903038900>
- [18] D. J. Amit, H. Gutfreund, and H. Sompolinsky, “Storing infinite numbers of patterns in a spin-glass model of neural networks,” *Phys. Rev. Lett.*, vol. 55, pp. 1530–1533, Sep 1985. [Online]. Available: <https://link.aps.org/doi/10.1103/PhysRevLett.55.1530>
- [19] H. Ramsauer, B. Schäfl, J. Lehner, P. Seidl, M. Widrich, L. Gruber, M. Holzleitner, T. Adler, D. Kreil, M. K. Kopp, G. Klambauer, J. Brandstetter, and S. Hochreiter, “Hopfield networks is all you need,” in *International Conference on Learning Representations*, 2021. [Online]. Available: <https://openreview.net/forum?id=tL89RnzIiCd>
- [20] D. Krotov and J. Hopfield, “Dense Associative Memory Is Robust to Adversarial Inputs,” *Neural Computation*, vol. 30, no. 12, pp. 3151–3167, 12 2018. [Online]. Available: https://doi.org/10.1162/neco_a_01143
- [21] R. Thériault and D. Tantari, “Dense Hopfield networks in the teacher-student setting,” *SciPost Phys.*, vol. 17, p. 040, 2024. [Online]. Available: <https://scipost.org/10.21468/SciPostPhys.17.2.040>
- [22] B. Hoover, H. Strobelt, D. Krotov, J. Hoffman, Z. Kira, and D. H. Chau, “Memory in Plain Sight: A Survey of the Uncanny Resemblances between Diffusion Models and Associative Memories,” *arXiv e-prints*, p. arXiv:2309.16750, Sep. 2023.
- [23] L. Ambrogioni, “In search of dispersed memories: Generative diffusion models are associative memory networks,” *arXiv e-prints*, p. arXiv:2309.17290, Sep. 2023.
- [24] M. Widrich, B. Schäfl, M. Pavlović, H. Ramsauer, L. Gruber, M. Holzleitner, J. Brandstetter, G. K. Sandve, V. Greiff, S. Hochreiter, and G. Klambauer, “Modern hopfield networks and attention for immune repertoire classification,” in *Advances in Neural Information Processing Systems*, H. Larochelle, M. Ranzato, R. Hadsell, M. Balcan, and H. Lin, Eds., vol. 33. Curran Associates, Inc., 2020, pp. 18 832–18 845. [Online]. Available: https://proceedings.neurips.cc/paper_files/paper/2020/file/da4902cb0bc38210839714ebdcf0efc3-Paper.pdf
- [25] D. Krotov and J. J. Hopfield, “Large associative memory problem in neurobiology and machine learning,” in *International Conference on Learning Representations*, 2021. [Online]. Available: https://openreview.net/forum?id=X4y_10OX-hX
- [26] B. Millidge, T. Salvatori, Y. Song, T. Lukasiewicz, and R. Bogacz, “Universal hopfield networks: A general framework for single-shot associative memory models,” in *Proceedings of the 39th International Conference on Machine Learning*, ser. Proceedings of Machine Learning Research,

K. Chaudhuri, S. Jegelka, L. Song, C. Szepesvari, G. Niu, and S. Sabato, Eds., vol. 162. PMLR, 17–23 Jul 2022, pp. 15 561–15 583. [Online]. Available: <https://proceedings.mlr.press/v162/millidge22a.html>

[27] T. Ota and R. Karakida, “Attention in a Family of Boltzmann Machines Emerging From Modern Hopfield Networks,” *Neural Computation*, vol. 35, no. 8, pp. 1463–1480, 07 2023. [Online]. Available: https://doi.org/10.1162/neco_a_01597

[28] B. Hoover, Y. Liang, B. Pham, R. Panda, H. Strobel, D. H. Chau, M. J. Zaki, and D. Krotov, “Energy Transformer,” *arXiv e-prints*, p. arXiv:2302.07253, Feb. 2023.

[29] C. Lucibello and M. Mézard, “Exponential capacity of dense associative memories,” *Phys. Rev. Lett.*, vol. 132, p. 077301, Feb 2024. [Online]. Available: <https://link.aps.org/doi/10.1103/PhysRevLett.132.077301>

[30] A. Fürst, E. Rumerthofer, J. Lehner, V. T. Tran, F. Tang, H. Ramsauer, D. Kreil, M. Kopp, G. Klambauer, A. Bitto, and S. Hochreiter, “Cloob: Modern hopfield networks with infoloob outperform clip,” in *Advances in Neural Information Processing Systems*, S. Koyejo, S. Mohamed, A. Agarwal, D. Belgrave, K. Cho, and A. Oh, Eds., vol. 35. Curran Associates, Inc., 2022, pp. 20 450–20 468. [Online]. Available: https://proceedings.neurips.cc/paper_files/paper/2022/file/8078e76f913e31b8467e85b4c0f0d22b-Paper-Conference.pdf

[31] A. Auer, M. Gauch, D. Klotz, and S. Hochreiter, “Conformal prediction for time series with modern hopfield networks,” in *Advances in Neural Information Processing Systems*, A. Oh, T. Naumann, A. Globerson, K. Saenko, M. Hardt, and S. Levine, Eds., vol. 36. Curran Associates, Inc., 2023, pp. 56 027–56 074. [Online]. Available: https://proceedings.neurips.cc/paper_files/paper/2023/file/aef75887979ae1287b5deb54a1e3cbda-Paper-Conference.pdf

[32] D. H. Ackley, G. E. Hinton, and T. J. Sejnowski, “A learning algorithm for boltzmann machines,” *Cognitive Science*, vol. 9, no. 1, pp. 147–169, 1985. [Online]. Available: <https://www.sciencedirect.com/science/article/pii/S0364021385800124>

[33] P. Smolensky, “Information Processing in Dynamical Systems: Foundations of Harmony Theory,” in *Parallel Distributed Processing, Volume 1: Explorations in the Microstructure of Cognition: Foundations*. The MIT Press, 07 1986. [Online]. Available: <https://doi.org/10.7551/mitpress/5236.003.0009>

[34] Y. Freund and D. Haussler, “Unsupervised learning of distributions on binary vectors using two layer networks,” in *Advances in Neural Information Processing Systems*, J. Moody, S. Hanson, and R. Lippmann, Eds., vol. 4. Morgan-Kaufmann, 1991. [Online]. Available: https://proceedings.neurips.cc/paper_files/paper/1991/file/33e8075e9970de0cfea955af4644bb2-Paper.pdf

[35] G. E. Hinton, “Training products of experts by minimizing contrastive divergence,” *Neural Computation*, vol. 14, no. 8, pp. 1771–1800, 2002.

[36] L. Wu, D. Wang, and Q. Liu, “Splitting steepest descent for growing neural architectures,” in *Advances in Neural Information Processing Systems*, H. Wallach, H. Larochelle, A. Beygelzimer, F. d’Alché-Buc,

E. Fox, and R. Garnett, Eds., vol. 32. Curran Associates, Inc., 2019. [Online]. Available: https://proceedings.neurips.cc/paper_files/paper/2019/file/3a01fc0853ebeba94fde4d1cc6fb842a-Paper.pdf

[37] D. Wang, M. Li, L. Wu, V. Chandra, and Q. Liu, “Energy-Aware Neural Architecture Optimization with Fast Splitting Steepest Descent,” *arXiv e-prints*, p. arXiv:1910.03103, Oct. 2019.

[38] R. Thériault, 2025. [Online]. Available: https://github.com/RobinTher/Dense_Associative_Network_vMF

[39] N. Le Roux and Y. Bengio, “Representational power of restricted boltzmann machines and deep belief networks,” *Neural Computation*, vol. 20, no. 6, pp. 1631–1649, 2008.

[40] R. Salakhutdinov, A. Mnih, and G. Hinton, “Restricted boltzmann machines for collaborative filtering,” in *Proceedings of the 24th International Conference on Machine Learning*, ser. ICML ’07. New York, NY, USA: Association for Computing Machinery, 2007, p. 791–798. [Online]. Available: <https://doi.org/10.1145/1273496.1273596>

[41] J. Kivinen and C. Williams, “Multiple texture boltzmann machines,” in *Proceedings of the Fifteenth International Conference on Artificial Intelligence and Statistics*, ser. Proceedings of Machine Learning Research, N. D. Lawrence and M. Girolami, Eds., vol. 22. La Palma, Canary Islands: PMLR, 21–23 Apr 2012, pp. 638–646. [Online]. Available: <https://proceedings.mlr.press/v22/kivinen12.html>

[42] N. Srivastava, R. Salakhutdinov, and G. Hinton, “Modeling documents with a deep boltzmann machine,” in *Proceedings of the Twenty-Ninth Conference on Uncertainty in Artificial Intelligence*, ser. UAI’13. Arlington, Virginia, USA: AUAI Press, 2013, p. 616–624.

[43] R. Salakhutdinov and G. Hinton, “Deep boltzmann machines,” in *Proceedings of the Twelfth International Conference on Artificial Intelligence and Statistics*, ser. Proceedings of Machine Learning Research, D. van Dyk and M. Welling, Eds., vol. 5. Hilton Clearwater Beach Resort, Clearwater Beach, Florida USA: PMLR, 16–18 Apr 2009, pp. 448–455. [Online]. Available: <https://proceedings.mlr.press/v5/salakhutdinov09a.html>

[44] G. Salton and M. J. McGill, *Introduction to Modern Information Retrieval*. McGraw-Hill, Inc., 1986.

[45] I. S. Dhillon and D. S. Modha, “Concept decompositions for large sparse text data using clustering,” *Machine Learning*, vol. 42, no. 1, pp. 143–175, Jan 2001. [Online]. Available: <https://doi.org/10.1023/A:1007612920971>

[46] A. Banerjee, I. S. Dhillon, J. Ghosh, and S. Sra, “Clustering on the unit hypersphere using von mises-fisher distributions,” *Journal of Machine Learning Research*, vol. 6, no. 46, pp. 1345–1382, 2005. [Online]. Available: <http://jmlr.org/papers/v6/banerjee05a.html>

[47] M. Carandini and D. J. Heeger, “Normalization as a canonical neural computation,” *Nature Reviews Neuroscience*, vol. 13, no. 1, pp. 51–62, Jan 2012. [Online]. Available: <https://doi.org/10.1038/nrn3136>

[48] R. B. Potts, “Some generalized order-disorder transformations,” in *Mathematical proceedings of the cambridge philosophical society*, vol. 48, no. 1. Cambridge University Press, 1952, pp. 106–109.

[49] F.-Y. Wu, “The potts model,” *Reviews of modern physics*, vol. 54, no. 1, p. 235, 1982.

[50] B. Kappen, “Using boltzmann machines for probability estimation,” in *ICANN '93*, S. Gielen and B. Kappen, Eds. London: Springer London, 1993, pp. 521–526.

[51] H. J. Kappen, “Deterministic learning rules for boltzmann machines,” *Neural Networks*, vol. 8, no. 4, pp. 537–548, 1995. [Online]. Available: <https://www.sciencedirect.com/science/article/pii/089360809400112Y>

[52] M. J. Nijman and H. J. Kappen, “Symmetry breaking and training from incomplete data with radial basis boltzmann machines,” *International Journal of Neural Systems*, vol. 08, no. 03, pp. 301–315, 1997. [Online]. Available: <https://doi.org/10.1142/S0129065797000318>

[53] M. C. Mozer and P. Smolensky, “Skeletonization: A technique for trimming the fat from a network via relevance assessment,” in *Advances in Neural Information Processing Systems*, D. Touretzky, Ed., vol. 1. Morgan-Kaufmann, 1988. [Online]. Available: https://proceedings.neurips.cc/paper_files/paper/1988/file/07e1cd7dca89a1678042477183b7ac3f-Paper.pdf

[54] T. Hoefler, D. Alistarh, T. Ben-Nun, N. Dryden, and A. Peste, “Sparsity in deep learning: pruning and growth for efficient inference and training in neural networks,” *J. Mach. Learn. Res.*, vol. 22, no. 1, jan 2021.

[55] Y. Guo, C. Zhang, C. Zhang, and Y. Chen, “Sparse dnns with improved adversarial robustness,” in *Advances in Neural Information Processing Systems*, S. Bengio, H. Wallach, H. Larochelle, K. Grauman, N. Cesa-Bianchi, and R. Garnett, Eds., vol. 31. Curran Associates, Inc., 2018. [Online]. Available: https://proceedings.neurips.cc/paper_files/paper/2018/file/4c5bde74a8f110656874902f07378009-Paper.pdf

[56] S. Gopalakrishnan, Z. Marzi, U. Madhow, and R. Pedarsani, “Combating Adversarial Attacks Using Sparse Representations,” *arXiv e-prints*, p. arXiv:1803.03880, Mar. 2018.

[57] J. Cosentino, F. Zaiter, D. Pei, and J. Zhu, “The Search for Sparse, Robust Neural Networks,” *arXiv e-prints*, p. arXiv:1912.02386, Dec. 2019.

[58] D. Madaan, J. Shin, and S. J. Hwang, “Adversarial neural pruning with latent vulnerability suppression,” in *Proceedings of the 37th International Conference on Machine Learning*, ser. Proceedings of Machine Learning Research, H. D. III and A. Singh, Eds., vol. 119. PMLR, 13–18 Jul 2020, pp. 6575–6585. [Online]. Available: <https://proceedings.mlr.press/v119/madaan20a.html>

[59] A. Rakin, Z. He, L. Yang, Y. Wang, L. Wang, and D. Fan, “Robust sparse regularization: Defending adversarial attacks via regularized sparse network,” in *GLSVLSI 2020 - Proceedings of the 2020 Great Lakes Symposium on VLSI*, ser. Proceedings of the ACM Great Lakes Symposium on VLSI, GLSVLSI. Association for Computing Machinery, Sep. 2020, pp. 125–130, funding Information: This work is supported in part by the National Science Foundation under Grant No.1931871. Publisher Copyright: © 2020 Association for Computing Machinery.; 30th Great Lakes Symposium on VLSI, GLSVLSI 2020 ; Conference date: 07-09-2020 Through 09-09-2020.

[60] T. Jian, Z. Wang, Y. Wang, J. Dy, and S. Ioannidis, “Pruning adversarially robust neural networks without adversarial examples,” in *2022 IEEE International Conference on Data Mining (ICDM)*, 2022, pp. 993–998.

[61] K. Friston, “Hierarchical Models in the Brain,” *PLoS Computational Biology*, vol. 4, no. 11, p. e1000211, Nov. 2008.

[62] A. Decelle and C. Furtlehner, “Restricted boltzmann machine: Recent advances and mean-field theory*,” *Chinese Physics B*, vol. 30, no. 4, p. 040202, apr 2021. [Online]. Available: <https://dx.doi.org/10.1088/1674-1056/abd160>

[63] T. Hastie and R. Tibshirani, “Discriminant Analysis by Gaussian Mixtures,” *Journal of the Royal Statistical Society: Series B (Methodological)*, vol. 58, no. 1, pp. 155–176, 1 1996. [Online]. Available: <https://doi.org/10.1111/j.2517-6161.1996.tb02073.x>

[64] S. Christian, V. Vincent, I. Sergey, S. Jon, and W. Zbigniew, “Rethinking the inception architecture for computer vision,” *2016 IEEE Conference on Computer Vision and Pattern Recognition (CVPR)*, vol. 2016, pp. 2818–2826, 06 2016. [Online]. Available: <https://cir.nii.ac.jp/crid/1361418519657311872>

[65] Y. Lecun, L. Bottou, Y. Bengio, and P. Haffner, “Gradient-based learning applied to document recognition,” *Proceedings of the IEEE*, vol. 86, no. 11, pp. 2278–2324, 1998.

[66] J. Barbier, F. Krzakala, N. Macris, L. Miolane, and L. Zdeborová, “Optimal errors and phase transitions in high-dimensional generalized linear models,” *Proceedings of the National Academy of Sciences*, vol. 116, no. 12, pp. 5451–5460, 2019. [Online]. Available: <https://www.pnas.org/doi/abs/10.1073/pnas.1802705116>

[67] S. Goldt, M. Mézard, F. Krzakala, and L. Zdeborová, “Modeling the influence of data structure on learning in neural networks: The hidden manifold model,” *Phys. Rev. X*, vol. 10, p. 041044, Dec 2020. [Online]. Available: <https://link.aps.org/doi/10.1103/PhysRevX.10.041044>

[68] B. Loureiro, G. Sicuro, C. Gerbelot, A. Pacco, F. Krzakala, and L. Zdeborová, *Learning Gaussian Mixtures with Generalised Linear Models: Precise Asymptotics in High-dimensions*, ser. Advances in Neural Information Processing Systems. Neural information processing systems foundation, 2021, pp. 10 144–10 157.

[69] K. Okajima, X. Meng, T. Takahashi, and Y. Kabashima, “Average case analysis of lasso under ultra sparse conditions,” in *Proceedings of The 26th International Conference on Artificial Intelligence and Statistics*, ser. Proceedings of Machine Learning Research, F. Ruiz, J. Dy, and J.-W. van de Meent, Eds., vol. 206. PMLR, 25–27 Apr 2023, pp. 11 317–11 330. [Online]. Available: <https://proceedings.mlr.press/v206/okajima23a.html>

[70] A. Decelle, G. Fissore, and C. Furtlehner, “Spectral dynamics of learning in restricted boltzmann machines,” *Europhysics Letters*, vol. 119, no. 6, p. 60001, nov 2017. [Online]. Available: <https://dx.doi.org/10.1209/0295-5075/119/60001>

[71] ——, “Thermodynamics of restricted boltzmann machines and related learning dynamics,” *Journal of Statistical Physics*, vol. 172, no. 6, pp. 1576–1608, Sep 2018. [Online]. Available: <https://doi.org/10.1007/s10955-018-2105-y>

[72] A. Decelle and C. Furtlehner, “Gaussian-spherical restricted boltzmann machines,” *Journal of Physics A: Mathematical and Theoretical*, vol. 53, no. 18, p. 184002, apr 2020. [Online]. Available: <https://dx.doi.org/10.1088/1751-8121/ab79f3>

[73] D. Bachtis, G. Biroli, A. Decelle, and B. Seoane, “Cascade of phase transitions in the training of energy-based models,” in *Advances in Neural Information Processing Systems*, A. Globerson, L. Mackey, D. Belgrave, A. Fan, U. Paquet, J. Tomczak, and C. Zhang, Eds., vol. 37. Curran Associates, Inc., 2024, pp. 55 591–55 619. [Online]. Available: https://proceedings.neurips.cc/paper_files/paper/2024/file/648a5a590ca6f2bb5de53f938e230160-Paper-Conference.pdf

[74] M. Harsh, J. Tubiana, S. Cocco, and R. Monasson, “‘place-cell’ emergence and learning of invariant data with restricted boltzmann machines: breaking and dynamical restoration of continuous symmetries in the weight space,” *Journal of Physics A: Mathematical and Theoretical*, vol. 53, no. 17, p. 174002, apr 2020. [Online]. Available: <https://dx.doi.org/10.1088/1751-8121/ab7d00>

[75] Y. Xu, F. Krzakala, and L. Zdeborová, “Learning with restricted boltzmann machines: Asymptotics of amp and gd in high dimensions,” 2025. [Online]. Available: <https://arxiv.org/abs/2505.18046>

[76] H. Huang and T. Toyoizumi, “Unsupervised feature learning from finite data by message passing: Discontinuous versus continuous phase transition,” *Phys. Rev. E*, vol. 94, p. 062310, Dec 2016. [Online]. Available: <https://link.aps.org/doi/10.1103/PhysRevE.94.062310>

[77] H. Huang, “Statistical mechanics of unsupervised feature learning in a restricted boltzmann machine with binary synapses,” *Journal of Statistical Mechanics: Theory and Experiment*, vol. 2017, no. 5, p. 053302, may 2017. [Online]. Available: <https://dx.doi.org/10.1088/1742-5468/aa6ddc>

[78] A. Barra, G. Genovese, P. Sollich, and D. Tantari, “Phase transitions in restricted boltzmann machines with generic priors,” *Phys. Rev. E*, vol. 96, p. 042156, Oct 2017. [Online]. Available: <https://link.aps.org/doi/10.1103/PhysRevE.96.042156>

[79] ——, “Phase diagram of restricted boltzmann machines and generalized hopfield networks with arbitrary priors,” *Phys. Rev. E*, vol. 97, p. 022310, Feb 2018. [Online]. Available: <https://link.aps.org/doi/10.1103/PhysRevE.97.022310>

[80] H. Huang, “Role of zero synapses in unsupervised feature learning,” *Journal of Physics A: Mathematical and Theoretical*, vol. 51, no. 8, p. 08LT01, jan 2018. [Online]. Available: <https://dx.doi.org/10.1088/1751-8121/aaa631>

[81] T. Hou, K. Y. M. Wong, and H. Huang, “Minimal model of permutation symmetry in unsupervised learning,” *Journal of Physics A: Mathematical and Theoretical*, vol. 52, no. 41, p. 414001, sep 2019. [Online]. Available: <https://dx.doi.org/10.1088/1751-8121/ab3f3f>

[82] F. Alemanno, L. Camanzi, G. Manzan, and D. Tantari, “Hopfield model with planted patterns: A teacher–student self-supervised learning model,” *Applied Mathematics and Computation*, vol. 458, p. 128253, 2023. [Online]. Available: <https://www.sciencedirect.com/science/article/pii/S0096300323004228>

[83] G. Manzan and D. Tantari, “The effect of priors on learning with restricted boltzmann machines,” *Physica A: Statistical Mechanics and its Applications*, p. 130766, 2025.

[84] R. Thériault, F. Tosello, and D. Tantari, “Modeling structured data learning with restricted boltzmann machines in the teacher–student setting,” *Neural Networks*, vol. 189, p. 107542, 2025. [Online]. Available: <https://www.sciencedirect.com/science/article/pii/S0893608025004216>

[85] E. Gardner and B. Derrida, “Three unfinished works on the optimal storage capacity of networks,” *Journal of Physics A: Mathematical and General*, vol. 22, no. 12, p. 1983, jun 1989. [Online]. Available: <https://dx.doi.org/10.1088/0305-4470/22/12/004>

[86] A. Decelle, S. Hwang, J. Rocchi, and D. Tantari, “Inverse problems for structured datasets using parallel TAP equations and restricted Boltzmann machines,” *Scientific Reports*, vol. 11, p. 19990, Oct. 2021.

[87] H. Nishimori, *Statistical Physics of Spin Glasses and Information Processing: An Introduction*. Oxford University Press, 07 2001. [Online]. Available: <https://doi.org/10.1093/acprof:oso/9780198509417.001.0001>

[88] P. Charbonneau, “From the replica trick to the replica symmetry breaking technique,” *arXiv e-prints*, p. arXiv:2211.01802, Nov. 2022.

[89] L. Zdeborová and F. Krzakala, “Statistical physics of inference: thresholds and algorithms,” *Advances in Physics*, vol. 65, no. 5, pp. 453–552, 2016. [Online]. Available: <https://doi.org/10.1080/00018732.2016.1211393>

[90] S. Kirkpatrick, C. D. Gelatt, and M. P. Vecchi, “Optimization by simulated annealing,” *Science*, vol. 220, no. 4598, pp. 671–680, 1983. [Online]. Available: <https://www.science.org/doi/abs/10.1126/science.220.4598.671>

[91] K. Rose, E. Gurewitz, and G. C. Fox, “Statistical mechanics and phase transitions in clustering,” *Phys. Rev. Lett.*, vol. 65, pp. 945–948, Aug 1990. [Online]. Available: <https://link.aps.org/doi/10.1103/PhysRevLett.65.945>

[92] E. Fix and J. L. Hodges, “Discriminatory analysis. nonparametric discrimination: Consistency properties,” *International Statistical Review / Revue Internationale de Statistique*, vol. 57, no. 3, pp. 238–247, 1989. [Online]. Available: <http://www.jstor.org/stable/1403797>

[93] Y. Grandvalet and Y. Bengio, “Semi-supervised learning by entropy minimization,” in *Proceedings of the 18th International Conference on Neural Information Processing Systems*, ser. NIPS’04. Cambridge, MA, USA: MIT Press, 2004, p. 529–536.

[94] S. Khalid, T. Khalil, and S. Nasreen, “A survey of feature selection and feature extraction techniques in machine learning,” in *2014 Science and Information Conference*, 2014, pp. 372–378.

[95] M. Kloppenburg and P. Tavan, “Deterministic annealing for density estimation by multivariate normal mixtures,” *Phys. Rev. E*, vol. 55, pp. R2089–R2092, Mar 1997. [Online]. Available: <https://link.aps.org/doi/10.1103/PhysRevE.55.R2089>

[96] S. Akaho and H. J. Kappen, “Nonmonotonic generalization bias of gaussian mixture models,” *Neural Computation*, vol. 12, no. 6, pp. 1411–1427, 06 2000. [Online]. Available: <https://doi.org/10.1162/089976600300015439>

[97] L. McInnes, J. Healy, N. Saul, and L. Großberger, “Umap: Uniform manifold approximation and projection,” *Journal of Open Source Software*, vol. 3, no. 29, p. 861, 2018. [Online]. Available: <https://doi.org/10.21105/joss.00861>

[98] K. ROSE, E. GUREWITZ, and G. C. FOX, “Constrained clustering as an optimization method,” *IEEE transactions on pattern analysis and machine intelligence*, vol. 15, no. 8, pp. 785–794, 1993.

[99] K. ROSE, “Deterministic annealing for clustering, compression, classification, regression, and related optimization problems,” *Proceedings of the IEEE*, vol. 86, no. 11, pp. 2210–2239, 1998.

[100] A. Decelle and C. Furtlechner, “Exact training of restricted boltzmann machines on intrinsically low dimensional data,” *Phys. Rev. Lett.*, vol. 127, p. 158303, Oct 2021. [Online]. Available: <https://link.aps.org/doi/10.1103/PhysRevLett.127.158303>

[101] N. Béreux, A. Decelle, C. Furtlechner, L. Rosset, and B. Seoane, “Fast training and sampling of restricted boltzmann machines,” 2024. [Online]. Available: <https://arxiv.org/abs/2405.15376>

[102] A. Grishechkin, A. Mukherjee, and O. Karin, “Hierarchical cell identities emerge from animal gene regulatory mechanisms,” 2025. [Online]. Available: <https://arxiv.org/abs/2412.11336>

[103] J. A. D. Loera and E. D. Kim, “Combinatorics and geometry of transportation polytopes: An update,” 2013. [Online]. Available: <https://arxiv.org/abs/1307.0124>

[104] K. Mardia and P. Jupp, *Directional Statistics*. United States: John Wiley & Sons, Ltd, 2000.

[105] “NIST Digital Library of Mathematical Functions,” <https://dlmf.nist.gov/>, Release 1.2.2 of 2024-09-15, f. W. J. Olver, A. B. Olde Daalhuis, D. W. Lozier, B. I. Schneider, R. F. Boisvert, C. W. Clark, B. R. Miller, B. V. Saunders, H. S. Cohl, and M. A. McClain, eds. [Online]. Available: <https://dlmf.nist.gov/10.9.E4>

[106] J. Fröhlich and T. Spencer, “The kosterlitz-thouless transition in two-dimensional abelian spin systems and the coulomb gas,” *Communications in Mathematical Physics*, vol. 81, no. 4, pp. 527–602, Dec 1981, appendix B. [Online]. Available: <https://doi.org/10.1007/BF01208273>

[107] “NIST Digital Library of Mathematical Functions,” <https://dlmf.nist.gov/>, Release 1.2.0 of 2024-03-15, f. W. J. Olver, A. B. Olde Daalhuis, D. W. Lozier, B. I. Schneider, R. F. Boisvert, C. W. Clark, B. R. Miller, B. V. Saunders, H. S. Cohl, and M. A. McClain, eds. [Online]. Available: <https://dlmf.nist.gov/10.41.E4>

[108] D. Barilari, “Lecture notes on differential geometry,” p. 127, March 2023.

[109] P. Uribe, C. G. de Leeuw, and H. Theil, “The Information Approach to the Prediction of Interregional Trade Flows1,” *The Review of Economic Studies*, vol. 33, no. 3, pp. 209–220, 07 1966. [Online]. Available: <https://doi.org/10.2307/2974414>

[110] G. J. D. Hewings and B. N. Janson, “Exchanging regional input—output coefficients: A reply and further comments,” *Environment and Planning A: Economy and Space*, vol. 12, no. 7, pp. 843–854, 1980. [Online]. Available: <https://doi.org/10.1068/a120843>

[111] S. McNeil and C. Hendrickson, “A note on alternative matrix entry estimation techniques,” *Transportation Research Part B: Methodological*, vol. 19, no. 6, pp. 509–519, 1985. [Online]. Available: <https://www.sciencedirect.com/science/article/pii/0191261585900451>

[112] R. Sinkhorn, “A relationship between arbitrary positive matrices and doubly stochastic matrices,” *The Annals of Mathematical Statistics*, vol. 35, no. 2, pp. 876–879, 1964. [Online]. Available: <http://www.jstor.org/stable/2238545>

[113] P. Knopp and R. Sinkhorn, “Concerning nonnegative matrices and doubly stochastic matrices.” *Pacific Journal of Mathematics*, vol. 21, no. 2, pp. 343 – 348, 1967.

[114] M. Idel, “A review of matrix scaling and Sinkhorn’s normal form for matrices and positive maps,” *arXiv e-prints*, p. arXiv:1609.06349, Sep. 2016.

[115] M. Menon and H. Schneider, “The spectrum of a nonlinear operator associated with a matrix,” *Linear Algebra and its Applications*, vol. 2, no. 3, pp. 321–334, 1969. [Online]. Available: <https://www.sciencedirect.com/science/article/pii/0024379569900342>

[116] D. Hershkowitz, U. G. Rothblum, and H. Schneider, “Classifications of nonnegative matrices using diagonal equivalence,” *SIAM Journal on Matrix Analysis and Applications*, vol. 9, no. 4, pp. 455–460, 1988. [Online]. Available: <https://doi.org/10.1137/0609038>

[117] W. E. Deming and F. F. Stephan, “On a least squares adjustment of a sampled frequency table when the expected marginal totals are known,” *The Annals of Mathematical Statistics*, vol. 11, no. 4, pp. 427–444, 1940. [Online]. Available: <http://www.jstor.org/stable/2235722>

[118] A. Douik and B. Hassibi, “Manifold optimization over the set of doubly stochastic matrices: A second-order geometry,” *IEEE Transactions on Signal Processing*, vol. 67, no. 22, pp. 5761–5774, 2019.

[119] M. E. Muller, “A note on a method for generating points uniformly on n-dimensional spheres,” *Commun. ACM*, vol. 2, no. 4, p. 19–20, Apr. 1959. [Online]. Available: <https://doi.org/10.1145/377939.377946>

[120] C. Pinzón and K. Jung, “Fast Python sampler for the von Mises Fisher distribution,” Aug. 2023, working paper or preprint. [Online]. Available: <https://hal.science/hal-04004568>

[121] A. BARVINOK, “What does a random contingency table look like?” *Combinatorics, Probability and Computing*, vol. 19, no. 4, p. 517–539, 2010.

[122] I. J. Good, “Maximum entropy for hypothesis formulation, especially for multidimensional contingency tables,” *The Annals of Mathematical Statistics*, vol. 34, no. 3, pp. 911–934, 1963. [Online]. Available: <http://www.jstor.org/stable/2238473>